

SYNTHESIS OF ZEOLITE FERRIERITE FROM RICE HUSK ASH,
CHARACTERIZATION AND ACTIVITY TOWARDS FRIEDEL-CRAFTS
ACYLATION FOR THE FORMATION OF *p*-METHOXYPROPIOPHENONE

HASLIZA BAHRUJI

UNIVERSITI TEKNOLOGI MALAYSIA

UNIVERSITI TEKNOLOGI MALAYSIA

BORANG PENGESAHAN STATUS TESIS^u

JUDUL: SYNTHESIS OF ZEOLITE FERRIERITE FROM RICE HUSK ASH, CHARACTERIZATION AND ACTIVITY TOWARDS FRIEDEL CRAFTS ACYLATION FOR THE FORMATION OF p-METHOXYPROPIOPHENONE

SESI PENGAJIAN: 2004/2005

Saya: HASLIZA BINTI BAHRUJI
(HURUF BESAR)

mengaku membenarkan thesis (~~PSM/Sarjana/Doktor Falsafah~~)* ini disimpan di Perpustakaan Universiti Teknologi Malaysia dengan syarat-syarat kegunaan seperti berikut:

1. Tesis ini hakmilik Universiti Teknologi Malaysia.
2. Perpustakaan Universiti Teknologi Malaysia dibenarkan membuat salinan untuk tujuan pengajian sahaja.
3. Perpustakaan dibenarkan membuat salinan tesis ini sebagai bahan pertukaran antara institusi pengajian tinggi.
4. **Sila tandakan (✓)

SULIT

(Mengandungi maklumat yang berdarjah keselamatan atau kepentingan Malaysia seperti yang termaktub di dalam AKTA RAHSIA RASMI 1972)

TERHAD

(Mengandungi maklumat TERHAD yang telah ditentukan oleh organisasi/badan di mana penyelidikan dijalankan)

TIDAK TERHAD

Disahkan oleh



(TANDATANGAN PENULIS)



(TANDATANGAN PENYELIA)

Alamat Tetap:

136 B6 Felda Air Tawar 4,
81900 Kota Tinggi Johor.


P.M. DR. ZAINAB RAMLI
(Nama Penyelia)

Tarikh: 2 Jun 2005Tarikh: 2 Jun 2005

CATATAN: * Potong yang tidak berkenaan
** Jika tesis ini SULIT atau TERHAD, sila lampirkan surat daripada pihak berkuasa/organisasi berkenaan dengan menyatakan sekali sebab dan tempoh tesis ini perlu dikelaskan sebagai SULIT atau TERHAD

^u Tesis dimaksudkan sebagai tesis bagi Ijazah Doktor Falsafah dan Sarjana secara penyelidikan, atau disertasi bagi pengajian secara kerja kursus dan penyelidikan, atau Laporan Projek Sarjana Muda (PSM).

“I hereby declare that I have read this thesis and in my opinion this thesis is sufficient in terms of scope and quality for the award of the degree of Master of Science (Chemistry)”.

Signature :  _____
Name of Supervisor I : Prof. Madya Dr. Zainab Ramli
Date : 2 June 2005

BAHAGIAN A – PENGESAHAN KERJASAMA*

Adalah disahkan bahawa projek penyelidikan tesis ini telah dilaksanakan melalui kerjasama antara _____ dengan _____

Disahkan oleh:

Tandatangan : Tarikh :

Nama :

Jawatan :

(Cop Rasmi)

**Jika penyediaan tesis / projek melibatkan kerjasama.*

BAHAGIAN B – Untuk Kegunaan Pejabat Sekolah Pengajian Siswazah

Tesis ini telah diperiksa dan di akui oleh:

Nama dan Alamat : Prof Dr. Mohd Zobir B Hussien
Pemeriksa Luar : Dept. of Chemistry
Faculty of Sciences and Environmental Study
Universiti Putra Malaysia,
43400 Serdang Selangor

Nama dan Alamat : Prof Madya Dr. Abdul Rahim B Yaacob
Pemeriksa Dalam I : Dept. of Chemistry, Faculty of Science
Universiti Teknologi Malaysia,
81300 Skudai Johor

Disahkan oleh Penolong Pendaftar di SPS :

Tandatangan : Tarikh :

Nama :

SYNTHESIS OF ZEOLITE FERRIERITE FROM RICE HUSK ASH,
CHARACTERIZATION AND ACTIVITY TOWARDS FRIEDEL-CRAFTS
ACYLATION FOR THE FORMATION OF *p*-METHOXYPROPIOPHENONE

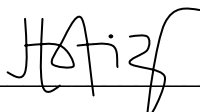
HASLIZA BAHRUJI

A thesis submitted in fulfilment of the
requirements for the award of the degree of
Master of Science (Chemistry)

Faculty of Science
Universiti Teknologi Malaysia

JUNE 2005

I declare that this thesis entitled “SYNTHESIS OF ZEOLITE FERRIERITE FROM RICE HUSK ASH, CHARACTERIZATION AND ACTIVITY TOWARDS FRIEDEL-CRAFTS ACYLATION FOR THE FORMATION OF *p*-METHOXYPROPIOPHENONE” is the result of my own research except as cited in the references. The thesis has not been accepted for any degree and is not concurrently submitted in candidature of any other degree.

Signature : 
Name : Hasliza binti Bahruji
Date : 2 June 2005

*Teristimewa buat:
mak, Amnah Mohd Nor, abah, Bahruji Abdullah dan keluarga,
suami tersayang, Muhammad Islahuddin,
dan cahaya mata ku, Afif Aizuddin
semoga usaha ini direstuhainya*

ACKNOWLEDGEMENT

In the name of Allah, the most Gracious, the most Merciful

Alhamdulillah, All praise be to Allah, The supreme Lord of the universe. Piece and blessing to Nabi Muhammad S.A.W, all the prophets, their families and all the Muslims.

Firstly, I wish to thank to my project supervisor, Assoc. Prof. Dr. Zainab Ramli for her guidance, encouragement and patience throughout this research. Her understanding and supervision is very much appreciated.

I would like to thank MARA and UTM under vote no: 74507 for scholarship and financial support. I would also like to express my gratitude to all lecturers and researchers of the Department of Chemistry, UTM and Institute Ibnu Sina, in particular, Prof Dr Halimaton Hamdan, Assoc. Prof Dr Salasiah Endud, Dr Hadi, Mr Didik and Mr Lim Kheng Wei, who have in many ways contributed to the success of my study.

Thanks to all the laboratory assistants in the Chemistry Department, En Kadir, Pn Mariam, Pn Asmah, Pn Mek Zum, En Rahim, En Azmi and others for their kindness and wonderful co-operation. To my friends, Marzita, Azmi, Wong Kah Man and others, thank you for your support and help. Thanks also to Hafiz (Apak), Hasmerya, Annie and Angela who helped me read this thesis.

Finally, I am grateful to my parents, husband and family for their love, understanding, encouragement and support.

ABSTRACT

Rice husk ash (RHA) consisting more than 90% of amorphous silica obtained under controlled burning of rice husk was directly used in the synthesis of ferrierite type-zeolite. The synthesis was performed under hydrothermal condition in the presence of different organic templates, oxide compositions and at various crystallization periods. Solid products obtained from the synthesis were characterized by XRD, FTIR, ^{29}Si MAS NMR, N_2 (g) adsorption and SEM techniques. Results showed that pure ferrierite can be formed from the initial molar oxide ratios in the range of 1.31 – 1.5 $\text{Na}_2\text{O} : \text{Al}_2\text{O}_3 : 10 - 30 \text{SiO}_2 : 4 - 10.0$ template : 410 H_2O with only pyrrolidine (Py) as the organic template. In general, quartz was obtained at higher $\text{SiO}_2/\text{Al}_2\text{O}_3$ and lower $\text{Py}/\text{Al}_2\text{O}_3$ ratios. The crystal phase changes from ferrierite to analcime and lastly to quartz, with increasing SiO_2/Py ratios. RHA was directly transformed to ferrierite phase within one day and reached equilibrium after 4 days crystallization. The acidity study of the H-ferrierite samples at different $\text{SiO}_2/\text{Al}_2\text{O}_3$ ratios (12, 20 and 30) using IR-pyridine adsorption method showed the increase of acid sites with the decrease of $\text{SiO}_2/\text{Al}_2\text{O}_3$ ratios in ferrierite framework. In each case, the Brønsted acid site is higher than Lewis acid sites. The catalytic activity of ferrierite at different $\text{SiO}_2/\text{Al}_2\text{O}_3$ ratios towards Friedel-Crafts reaction between anisole and acid anhydrides was investigated. Results from the catalytic activity showed that only *p*-methoxypropionophenone and propionic acid was produced as the main product and side product respectively when propionic acid was used as acylating agent. The optimum temperature for the reaction was 120°C and ferrierite catalyst with $\text{SiO}_2/\text{Al}_2\text{O}_3$ ratio 12 gave the highest conversion of anisole (66 %) and the selectivity of the main product (80 %). When acetic anhydride was employed as acylating agent, the conversion of anisole (55 %) and the selectivity of desired product (98 %) showed a higher percentage as compared with propionic anhydride. In both cases, the main product obtained is in *para* orientations with higher selectivity proved that H-ferrierite is a selective catalyst for the production of *para* orientation products.

ABSTRAK

Abu sekam padi (RHA) mengandungi lebih daripada 90% silika amorfus yang diperolehi daripada pembakaran terkawal digunakan untuk menyediakan zeolit ferrierit. Sintesis dijalankan secara hidroterma dengan mengubah pelbagai templat organik, nisbah komposisi oksida dan masa penghabluran. Hasil pepejal yang diperolehi di cirikan dengan menggunakan kaedah XRD, FTIR, ^{29}Si MAS NMR, penjerapan $\text{N}_2(\text{g})$ dan SEM. Keputusan menunjukkan ferrierit tulen telah berjaya disintesis dalam julat $1.31 - 1.5 \text{ Na}_2\text{O} : \text{Al}_2\text{O}_3 : 10 - 30 \text{ SiO}_2 : 4 - 10.0 \text{ templat} : 410 \text{ H}_2\text{O}$ dengan hanya menggunakan pyrrolidin (Py) sebagai templat organik. Apabila nisbah $\text{SiO}_2/\text{Al}_2\text{O}_3$ ditingkatkan dan nisbah $\text{Py}/\text{Al}_2\text{O}_3$ direndahkan, tindakbalas akan menghasilkan kuartz. Fasa hablur berubah dari ferrierit kepada analsim dan diikuti oleh kuartz dengan pertambahan nisbah SiO_2/Py . Pembentukan zeolit ferrierit secara langsung daripada RHA berlaku dalam tempoh satu hari dan mencapai keseimbangan selepas 4 hari penghabluran. Kaedah penjerapan piridin – IR terhadap H-ferrierit dengan pelbagai nisbah $\text{SiO}_2/\text{Al}_2\text{O}_3$ (12, 20 dan 30) telah menunjukkan pertambahan tapak asid dengan berkurangnya nisbah $\text{SiO}_2/\text{Al}_2\text{O}_3$, tetapi bagi setiap sampel, kehadiran tapak asid Brønsted adalah lebih tinggi berbanding tapak asid Lewis. Keaktifan mangkin zeolit ferrierit telah dikaji terhadap tindak balas pengasilan Friedel-Crafts antara anisol dan asid anhidrida. Keputusan menunjukkan hanya *p*-metoksipropiofenon dan asid propionik terbentuk dengan masing-masing sebagai hasil utama dan hasil sampingan apabila propionik anhidrida digunakan sebagai agen pengasilan. Suhu optimum tindak balas adalah pada 120°C dengan mangkin ferrierit pada nisbah $\text{SiO}_2/\text{Al}_2\text{O}_3$ 12 memberikan peratus penukaran bagi anisol yang tertinggi dengan 66 % dan peratus kepilihan terhadap produk utama sebanyak 80%. Apabila asetik anhidrida digunakan sebagai agen pengasilan, peratus pertukaran anisol dan peratus kepilihan hasil utama meningkat berbanding propionik anhidrida sebagai agen pengasilan. Hasil utama yang terbentuk dalam kedua-dua tindak balas adalah dalam orientasi *para* dengan kepilihan yang tinggi, di mana ini membuktikan bahawa H-ferrierit adalah mangkin yang baik bagi menghasilkan sebatian dengan orientasi *para*.

TABLE OF CONTENTS

CHAPTER	TITLE	PAGE
	TITLE	
	DECLARATION	ii
	DEDICATION	iii
	ACKNOWLEDGEMENT	iv
	ABSTRACT	v
	ABSTRAK	vi
	TABLE OF CONTENT	vii
	LIST OF TABLES	xi
	LIST OF FIGURES	xii
	LIST OF ABBREVIATIONS	xv
	LIST OF APPENDICES	xvi
1	INTRODUCTION	
	1.1 General Introduction	1
	1.2 Research Background	2
	1.3 Objectives of Research	3
	1.4 Scope of the Research	4
2	LITERATURE REVIEW	
	2.1 Rice husk ash	5
	2.2 Zeolites	7

2.2.1	Structure and properties	10
2.2.2	Synthesis of zeolite	15
2.3	Ferrierite	18
2.3.1	Structure of Ferrierite	18
2.3.2	Synthesis of Ferrierite	21
2.3.3	Application of Ferrierite	22
2.4	Friedel-Crafts Acylation	23
2.5	Characterization Technique	26
2.5.1	X-ray Powder Diffraction (XRD)	26
2.5.2	Infrared Spectroscopy	28
2.5.3	²⁹ Si Magic Angle Spinning Nuclear Magnetic Resonance	30
2.5.4	N ₂ adsorption	34

3 EXPERIMENTAL

3.1	Synthesis of Ferrierite	36
3.1.1	Chemicals	36
3.1.2	Synthesis of Ferrierite from Rice Husk Ash	37
3.1.3	Optimization Synthesis of Ferrierite from Rice Husk Ash	39
3.1.4	Method to study the Transformation of Rice Husk Ash to ferrierite	39
3.2	Characterizations of Solid Product	40
3.2.1	X-Ray Diffraction (XRD)	40
3.2.2	Fourier Transformed Infrared Spectroscopy	41
3.2.3	²⁹ Si MAS NMR	41
3.2.4	N ₂ adsorption	42
3.2.5	Scanning Electron Microscopy	42

3.3	Acidity Measurement	42
3.3.1	Ammonium ion-exchange method	42
3.3.2	Pyridine Adsorption	43
3.3.3	Temperature-Programmed Desorption	44
	Ammonia	
3.4	Catalyst Activity Testing	45
3.4.1	Gas Chromatography	
3.4.2	Gas Chromatography-Mass Spectroscopy Detector	

4 RESULTS AND DISCUSSION

4.1	Synthesis of Zeolite Ferrierite with Different Initial Oxides Compositions	48
4.1.1	Effect of different Template	49
4.1.1.1	X-ray Diffractogram	49
4.1.1.2	Fourier Transform Infrared	52
4.1.2	Effects of Different Molar Compositions of the Initial Gel	55
4.2	Transformation of Rice Husk Ash to Ferrierite Type Zeolite	64
4.2.1	X-Ray Diffraction	64
4.2.2	The Solid Weight	68
4.2.3	Fourier Transform Infrared	69
4.2.4	Nitrogen Adsorption	73
4.2.5	²⁹ Si MAS NMR Spectroscopy	76
4.2.6	Scanning Electron Microscopy (SEM)	79
4.3	Acidity Study	82
4.3.1	²⁹ Si MAS NMR for H-ferrierite	82
4.3.2	Infrared Spectroscopy of Pyridine Adsorption	84
4.3.3	Temperature-Programmed Desorption	90

(TPD) of Ammonia

4.4	Friedel Crafts Acylation of Anisole and Acid Anhydrides	93
4.4.1	Effect of SiO ₂ /Al ₂ O ₃ Ratios	97
4.4.2	Effect of Reaction Times	99
4.4.3	Effect of Reaction Temperature	102
4.4.4	Effects of the Size of Acylating Agent	103
4.4.5	Correlations Between the Reactivity of Catalysts with their Acidity	105
5	CONCLUSIONS AND RECOMMENDATION	
5.1	Conclusions	106
5.2	Recommendation	109
	REFERENCES	110
	APPENDICES	124

LIST OF TABLES

NO.TABLE	TITLE	PAGES
3.1	The oxides composition of rice husk ash	37
3.2	Molar oxides composition for synthesis ferrierite using various type of templates	38
3.3	The oven-programmed setup for GCMS	46
4.1	Comparison of lattice spacing, d between commercial ferrierite with Fer-12-Py and Fer-12-Py-FS samples	52
4.2	Initial reaction mixtures for samples at different SiO ₂ /Al ₂ O ₃ ratios	57
4.3	Initial reaction mixture for modified samples with different SiO ₂ , Na ₂ O and Py ratio.	57
4.4	The influence of crystallization periods on the solid weight of the products for the formation of ferrierite	66
4.5	FTIR wavenumbers observed for each sample	71
4.6	The BET surface area, average pore diameter and pore volume of sample Fer-12 crystallized at different periods	75
4.7	The chemical shifting and Si/Al ratio of samples H-ferrierite	82
4.8	The amount of Brønsted and Lewis acid sites in catalysts	89
4.9	Quantitative results of H-Ferrierite at different SiO ₂ /Al ₂ O ₃ ratios from the TPD analysis	91

LIST OF FIGURES

NO. FIGURE	TITLE	PAGES
2.1	Zeolite utilization demand in United State of America on 1995	8
2.2	The Secondary Building Units (SBU) in zeolite framework. The oxygen atoms between silicons and aluminiums are omitted for simplicity	13
2.3	Framework lattices: (a) α , (b) Zeolite A, (c) Y and (d) Faujasite	14
2.4	Brønsted and Lewis acid sites in zeolite framework	14
2.5	Framework structure of zeolite ferrierite	20
2.6	Friedel-Crafts acylation between anisole and acid anhydride	25
2.7	Schematic representation of diffracted beams in crystal lattice	27
2.8	Range of ^{29}Si chemical shifts of Q^n in solid silicate	33
2.9	Range of ^{29}Si chemical shifts of $Q^4(mAl)$ units in aluminosilicates	33
2.10	Six types of adsorption isotherm and adsorption and desorption isotherm for mesoporous and microporous materials.	34
2.11	The α_s plot that determined the type of adsorption isotherms	
3.1	Experimental setup for acidity measurement	43
3.2	Heterogeneous batch reaction apparatus	46
4.1	X-Ray Diffractogram for sample Fer-STD, Fer-12-Py, Fer-12-Py(FS), Fer-1-Gly, Fer-2-En, Fer-7-Pn and Fer-8-PnGLy; Effect of different template and silica sources	50
4.2	FTIR spectra for sample Fer-12-Py, Fer-12-Py-FS, Fer-1-Gly, Fer-2-En, Fer-7-Pn and Fer-8-PnGLy	53
4.3	XRD diffractogram of samples at different $\text{SiO}_2/\text{Al}_2\text{O}_3$ ratios	57
4.4	XRD patterns of ferrierite synthesized with different concentrations of pyrrolidine.	59

4.5	The distribution of formation of zeolite phase along the range of SiO ₂ /Py ratios and Na ₂ O/Al ₂ O ₃ ratios	59
4.6	Phase diagram showing the ferrierite and quartz phase produced when the reaction mixture compositions of SiO ₂ /Py/Na ₂ O were varied within the range of 10-50 SiO ₂ : 2-10 Py : 1.31-6 Na ₂ O	61
4.7	X-ray diffractogram pattern for sample Fer-12 under various crystallization periods	64
4.8	Crystallization curve for ferrierite from rice husk ash in sample Fer-12	65
4.9	The percentage of solid products obtained over the initial rice husk ash with time of crystallization	67
4.10	FTIR spectra for sample FER-12 at various crystallization period	69
4.11	The changes of asymmetric and symmetric stretching for TO ₄ bending with crystallization periods	70
4.12	N ₂ adsorption isotherm of calcined samples at various crystallization period	73
4.13	α _s plot for sample at different crystallization period	74
4.14	Correlation between surface areas, pore diameter and pore volume of sample Fer-4-Py at different crystallization period	75
4.15	²⁹ Si MAS NMR spectrum for samples Fer-12 at various crystallization periods	77
4.16	Scanning electron micrograph for ferrierite at different crystallization period (a) 1 day (b) 5days (c) 9 days (d) 12 days	78
4.17	²⁹ Si MAS NMR spectra for sample H-ferrierite at different SiO ₂ /Al ₂ O ₃ ratios	81
4.18	Proposed mechanism of interaction between pyridine molecules with Brønsted acid sites in zeolite.	84
4.19	FTIR spectra of H-Fer 12 after (a) heated at 400°C, following thermal treatment of (b) pyridine desorbed at room temperature, (c) pyridine desorbed at 150°C and (d) pyridine desorbed at 400°C	85
4.20	Infrared spectra of pyridine absorbed at 150°C on H-ferrierite with various SiO ₂ /Al ₂ O ₃ ratios; (a) H-Fer 12, (b) H-Fer 20 and (c) H-Fer 30	87

4.21	TPD of ammonia thermogram of H-Ferrierite with various SiO ₂ /Al ₂ O ₃ ratios denoted as (a) H-Fer 12, (b) H-Fer 20 and (c) H-Fer 30	90
4.22	Friedel-Crafts acylation between anisole and propionic anhydride	92
4.23	GC chromatogram of yield product over acylation of anisole (H-Fer 12)	93
4.24	GCMS spectra of yield product for acylation of anisole over H-ferrierite catalysts.	94
4.25	Quantitative calibration plot of anisole contain internal standard (IS) as analysed by Gas Chromatograph	96
4.26	Effect of SiO ₂ /Al ₂ O ₃ ratios of H-ferrierite on the conversion and selectivity of product.	96
4.27	The reactivity of H-Fer 12 in Friedel-Crafts acylation of anisole with time	98
4.28	The percentage of concentrations for every compound in organic yield	98
4.29	Correlation between the concentrations of anisole and propionic acid with the concentrations of <i>p</i> -methoxypropiophenone	99
4.30	Effect of reaction temperature on the conversion of anisole as substrate with using H-Fer4	100
4.31	The percentage of conversion, selectivity and yield for reaction of anisole with acetic anhydride	102
4.32	Proposed mechanism of electrophile substitution of anisole using H-ferrierite as catalyst	105

LIST OF SYMBOL / ABBREVIATIONS

RHA	-	rice husk ash
FER	-	Ferrierite
Py	-	pyrrolidine
Pn	-	piperidine
Gly	-	glycerol
GC	-	gas chromatography
H-Fer	-	ferrierite zeolite in hydrogen formed
H-Fer-12	-	ferrierite zeolite in hydrogen formed with SiO ₂ /Al ₂ O ₃ ratio 12
Fer-12	-	ferrierite zeolite with SiO ₂ /Al ₂ O ₃ ratio 12
Si-12	-	sample with SiO ₂ /Al ₂ O ₃ ratio 12
N-5	-	sample with Na ₂ O/Al ₂ O ₃ ratio 5
Py-10	-	sample with Py/Al ₂ O ₃ ratio 10
Fer-12-0.25	-	sample Fer-12 with 0.25 day crystallization period
PBU	-	primary building unit
SBU	-	secondary building unit
TBU	-	tertiary building unit
GC	-	gas chromatography
BET	-	Brunauer, Emmett, Teller
FS	-	fume silica
JBW	-	NaJ (Barrer and White)
MTBE	-	methyl tert-butyl ether
JCPDS	-	Joint-Committees on Powder Diffraction Standards

LIST OF APPENDICES

APPENDICES	TITLE	PAGES
A	GC chromatogram for the reaction of propionic anhydride with anisole	123
B	Data obtained from GC-FID Chromatograms (Friedel-Crafts acylation of anisole and propionic acid)	125
C	GC chromatogram for the reaction of acetic anhydride and anisole using H-Fer 12 as catalyst	126
D	List of Publications	127

CHAPTER 1

INTRODUCTION

1.1 General Introduction

According to the Malaysian Budget 2005, Malaysia will focus on research and development activities, which can be divided into four main fields, including the finding of advanced materials. Zeolites that are classified under advanced materials show a higher demand in worldwide market, reaching around USD 2.15 billion per year in 2001 and is expected to increase to \$2.52 billion by 2005 and 2.94 billion by 2010. The utilization of zeolite as catalysts in industrial processes occupies 40 % followed by the oxides, complex oxides and ion-exchange resins [Tanabe *et al.* 1999]. The average utilization worldwide for zeolite in fine chemicals industries is thought to be around 60% of its uses worldwide, either as a parent form or after its modification. Nowadays, zeolites are employed as alternative heterogeneous catalysts to substitute homogenous catalysts in many organic processes such as in Friedel-Crafts reaction because of its more efficient and environmentally-friendly which can eventually reduce plant corrosion and eliminate environmental problems.

The synthetic zeolites give alternative sources for natural zeolites in which it is exists in minor quantity and always in the mixture of other constituents makes natural zeolites unfavorable and uneconomical to be used for specific applications such as catalysts. Ferrierite for example only can be found in three places in the world [Nadimi, 1993]. Based on these, the research in the synthesis of zeolites and other mesoporous materials has been widely explored by researchers all around the world. Studies including the choice of raw materials, optimization of experimental

condition for synthesis and the modifications of zeolites structure are the step to increase the potential of zeolite in order to fulfill the market demand.

1.2 Research Background

The main synthesis component for preparing zeolite is silica besides aluminium, mineralized reagent and water. It is known that the rice husk ash contains silica in which the white ash contains up to 96 % to 99 %. The abundant rice husk ash in Malaysia is giving alternative economical sources for synthesizing zeolites. Several types of zeolites such as zeolite Y [Ramli, 1995], zeolite ZSM-5 [Rawtani *et al.* 1989] and zeolite β [Didik, 2001] have been prepared by using rice husk ash as silica source. The silica was used either directly or by extracting the silica from the ash. The encouraging results from previous works have prompted us to synthesize another type of zeolite namely ferrierite which has great potential as catalysts in organic synthesis as well as in the reduction of nitrous oxides gaseous. In this research, rice husk ash was directly used for the first time in the synthesis of ferrierite.

Synthetic ferrierite is being commercialized either as it is or in the modified form as catalysts in skeletal isomerization of n-alkenes and for reduction of nitrous oxides gaseous. The great potential of ferrierite as catalysts has been widely explored by researchers. Ferrierite with the unique bidimensional pore systems shows the best performance in the isomerization of alkenes for petrochemicals industry compared to other types of catalysts [Yokomori *et al.* 2001]. Recent uses of ferrierite in the form of metal-exchange ferrierite (Ce and Ar) are efficient catalysts for nitrous oxide gaseous reduction. The high selectivity of ferrierite towards NO_x reduction and the capability of Brønsted acid sites which promoted the activation of propene for the pairing with NO or NO_2 , make ferrierite as a good catalyst for NO_x reduction [Seijger *et al.* 2003]. Nowadays, the capability of ferrierite as a hydrocarbon trap in automobile exhaust is still being explored by researchers in order to reduce the hydrocarbon emissions.

The great potential of ferrierite as catalysts whether in petrochemical industry or automobile and environment technology was encouraged in this study to prepare ferrierite in optimum conditions that can reduce the cost of ferrierite production. Usually, in the synthesis of ferrierite using commercial silica as silica sources requires high temperature and long crystallization period with the presence of certain amounts of template to ensure the formation of ferrierite. In this research, the use of rice husk ash as the substitute of commercial silica will lower the overall cost of ferrierite production in term of low cost of raw materials, short crystallization period than commercial silica and the low amount of template used. This study will focus in the optimization of ferrierite in order to find the optimum formulation for synthesizing ferrierite from rice husk ash. In order to cut down the cost of producing ferrierite, the small amount of template or free template system is needed. The template is the main component in the synthesis ferrierite that contributes almost 60% of the cost of zeolite production.

1.3 Objectives of research

The main objective of this research is to explore the capability of rice husk ash as raw material in the synthesis of ferrierite and also to obtain the optimum composition and synthesis conditions for ferrierite. As ferrierite is classified as a medium pore zeolite and having both Lewis and Brønsted acid sites, the potential of ferrierite for Friedel-Crafts acylation was also explored. The objectives of this research are listed as follows:

1. To synthesize ferrierite using rice husk ash as silica source
2. To optimize the metal oxides composition of the initial gel in ferrierite synthesis and the reaction conditions
3. To study the transformation of rice husk ash to ferrierite
4. To test the reactivity of the as-synthesized ferrierite as catalyst in the Friedel-Crafts acylations.

1.4 Scope of the Research

The work reported in this study focuses on the synthesis of ferrierite using amorphous rice husk ash which was obtained by controlled burning of rice husk, as silica sources. Several templates namely pyrrolidine, piperidine and ethylenediamine were used in the synthesis. The templates that gave the best ferrierite were chosen for the optimization study of preparing ferrierite from rice husk ash.

The initial oxides compositions were varied to obtain the ranges of oxides that can produce pure ferrierite. The transformation study of rice husk ash to ferrierite was performed at different crystallization period starting from 0 up to 12 days of crystallization. Characterization of each sample was carried out using Fourier Transform Infrared (FTIR), X-ray Diffractogram (XRD), ^{29}Si Magic Angle Spinning NMR (MAS NMR), Scanning Electron Microscopy (SEM), N_2 (g) adsorption and also the weight of the sample at the end of each crystallization time.

Modification of the as-synthesized ferrierite to the hydrogen form of ferrierite was carried out by ion exchanged with NH_4Cl solution followed by calcinations. The Si/Al ratio in ferrierite framework was measured using ^{29}Si MAS NMR and the acid strength and the type of acid sites were measured using Temperature Programmed Desorption (TPD) of ammonia and Fourier Transform Infrared spectroscopy (FTIR) using pyridine as the probe base molecule.

The final part in this study is to test the catalytic capability of ferrierite in hydrogen form from rice husk ash towards Friedel-craft acylation of anisole with propionic and acetic anhydride as the acylating agents. The reaction was performed in a batch reactor and the products were separated and analyzed by gas chromatography (GC) and the identification of products were carried out using gas chromatography with mass spectrometry detector (GC-MSD).

CHAPTER 2

LITERATURE REVIEW

2.1 Rice husk ash

Rice husk is one of the major agricultural wastes. It is a fibrous material containing cellulose as the major constituent, lignin and ash [Endang, 1995]. The local annual production of rice left behind about 2.4 million tonnes of husk as waste product; usually disposed by combustion. The large amount of silica freely obtained from this source provides an abundant and cheap alternative of silica for many uses such as for the synthesis of zeolites, to generate heat or electric power [Kapur *et al.* 1998] and also to produce metallurgical silicon [Amick, 1982]. Previously, the content of rice husk ash at different combustion temperatures has been studied. The white ash that was obtained from combustion is generally 10-15% of the total dry weight of rice husk. The water content may affect the combustion temperature and the rice husk that has been treated with hot-water and some steam-explosion processes give a lower level of metallic impurities [Mochidzuki *et al.* 2001].

The EC-ASEAN COGEN data indicates that Malaysia produced 2.2 million tonnes of paddy in 1996. Rice manufacturing in Malaysia has increased from 1.2 million tonnes in 1990 to 2.2 million tonnes in 1998 [FAOstat, 1998]. Rice husk is generated at the rice mills. Rice husk ash can be considered as fuel for heat and power generation, provided it comes in regular and sufficient quantities.

The abundant rice husk ash left behind after every harvesting season causes an environmental pollutant. These ashes which are nonbiodegradable are a source of

pollutant in air and water systems. Researches are being carried out to overcome this problem which includes generating valuable products from such waste materials. As such the utilization of these materials will not only reduce the pollution problem caused by the ash but also produced value added products for economic prospective.

As the main component in the rice husk ash is the silica, it can be used as an added component in cement sand bricks and could be seen as a potential low cost building element. Burning the husk into ash under controlled conditions and milling, turns it into a powdery siliceous material that may be used as an aggregate in making bricks and blocks. If the ash is ground further it may have some pozzolanic properties beneficial to the strength of the product. Using rice husk ash in bricks can also lower the weight of each component since the ash has a lower specific weight than sand [Sugita *et al.* 1992].

Another potential uses of rice husk ash is in preparation of useful zeolite and aluminosilicate compounds. As the main constituent of zeolite is silica, rice husk ash that contains 96% to 99% silica can be used as an alternative and more economical silica source for zeolite synthesis. Rice husk ash as silica source has proven to be an active silica material for preparing zeolite Y [Ramli, 1995], zeolite ZSM-5 [Rawtani *et al.*, 1989] and zeolite Beta [Didik, 2001]. These encouraging results have prompted us to synthesize ferrierite, another type of zeolite that has potential industrial application. Ferrierite, in a class of medium pore zeolite with high thermal stability has an advantage compared to zeolite Y and ZSM-5 in the reduction of nitrous oxides gaseous (deNO_x reduction). Furthermore, numerous researches concerning modification of ferrierite to obtain better result for DeNO_x [Seiger *et al.* 2003] and skeletal isomerization of n-alkenes [Oneystak *et al.* 2002] have been done and this proved that ferrierite has a potential economical values. The uses of low cost material such as rice husk ash in producing ferrierite will lower the production cost of the product.

The type of silica phases of the rice husk ash depends on the combustion temperature [James *et al.* 1986]. Amorphous rice husk ash was formed when the rice husk was burnt below 800°C for 10 hours whereas crystalline rice husk ash of the crystalline silica of α -cristobalite and tridymite were formed when the combustion temperature was higher than 800°C [Chen *et al.* 1992].

2.2 Zeolites

Zeolite was first discovered in 1759, by a mineralogist from Sweden, A. F. Cronstedt. The name “zeolites” originates from the Greek words “zeo” means boiling and “lithos” means stone because when gently heated, the stones evolved water vapor [Breck, 1974]. There are 40 types of natural zeolites that have been found and to date, the number of synthetic zeolites has increased more than 150. Nowadays, the research in this area of science is still expanding, resulting to the discovery of synthetic zeolite with new topologies and new catalytic, sorption and separation properties.

The first synthetic zeolite that was synthesized is levinite in 1862 through hydrothermal synthesis. In the mid 1930s, R. M. Barrer attempted to synthesize zeolite in laboratory at elevated temperatures and variable pH rather than those used by nature due to a theory that it will influence the formation of zeolite with much shorter reaction time. In 1948, Barrer [1982] was successfully synthesized zeolite P using aluminosilicate mineral, barium chloride salts and water, which were heated in stainless steel autoclaves for 2 to 6 days in a temperature range of 180-270°C.

By mid-1980s, annual production and sales of natural zeolite was 10000 metric tons meanwhile in 2000 the natural zeolite production has increased up to 41800 metric tons [Robert, 2000] and continuing to increase around 3.8 million metric tons per year in 2001. This is about thirty times the production and sales in 1980 that shows the big growth of zeolite industries especially in fine chemical industries, animal food, waste water treatment, desiccant, water purification and gas

absorbent markets. The prices of natural zeolites is increasing in parallel with their unique properties that depends on zeolite properties and processing. For industrial or agricultural purposes, the price of zeolites was ranged from USD30 to USD 70 per metric ton for granular products down to 40 meshes and from USD 50 to USD 120 per ton for finer ground material. The utilization of zeolite in America around the year 1995 is divided into three main fields; catalysts 60 %, detergent 39 % and adsorbent 1 %, with a total sale of USD 845 million. Based on this increment of the demand of zeolite in industries, the research on zeolite either in exploring new techniques of synthesizing or modification of zeolite has been widely explored [Anonymous, 1996].

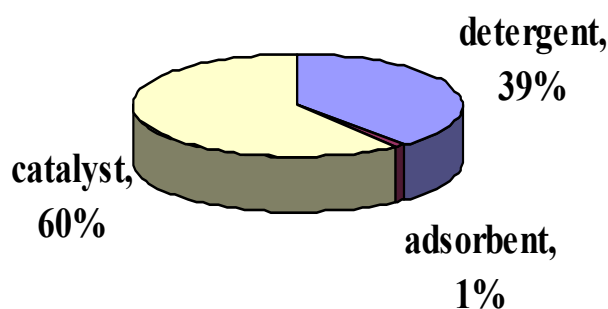


Figure 2.1: Zeolite utilization demand in United State of America on 1995

Following the discovery by Barrer, a lot of techniques to synthesize zeolite were established whereby it was not only to produce zeolites, but also was extended to the uses of the materials for industrial purposes. Zeolite has found their uses in many applications particularly in three main areas; as catalyst, absorbent and ion exchanger. Zeolite A, X and Y are the earlier synthesized zeolites produced commercially. Since 1982, the research has progress towards the synthesis of large pore molecular sieves, known as mesoporous material. MCM-41 is one of the

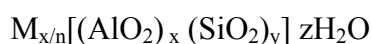
examples of molecular sieve with pore sizes of more than 20Å or in mesoporous range.

Nowadays, zeolites also play an important role in our environmental technologies. The unique properties, characteristics and selectivity of zeolite can provide an effective environmental solution by minimizing the output of pollutant or by secondary treatment of effluent produced. There are several areas in environmental technologies that zeolite shows their strong potential such as in the reduction of nitrous oxides (NO_x) gaseous and the emissions of volatile organic compound (VOC) from automobiles. NO_x is a major provider for acid rain and can also cause the green house phenomenon due to the capability of NO_x to absorb the infrared radiation [Bonnie *et al.* 1999]. Copper or cobalt ZSM-5, mordenite and beta zeolite have been defined as the preferred choices to be used to decompose these NO_x gaseous due to their selectivity, availability and relative cost [Li *et al.* 1992]. Another use of zeolite is in food industries. A new method for fast drying at low temperatures was develop to dry food in order to maintain the quality of product and also to prevent the degradation of the product [Bussmann, 2000]. The affinity of zeolite towards water which is extremely high compared to other adsorbents as well as inert materials makes it a preferred choice to be used in the food drying industries.

The present research trends in zeolite are more concentrated in the modification of the structure for catalytic purposes. Modifications include incorporation of metal oxides and substitution of aluminium in zeolite framework with other metal oxides in order to modify the properties of the zeolites. For an example, the modification of ferrierite with boron was carried out in order to decrease the acid strength but sufficient to catalyze several reaction [Perego *et al.* 2002]. This modified catalysts have a capability to catalyze the double-bond isomerization of linear olefins [Holderich *et al.* 1986], the cracking of MTBE [Taramasso *et al.* 1990] and also in the Beckmann rearrangement of cyclohexanone oxime [Roeseler *et al.* 1997].

2.2.1 Structure and properties

Zeolites are crystalline aluminosilicates with three-dimensional framework, in which the polyhedral sites, usually tetrahedral, are linked by oxygen atoms, comprises of corner-sharing TO_4 tetrahedra ($T=Si, Al$). The crystalline framework contains cages and channels of discrete size in 3-30 Å in diameter. The general formula of zeolite is



where M is an extra-framework cation that balances the anionic charge of the framework, n is the cation valence for M, x and y are the total number of aluminates and silicates per unit cell and z is the number of water molecules per unit cell. The oxygen atoms are the connectors between silicone and aluminium atoms, while the tetrahedral are arranged into the n-membered rings, where $n = 4$ or larger. The total y/x ratio is between 1 to 5 for low Si/Al ratio zeolite but can be as high as 1000 for highly siliceous zeolites. The low Si/Al ratio zeolites have high concentrations of cations. However, according to the Lowenstein law, the minimum Si/Al ratio must be one, in which each aluminium atoms will connect to 4 silicone atoms, such that Al-O-Al bonds are not accepted. The name silicalite has been proposed by Flanigen et al.[1978] for synthetic zeolite ZSM-5 with Si/Al ratio of 4000 which was synthesized by Olson [1980] in order to indicate that it is a silica phase and that the very small alumina content is a nonessential important.

The framework zeolite is constructed from individual tetrahedral unit called TO_4 which refers to as Primary Building Unit (PBU). The topology of all known zeolites framework types can be described in terms of a finite number of specific combinations of tetrahedra called "secondary building units" (SBU's). TO_4 can be combined with various methods to form "Secondary Building Unit" (SBU) [Davis, 1998] (Figure 2.2), where T atom is present at each corner and the oxygen atom is located at the midway between the T. SBUs are linked to each other to form an infinitely extended three-dimensional network forming the zeolite structure [Barrer, 1982]. Description of the framework topology of zeolites involves "tertiary" building

units corresponding to different arrangements of the SBU's in space. Various alternative ways have been proposed. The framework may be considered in terms of large polyhedral building blocks forming characteristic cages as shown in Figure 2.3. For example, sodalite, zeolite A and zeolite Y can all be generated by the truncated octahedron known as the β - cage. An alternative method of describing extended structures uses the two-dimensional sheet building units. Sometimes various kinds of chains can be used as the basis for constructing a molecular sieve framework [Barrer, 1982]

A topological description and classification of zeolite framework types has been proposed by previous researchers [Meier *et al.* 1979] who considered "coordination sequences", representing the numbers of T atoms in the first, second, third, etc. tetrahedral coordination sphere of each topologically non-equivalent T-site. The topology of the framework is then expressed by the sequences of these numbers. The concept of a coordination sequence has proved to be very useful in evaluating the degree of similarity among different zeolite structure types.

Zeolite pores consists of 8, 10, 12 and 14 membered of oxygen ring systems to form tube-like structure and pores that interconnected to each other. Tube-like structure can exists as one, two or three direction with different sizes. Zeolites can be classified based on their pore size; small pore within 5Å, such as zeolite A, carbazite and erionite; medium pore, within 4.5 Å to 6.4 Å, such as ZSM-5, ferrierite and TS-1 and large pore within 6.5 Å – 7 Å, such as faujasite, ZSM-12 and beta [Bekkum *et al.* 1991]. For example, ferrierite with ten membered ring pore openings has similar pore opening to that of ZSM-5 which is the intermediate between shape selective small pore (8-ring) zeolites like zeolite A and surface selective large pore (12-ring) zeolite such as zeolite X [Dessau, 1980].

An excellent example of the role of pore size is in a zeolite-catalyzed process such as in the conversion of methanol to higher hydrocarbons. The presence of extra framework cations is known to strongly affect the properties of zeolites. For example, the addition of silver and cerium to ferrierite, Beta and ZSM-5 were investigated in order to catalyze the decomposition of NO_x into N_2 and O_2 . Cerium

exchanged zeolites with the ferrierite exhibits enhanced conversion of nitrous oxides gaseous reduction [Seijger *et al.* 2003].

Another property of zeolite is possessed acid sites that results from the net negative framework charges. There are two types of acidic sites in zeolite framework that make it as a great heterogenic catalyst: Brønsted acid sites and Lewis acid sites. Brønsted acid sites associated with the protons attached to framework oxygen which is connected to the framework aluminium, meanwhile Lewis acid sites are provided by the non-framework aluminium. The Brønsted acid sites can be created by decomposition of the ammonium-exchange form of zeolite at 400⁰C, hydrolysis of water or by reduction of cations to a lower valency state [Breck, 1974]. Lewis acid sites that are believed to be more active than Brønsted acid sites usually generated with further heating at high temperature. Figure 2.4 shows the Lewis acid sites and Brønsted acid site in zeolite framework.

Zeolites occurred naturally or can chemically synthesize. Synthetic zeolites can be manufactured uniformly with good purity. They are produced under similar conditions with natural zeolites, but in shorter time and at lower temperatures. The reaction composition is the key point of the synthesis to obtain pure zeolites. Natural zeolites are generally formed by the reaction of mineralizing aqueous solutions with solid aluminosilicates at certain temperature and pressure.

Procedures to synthesize zeolites in the laboratory are similar to those of the natural zeolite which requires hydrothermal condition. The type of zeolite formed is determined by synthesis parameters such as alkalinity, temperature, crystallization period and gel ratio of the reactants. The crystallization of zeolites requires alkaline conditions. Alkalinity is related to the total sum of tetrahedron $[\text{Si}(\text{OH})_4]$ concentrations, where the optimum pH is between 11 to 13. The reaction mixture is composed of the various components with the main reactants are silica, alumina, sodium hydroxide and water with the amounts corresponding to the composition of the desired product. It is maintained for a period of time at constant pressure and temperature [Barrer, 1982].

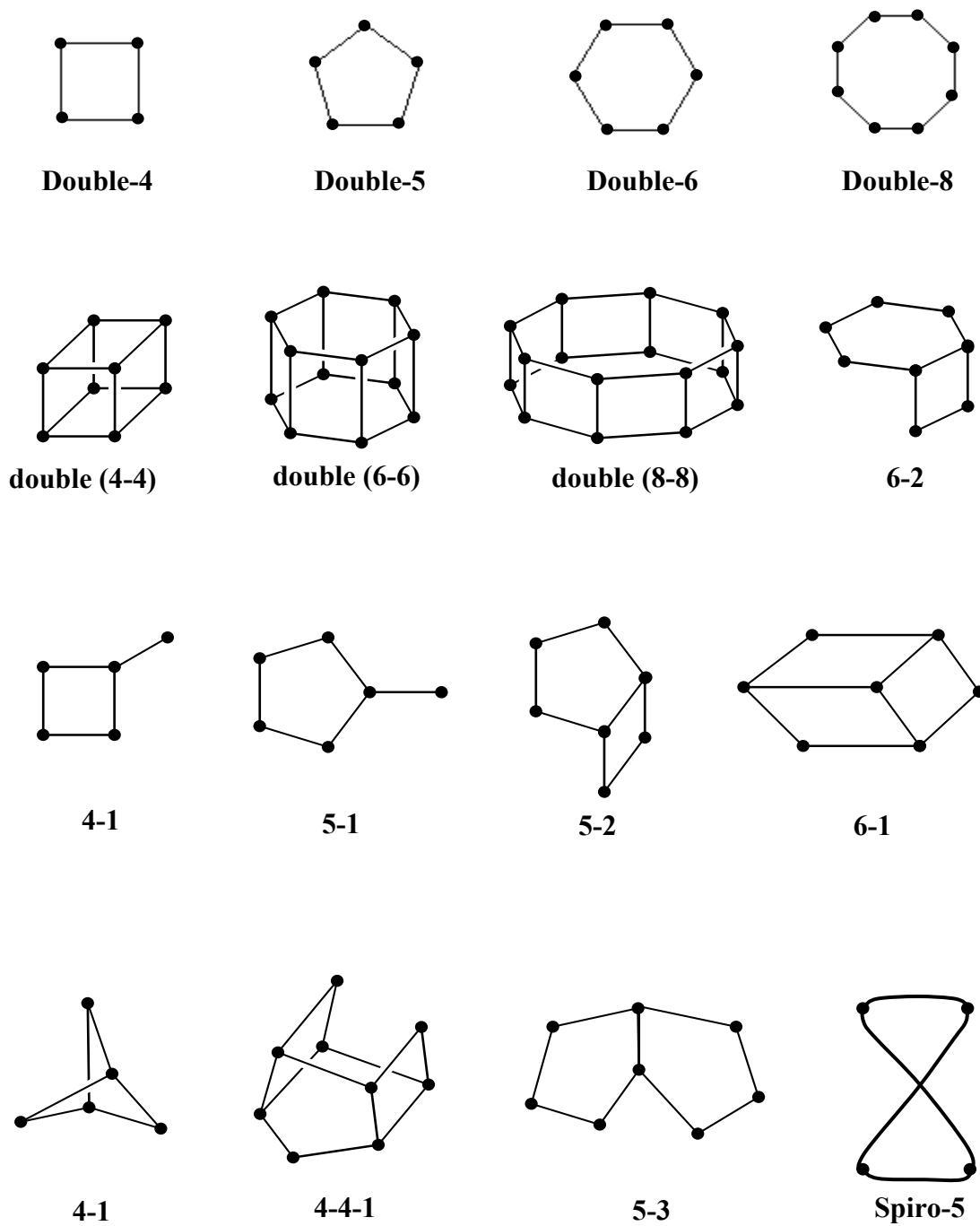


Figure 2.2: The Secondary Building Units (SBU) in zeolite framework. The oxygen atoms between silicons and aluminiums are omitted for simplicity
 ● = Si / Al

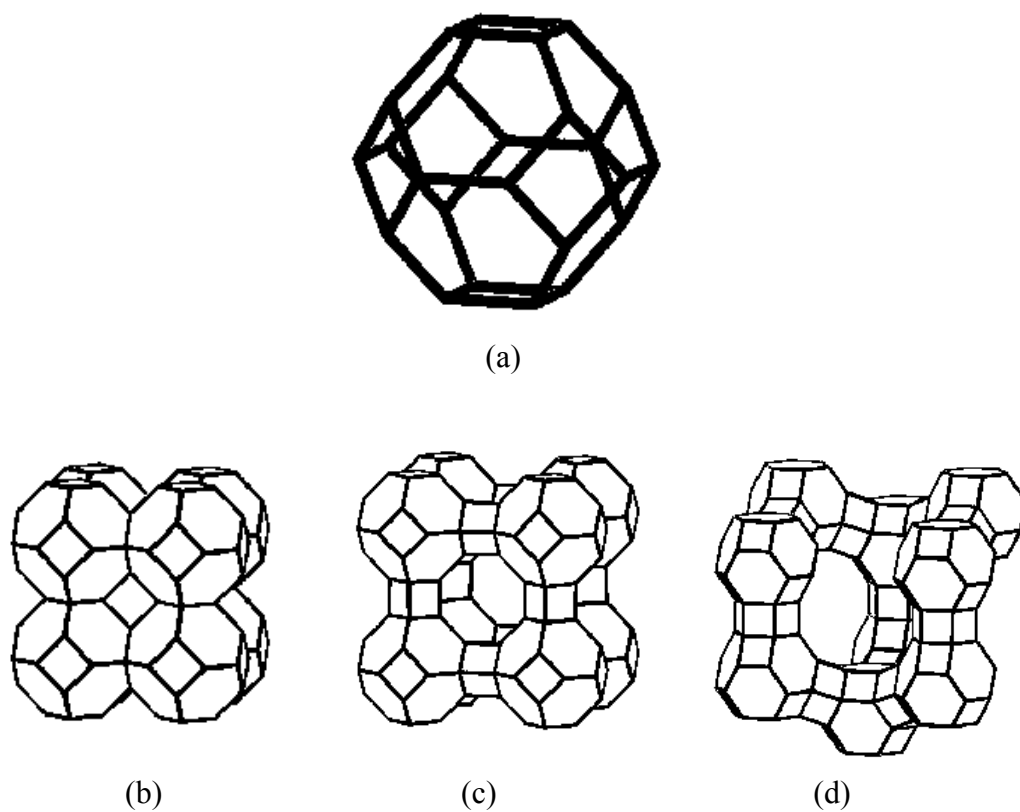


Figure 2.3: Framework lattices: (a) α , (b) Zeolite A, (c) Y and (d) Faujasite

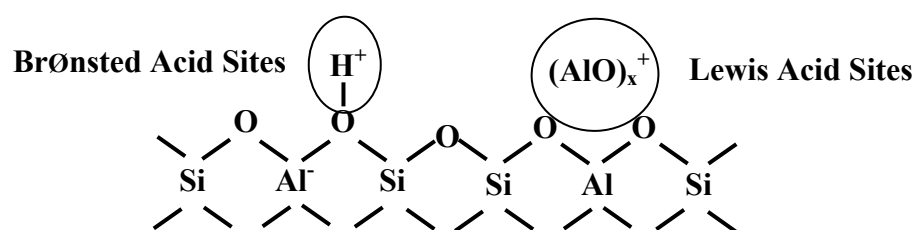


Figure 2.4: Brønsted and Lewis acid sites in zeolite framework

2.2.2 Synthesis of zeolite

The reaction mixture for the preparation of zeolite is monitored by its gel chemistry. In zeolite synthesis, the usual sources of aluminium are aluminium hydroxide or sodium aluminate. For certain purpose aluminium isopropoxide is used. Amorphous silica, sodium silicate, sodium metasilicate, silica glass, silicic acid and various concentrations of silica sol are the common silica sources. Besides the commercially available silica, the uses of high silica content of low cost and waste materials as the silica sources are desirable. Rice husk ash and fly ash were already known as a silica sources for synthesizing zeolites type Y, mordenite, ZSM-5 and beta. Many types of organic template are regularly used to synthesize zeolite with high silica content. Pyrrolidine and piperidine are commonly used in the synthesis of ferrierite. The template functioned as the structure directing agent either in organic or inorganic compound will be the cations neutralized for the anionic framework charge. One example to understand the role of template organic can be found in the synthesis of siliceous zeolites. By increasing the chain length of the amine that used as organic template, three different structures of zeolite were formed, ZSM-35, ZSM-5 and ZSM-11. The short chain of template ($C_2 - C_4$) preferred ZSM-35 framework, the medium chain ($C_5 - C_6$) generates ZSM-5 and the long chain ($C_7 - C_{10}$) produced ZSM-11 [Meisel *et al.*, 1967].

There are four main factors influencing zeolite crystallization, the gross composition, time of crystallization, temperature and also the history depending factor. All components in initials reaction mixture play their own role in influencing the crystallization of zeolite. The type of silica phase will determine the rate of solubility of the silica. The rate of solubility decreases from amorphous silica to crystalline silica (consist tridymite, cristobalite and quartz) [Barrer, 1982].

Another factor to zeolite crystallization is the concentration of hydroxyl ion. The high concentration of hydroxyl ion will increase the alkalinity of the solution and the crystalline phase obtained might differ from the lower concentration of hydroxyl. Alkaline solution will facilitate the solubility of silica which in turns increases the crystallization rate. At higher silicate ratio (SiO_2/Na_2O), it will produce

unstable solution due to the lack of charge compensation. This gradually results the formation of colloidal particles of silica instead of polymeric silicate anion which facilitate the production of zeolite [Scott, 1996]. For an example, at a fixed $\text{SiO}_2/\text{Al}_2\text{O}_3$ ratio and at a constant time of crystallization, increase of hydroxyl ion favors the formation of mordenite over ZSM-5 [Dutta *et al.* 1994].

The crystallization period of zeolite formation decreases rapidly with increasing temperature. At the same temperature, different phase of zeolite will be formed depending on the crystallization period. For example, the formation of zeolite A from meta koalin obtained in the first hour of reaction followed by the transformation of zeolite A to JBW type of zeolite. The work reported by Lin *et al.* [2004] shows that the JBW type of zeolite is relatively stable than zeolite A in the medium with high basicity which make the JBW as a dominant phase. According to Szostak [1989], the transformation of zeolite phase is due to the existence of metastable phase with respect to another.

Crystallization of zeolite involves three basic steps. First is the reaching of supersaturation, second is the formation of nucleus and finally the growth of crystal. Saturation solution can be defined as when the solution is in equilibrium with solid and supersaturation solution achieve when the solution contains more dissolved solid than at its saturation state. There are two categories of supersaturated solution: labile (unstable) and metastable. Labile supersaturated solution makes spontaneously deposition of the solid phase possible even in the absence of the solid nuclei, meanwhile the metastable supersaturated avoided the deposition of solid phase.

After supersaturation was achieved, the nucleation take placed. Before crystallization can occur, a number of nucleuses must exist in solution. Nucleation may occur spontaneously from solution or it may be formed by impurities or contaminants in the reactor walls. The formation of nucleus occurs step-by-step leading to the formation of short chains, flat monolayers and eventually the crystalline nucleus. As soon as stable nucleus has formed in a supersaturated solution, the process of crystal growth starts to occur. In the diffusion theory of crystal growth, the crystallization is the reverse of dissolution and the rate of

crystallization and diffusion is governed by the difference between the concentrations of the precursor species at the surface of the solid and in the bulk. Process of solid deposition on the crystal surface may occur in two different steps. One is when the solute molecules are transported from the bulk of the liquid phase to the solid surface which is called diffusion process. The second step involves the arrangement of solute molecules into the crystal lattice. The diffusion process is usually followed by the ordering and rearrangement of the precursor species on the growing crystal face. This ordering and rearrangement will reduce the crystallization rate and at the same time it will dissolve the crystal faster than the growth.

Two theories have been proposed to account for the mechanism of zeolite synthesis. In the solid-solid transformation mechanism, crystallization of the zeolite occurs directly from the amorphous gel to the crystalline phase [Zhdanov, 1971]. In the solution crystallization mechanism, nuclei form and grow in the liquid phase [Kerr, 1966]. The latter proposes that equilibrium exists between the solid-gel phase and the solution, and that nucleation occurs in the solution. The gel dissolves continuously, and the dissolved species are transported to the nuclei crystals in the solution. In addition to zeolite formation via either of the two transformations, there is evidence to indicate that both types of transformation can sometimes occur simultaneously. In some cases zeolites can also be crystallized from a single-solution system containing no secondary solid-gel phase [Ueda, 1979]. From the single-phase solution studies, it appears that nucleation and subsequent crystallization can occur readily in the solution phase, leading to the possibility that the presence of a solid-gel phase acts only to supply nutrients to the solution.

2.3 Ferrierite

2.3.1 Structure of Ferrierite

Natural ferrierite can only be found in three places; at Kamploops Lake, Canada; Gotaloves, Yugoslavia; and Chernichino, Bulgaria. Due to the difficulty in finding ferrierite in other places has lead to scientific research on finding an alternative way to get ferrierite i.e. by synthesis. Synthetic ferrierite was first obtained by Barrer and Marshall in 1964 [Barrer, 1982]. The types of silicon sources and organic templates are the important reactants in the synthesis of ferrierite because both reactants will influence the development of the ferrierite structure.

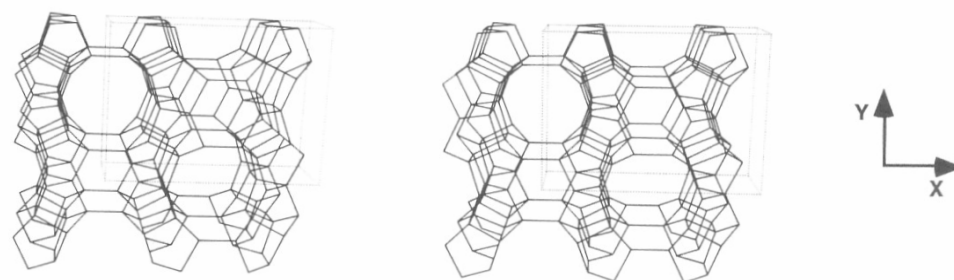
Ferrierite is a naturally-occurring silica-rich zeolite and was first discovered by W. F. Ferrier. The structural formula of ferrierite is $\text{Na}_5[\text{Al}_5\text{Si}_{31}\text{O}_{72}] w\text{H}_2\text{O}$ where w is equal to 18. The framework composition of natural ferrierite ranges from $(\text{Al}_{7.5}\text{Si}_{27.5}\text{O}_{72})$ to $(\text{Al}_5\text{Si}_{31}\text{O}_{72})$, which corresponds to a Si/Al ratio range of 3.2 to 6.2. Ferrierite structure is most closely resemble to mordenite and dachiarite [Breck, 1974]. The ferrierite structure type has an orthorhombic symmetry with unit cell values of $a = 19.2$, $b = 14.1$, $c = 7.5\text{\AA}$, $V = 2030\text{\AA}^3$ and $d = 1.996\text{ gcm}^{-3}$ and belongs to space group $Immm$. The unit cell contains 36 T-atoms, where T is Si or Al. A monoclinic variety of natural ferrierite with the space group $P2_1/n$ has also been found. The lower symmetry is mainly caused by deviation from T-O-T angle of 180° .

Ferrierite framework is based on 5-1 units SBU that are linked to form the ferrierite structure. Stacking of layers is an equally fruitful way of generating zeolite structures. Each layer is linked by Si – O – T (T = Al or Si) bonds parallel to the layer above and to those layers below. For ferrierite, the layer is puckered in various ways and cross-linked to identical layers above and below.

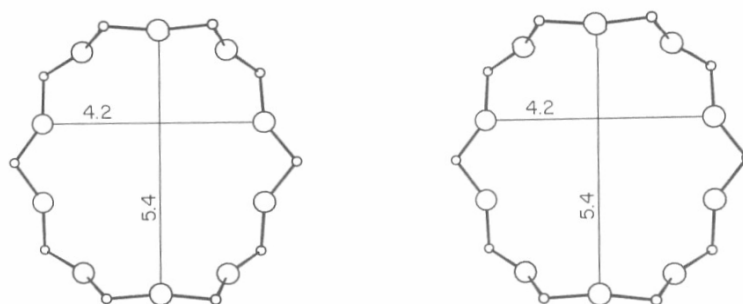
The ferrierite framework is based on chains of 5-rings, which are linked to give polyhedral units. There are two types of intersecting channels in the structure. The main channels are parallel to the orthorhombic c-axis of the crystal and are

outlined by elliptical 10-rings (4.3 x 5.5 Å in diameter), while the side channels parallel to the b-axis are formed by 8-rings (3.4 x 4.8 Å in diameter) as shown in Figure 2.5.

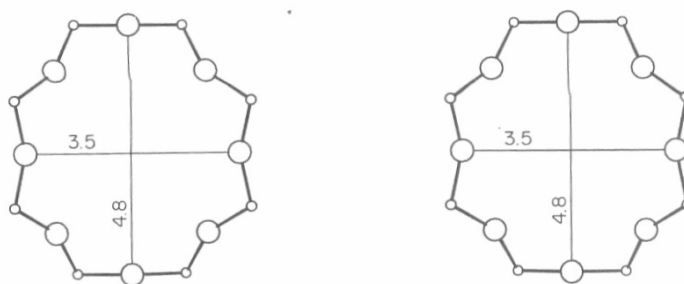
Ferrierite, a zeolite structurally related to mordenite and epistilbite, exhibits high ion exchange selectivity for magnesium and appears in nature preferentially in this cation form with Si/Al ratios between 3.5 to 5.5. Ferrierite formed in two types; monoclinic and orthorhombic. The ferrierite framework contains two systems of mutually perpendicular one-dimensional channels of 10- and 8- membered rings. The crystal structure of natural Mg-rich ferrierite was solved in the orthorhombic *Immm* space group. Mg-rich ferrierite is characterized by the presence of $\text{Mg}(\text{H}_2\text{O})_6^{2+}$ octahedron at the center of the so-called ferrierite-cage. A monoclinic symmetry, with the space group *P2₁/n*, was reported for natural Mg-poor, sodium and potassium-rich ferrierite.



framework viewed along [001]



10-ring viewed along [001]



8-ring viewed along [010]

Figure 2.5: Framework structure of zeolite ferrierite [Meier *et al.* 1992]

2.3.2 Synthesis of ferrierite

Ferrierite mineral has Si/Al ratio in the range of 4-7 and is considered one of the siliceous naturally occurring zeolites. They can be synthesized using inorganic or organic bases. Ferrierite can also be prepared in its siliceous form by both aqueous and nonaqueous routes. Some synthesis methods, depending on the initial reactant composition give pure ZSM-5 or ferrierite or mixtures of ZSM-5 and ferrierite [Meier *et al.* 1992]. There are many organic templates that have been used to synthesize ferrierite. The templates mostly are organic base including trimethylcetylsammonium hydroxide, glycerol [Sanyuang *et al.* 1997], diethanolamine [Neils *et al.*, 1995] pyrrolidine and piperidine [Tae *et al.*, 1996] at temperature around 150°C to 200°C. Even the aluminium-free end member of ferrierite has been synthesized [Gabriella *et al.*, 1998].

Recently Khomane *et al.* used nonionic surfactant as organic template to produce ferrierite such as poly(oxyethelene)sorbitan monolaurate [2001]. In all cases the small amount of pyrrolidine is still necessary. The results show that in the absence of pyrrolidine, ferrierite was co crystallized with ZSM-5, whereas in the absence of nonionic surfactant, the yield and crystallization of ferrierite is very poor. Ferrierite can also be prepared through non-aqueous route from dried aluminosilicates gels using triethylamine and in ethanol with piperidine or mixture of ethylenediamine and dibutylamine as templates [Kibby *et al.*, 1974].

Another novel method of synthesizing ferrierite is to crystallize ferrierite in the absence of liquid phase in the reaction mixture. ZSM-5 [Matsukata *et al.* 1996] and ferrierite [Sanyuang *et al.* 1997] have been prepared from amorphous alkaline silica or alumina by treating the dried gel at higher temperatures (about 200°C) in an atmosphere of steam and gaseous ethylenediamine and triethylamine. Another research that has been carried out was dealing with the dry-state recrystallization of megadiite containing tetrahedrally coordinated framework aluminium to high-silica ferrierite [Gabriella *et al.*, 1998].

A number of studies concerning the preparation of ferrierite through hydrothermal synthesis used silica sol as silica source. However, dry synthesis of

ferrierite technique has been carried out using aluminium-containing kenemite and aluminium-containing hydrated megadiite as starting materials. This technique is definitely different compared to hydrothermal synthesis, in which the conversion of starting materials into ferrierite was brought about simply by heating air-dry crystalline kanemite samples, intercalated with piperidine, in sealed vessels [Gabiella *et al.* 2000].

2.3.3 Application of Ferrierite

Ferrierite is a zeolite with a bidimensional pore structure, consisting of 10-membered rings (42 nm x 54 nm) channel intersected by 8-membered rings (35 nm x 48 nm) channel. The bidimensional pore structure of ferrierite was considered responsible for the high isobutene selectivity of the material, although it is reached after some time-on-stream (TOS) when a carbonaceous deposit is formed and suppresses undesirable side reactions. The acid sites distribution in ferrierite shows the weak and strong acid strength, respectively [Yokomori *et al.* 2001]. The high activity at short TOS is related to the strong acid sites. The external acid sites are non-shape selective for isomerization and are responsible for the side reactions, while the internal acid sites are selective for skeletal isomerization [Xu *et al.* 1995]. Both catalytic activity and isobutene selectivity have also been related to the density of acid sites and to the space around them. The special characteristics of ferrierite made it a good catalyst in skeletal isomerization.

Skeletal isomerization of *n*-alkenes is an important reaction to upgrade refinery and petrochemical feed streams. The isomerization of *n*- to *iso*-butene was the subject of many investigations due to it uses as starting material for the production of methyl-*tert*-butyl-ether (MTBE). MTBE is the most frequently used as additive to gasoline for boosting the octane number. Besides ether production, *iso*-butene is needed for alkylation in order to produce high-octane gasoline. Due to the importance of *iso*-butene, a lot of study have been done to find the best catalyst for skeletal isomerization of *n*-butene. Maurer and Kraushaar studied this reaction by using ZSM-5 as a catalyst, but encounter some problems. At low temperature, they

have found that only double bond isomerization was observed, whereas at high temperature the *n*-butene and *iso*-butene were reacted further to form by-products [Maurer *et al.* 1999]. This problem can be solved only when ferrierite was used as a catalyst.

Another potential application of ferrierite as a catalyst is in the reduction of nitrous oxides gaseous from automobile [Sobalik *et al.* 2000]. Ferrierite have been modified using cerium, silver, boron, cobalt (Co) or copper in order to increase the catalytic activity towards the processes. For an example, by increasing the amount of Co loading in ferrierite, it will increase the turnover of NO_x to nitrogen gas [Li *et al.* 1994]. As comparison between ferrierite, ZSM-5 and zeolite Beta, it shows that ferrierite exchange with cerium realizes the highest NO_x conversion even in higher temperature due to the high thermal stability of ferrierite [Seijger *et al.* 2003].

2.4 Friedel-Crafts Acylation

Aromatic acylation is important technique in producing aromatic ketones that was used in various areas in fine chemical and pharmaceutical industries. Zeolites and clays families are currently being widely studied for their application as a heterogeneous catalyst in the synthesis of aromatic ketone. The key opportunity for the use of zeolites as catalysts relies on their unique pores, which can control the selectivity of the products. The current use of conventional Lewis acid catalysts such as aluminium chloride implies a number of problems related to the fact that greater than stoichiometric amount of the catalyst is needed [Olah, 1964]. This is due to the formation of a complex between the product and the catalyst following the hydrolysis of which leads to the loss of the catalyst and the environmental consequences of its disposal. In industry, the uses of over-stoichiometric amount of metal halides as catalysts and acyl chlorides, results in substantial amount of by-products and also the corrosion problems cause by H₂SO₄ co-catalyzed.

To encounter the problems, attention to the alternative heterogeneous catalyst has increased due to the high selectivity of yield, good in separation and the recyclable of the catalyst. Zeolite as catalyst in Friedel-Crafts acylation was widely employed and the earliest results were published by previous researchers who studied the reaction of toluene and *p*-xylene with straight chain carboxylic acids catalysed by Ce-Na-Y zeolites in liquid phase [Chiche *et al.*, 1986]. Zeolite was used as heterogeneous catalysts due to their unique properties of acidity and framework structure. Pore size of zeolite also plays an important role in aromatic acylation in order to produce the desired products. Large pore zeolite such as zeolite Y, mordenite, Beta and medium pore zeolite like ZSM-5 was used either in hydrogen form or with metal substituted as catalysts in Friedel-Crafts acylation. Generally, large pore zeolite will give higher yield as compared to the medium pore zeolite which gives high in selectivity instead.

A lot of study has been carried out in order to study the effectiveness of zeolite catalysts in Friedel-Crafts acylation. Freese *et al.*, [1999] reported the catalytic activity of different zeolites on catalyzed Friedel-Crafts acylation of anisole with acetic anhydride. H-ZSM-5 which is a medium pore zeolites results only 14% of conversion due to the small pore size of ZSM-5 (10-ring) for penetration of the aromatic compound, or the intersections of the channels limit the formation of the transition state. However, for H-Beta with 12-ring pores was found to be the best catalyst with higher conversion and selectivity of *p*-methoxyacetophenone. Gaare *et al.* [1996] reported that modified zeolites were found to be active catalysts in the Friedel-Crafts acylation. Lanthanum modified zeolite was used as a catalysts and it was shown that the yield of the product increased with the increasing of lanthanum content in the framework. The methods of catalysts treatment also influence the selectivity of product which has been proposed by Casagrande *et al.* (2000). By increasing the temperature treatment, the selectivity towards desired product increased due to the extra framework aluminum deposition on the channel walls that reduces the mobility of the more bulky molecules in their inside.

Until today, the study concerning the capability of ferrierite as a catalyst in Friedel-Crafts acylation has not been reported. The bidimensional pore structure of

ferrierite and the distribution of acid strength of ferrierite have encouraged us to investigate its potential use as a catalyst for Friedel-Crafts acylation. Since ferrierite is medium pore zeolites, it is expected to give higher selectivity of the products obtained of the Friedel-Crafts acylation compared to other large pore zeolites.

Figure 2.6 illustrates the reaction of anisole and acid anhydride to produce *p*-methoxyacylphenone. The acid anhydride will generate a strong electrophile (RO^+) to further react with π electron from anisole benzene ring. Acid will produce as a side product.

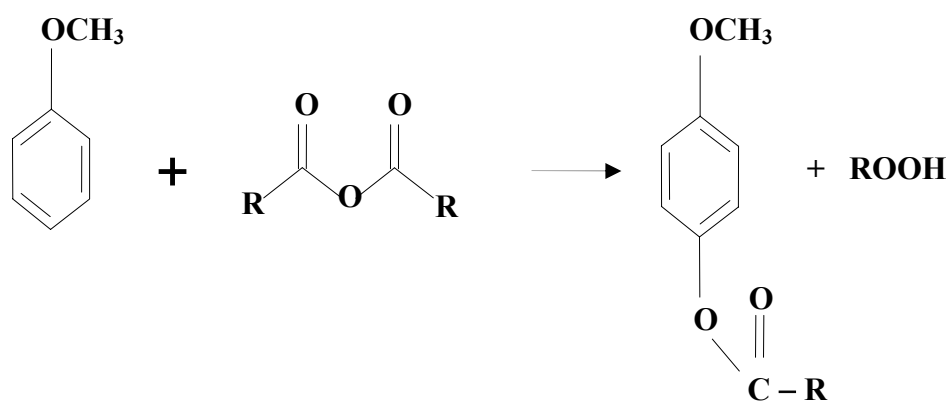


Figure 2.6: Friedel-Crafts acylation between anisole and acid anhydride

2.5 Characterization Techniques

Characterization was carried out in order to study the physical and chemical properties of the samples that were obtained from the experiments. Each sample was characterized using four main techniques which are X-ray Powder Diffraction (XRD), Fourier Transform Infrared (FTIR), ^{29}Si Magic Angle Spinning Nuclear Magnetic Resonance (^{29}Si MAS NMR) and nitrogen adsorption. Other techniques are Scanning Electron Micrograph (SEM), pyridine adsorption, Temperature Programmed Desorption Ammonia (TPD NH_3) and gas chromatography (GC).

2.5.1 X-ray Powder Diffraction (XRD)

X-ray Powder Diffraction technique is the best method to define the crystallographic structure of zeolite. Each zeolite has their own specific pattern that can be used as references for the determination of solid crystal phase and it is used as fingerprint for every zeolite. This technique can signify whether the solid sample is amorphous or crystalline phase, the degree of crystallinity and identification of phase present. The purity of solid crystal will be measured by comparing the X-ray diffractogram pattern of sample with X-ray diffractogram pattern of standard that can be obtained from International Zeolite Association (IZA). The presence or absence of some peaks of the diffractogram indicates to the existence of other crystal phase or zeolite was contaminated with other phases. The size and shape of unit cell for any crystal are easily determined by using the diffraction of the X-rays.

Bragg quoted that X-ray diffraction occurs when the beam is reflected by a set of planes. The diffraction pattern is plotted based on the intensity of the reflected beams, represents as a map of reciprocal lattice parameter of Miller indices (hkl) as a function of 2θ where θ is the diffraction angle which satisfies the Bragg's condition,

$$n\lambda = 2d \sin \theta \quad (2.1)$$

where d is the interplanar spacing and λ is the wavelength of the beam. The reflection diagram is shown in Figure 2.7 [West, 1988].

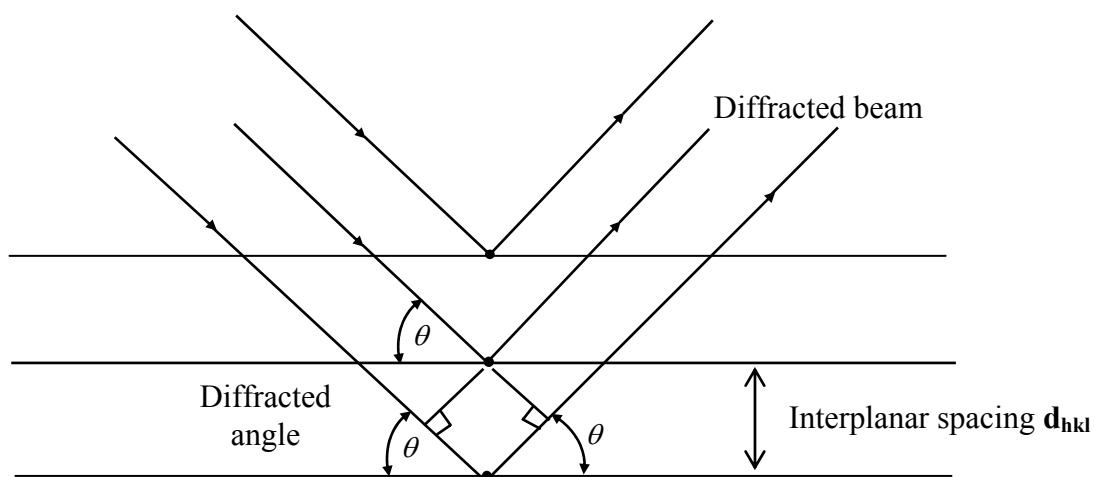


Figure 2.7: Schematic representation of diffracted beams in crystal lattice

The crystallinity of zeolite can be measured by comparing the intensity of the reflected beam with a standard pattern for each zeolite. For each differences in intensity between the sample and the standard XRD pattern shows a decreasing in the degree of crystallinity. Amorphous phases will produce no diffraction line at all and small particles will produce broad diffraction lines, whereas a crystalline particle gives a sharp and strong diffraction lines.

2.5.2 Infrared Spectroscopy

Infrared spectroscopy is commonly used to study the silica aluminate framework, hydroxyl group and also adsorbed molecules in zeolite. Zeolite infrared

vibration can be divided into two forms of vibration, the internal vibration and external vibration. The internal vibrations occur from the vibration of the TO_4 tetrahedral, which is insensitive to the structure changes and present in each zeolite framework and silica. This vibration includes the T-O asymmetric stretch at $1250 - 1000 \text{ cm}^{-1}$, T-O symmetric stretch at $750 - 650 \text{ cm}^{-1}$ and T-O bends at $500 - 400 \text{ cm}^{-1}$. T-O stretching is sensitive towards the composition of Al and Si in framework. The shifting of these stretching to higher wavenumber occurs when the aluminium contents in the framework decrease. The increase of wavenumber with the decreased in aluminium content is related to change of bond length and bond orders. The longer length of Al-O bond and the decrease in the electronegativity of Al, results to the decrease of the forces constant and hence the wavenumber [Flanigen *et al.*, 1971].

External vibrations on the other hand are assigned for vibration by linkage of TO_4 tetrahedral. It can be observed at $1050 - 1150 \text{ cm}^{-1}$ that assigned to asymmetric stretch for T-O and at $820 - 750 \text{ cm}^{-1}$ for symmetric stretch for T-O. Zeolites that have double ring in the framework will give a strong absorption band at $650-500 \text{ cm}^{-1}$. Usually, the adsorption band at 550 cm^{-1} will form in the presence of 5-membered rings in zeolite framework which can be formed in ZSM-5. Ferrierite structure contains only 5-3 block and usually exists at 563 cm^{-1} [Szoastak, 1989]. For zeolite contains no 5- membered ring such as epistilbite, a shoulder at 1175 cm^{-1} was observed corresponded to the presence of a pseudo-5-member ring chain. Finally, T-O bending for tetrahedron that formed large pore opening was observed at $420 - 300 \text{ cm}^{-1}$.

IR spectroscopy also can be used to determine the hydroxyl group in zeolite. In air, OH group will interact with water vapor and give a broad band around $3700 - 3400 \text{ cm}^{-1}$. For determination of OH group, zeolite was heated at high temperature under vacuum to remove water that was trapped in zeolite framework. There are three types of hydroxyl groups that give absorbance at different wavenumbers. Hydroxyl terminal of the silanol group (Si-OH) will shows an absorbance at 3742 cm^{-1} , hydroxyl terminal for Al-OH at 3641 cm^{-1} and vibration for bridging OH groups at 3604 cm^{-1} . For acidity measurement of zeolite, probe base pyridine is adsorbed into the zeolite. Pyridine will interact with acid sites in zeolite and give a

vibration at 1545 cm^{-1} and 1454 cm^{-1} , both assigned for Bronsted acid sites and Lewis acid sites.

2.5.3 Magic Angle Spinning Nuclear Magnetic Resonance

NMR spectroscopy is a powerful tool to determine the structure and dynamics of molecular sieves such as zeolites. NMR is used to measure atomic ordering in framework structure and quantitative measurement of certain site. NMR spectroscopy for solids cannot be managed in the same way as liquid or solution. In solids, the position of nuclei is fixed in the solid lattice instead of solution that the molecules tumbling are averaged and produce high resolution spectra. The random distribution of atomic ordering in solid give a broadline spectrum that may conceals some of the information of the solid structure. Magic Angle Spinning (MAS) technique was employed to reduce the spectrum broad line using a rotation of sample at an angle of $54^{\circ} 44'$ which is known as the magic angle. These techniques reduce dipolar interaction and chemical shift anisotropy which give rise to line broadening.

^{29}Si MAS NMR technique was used to determine the distribution of silicon and aluminium in zeolite framework. ^{29}Si MAS NMR spectrum may consist one or five possibilities signal that corresponding to five possible silicon environments in the zeolite framework. Silicon in zeolite framework can be classified into five environments depending on the total silicon and aluminium that coordinated to tetrahedral SiO_4 i.e. Si(0Al) represents $\text{Si}(\text{OSi})_4$, Si(1Al) represents $\text{Si}(\text{OSi}_3)(\text{OAl})$, Si(2Al) represents $\text{Si}(\text{OSi})_2(\text{OAl})_2$, Si(3Al) represents $\text{Si}(\text{OSi})(\text{OAl})_3$ and Si(4Al) represents for $\text{Si}(\text{OAl})_4$. With increasing number of aluminium atom in silicon tetrahedron, the signal shifted to low field where each added Al atom will contribute to 5 ppm shifting [Engelhardt *et al.* 1987].

The intensity of peak in ^{29}Si MAS NMR is proportional to the number of Si units. The quantitative ratio of silica to alumina in zeolite framework can be calculated from five peak intensities according to the following equation:

$$\text{Si / Al} = \frac{I_4 + I_3 + I_2 + I_1 + I_0}{I_4 + \frac{3}{4} I_3 + \frac{1}{2} I_2 + \frac{1}{4} I_1} \quad (2.2)$$

where I is the peak intensity of the NMR signal referred to $\text{Si}(n\text{Al})$ units, and n indicates the number of coordinated Al atoms in the first coordinated SiO_2 sphere for the given peak.

Figure 2.8 shows the ranges of ^{29}Si chemical shift for each of the five Q^n units in solid silicates. The substitution of one or more Si atoms by Al atoms in coordination sphere results in significant low-field shift, i.e. give less negative δ value.

In general, ^{29}Al NMR spectra of zeolite are relatively simple compare to ^{29}Si NMR since only one tetrahedral aluminium $\text{Al}(\text{OSi})_4$ exists in the zeolite framework. Systematic investigation of ^{27}Al NMR chemical shifts determines that the chemical shifts in the aluminium NMR spectrum depend primarily on the coordination of aluminium with respect to oxygen. ^{27}Al NMR permits the detection of tetrahedral aluminium in the framework of high silica zeolites which are not seen in the ^{29}Si NMR. For tetrahedral coordination, chemical shifts of 55 to 80 ppm from $\text{Al}(\text{H}_2\text{O})_6^{3+}$ were observed. Octahedral Al appears at 0 to 22 ppm. Both solid and solution spectra show similar ranges of chemical shift.

2.5.4 N_2 adsorption

When a gas molecule of adsorbate, such as nitrogen approaches a solid surface of porous material, at certain temperature, the molecule is acted on initially

by attractive force that called adsorption. Adsorption will provide the information of pore volume and the structure of materials which are the important properties in zeolite catalysts. The technique that used to measure these properties is the nitrogen adsorption measurement. A total volume of gaseous that adsorbed and desorbed depends on absolute temperature (T), pressure (P) of the vapors, surface area (Å), pore volume and solid-gas system. When total volume of gas adsorb, V_a was plotted as a function of P/P_o , results the adsorption isotherm which is shown in Figure 2.10

There are five types of adsorption isotherm which are shown in Figure 2.10 which was classified by Brunauer, Emmet and Teller (BET). Type I is characteristic of microporous materials like zeolite. Typical type I isotherm always show high adsorption capacity and very fast reaction saturation, followed by consistent adsorption over a wide range of P/P_o . Nonporous materials exhibit the adsorption isotherm Type II and type III for macroporous materials. Adsorption isotherm for nonporous materials show high adsorption capacity at low relative pressure (P/P_o), moderate adsorption capacity at the middle and high adsorption capacity at P/P_o in close proximity to 1. The most striking feature of the Type IV isotherm are the hysteresis loop and the plateau at high P/P_o . Isotherms of this type are typical of mesoporous adsorbents such as silica gels and M41S family. Type V isotherm shows a low adsorption of nitrogen at low relative pressure. These explain that the interaction between adsorbent and materials is weak. The rare type VI step-like isotherm is shown by nitrogen adsorbed on special carbon [Sing *et al.* 1985].

$$\text{BET equation: } q = \frac{q_m K_b C}{[C_a - C] \{1 + [K_b - 1][C/C_a]\}} \quad (2.3)$$

Where C_a = concentration at which all layer are filled

K_b = a coefficient

α_s method was employed when the capillary condensation occurred towards the adsorbent used. This method was employed by the comparison between the sample and reference (Aerosil 300). The volume of nitrogen adsorbed versus the α_s was

plotted and the α_s plot will determined the type of pore in sample. Figure 2.11 shows the α_s plot that identical with adsorption isotherm. The α_s value can be determined using the following equation:

$$\alpha_s = \frac{n}{n_{0.4}} \quad (2.4)$$

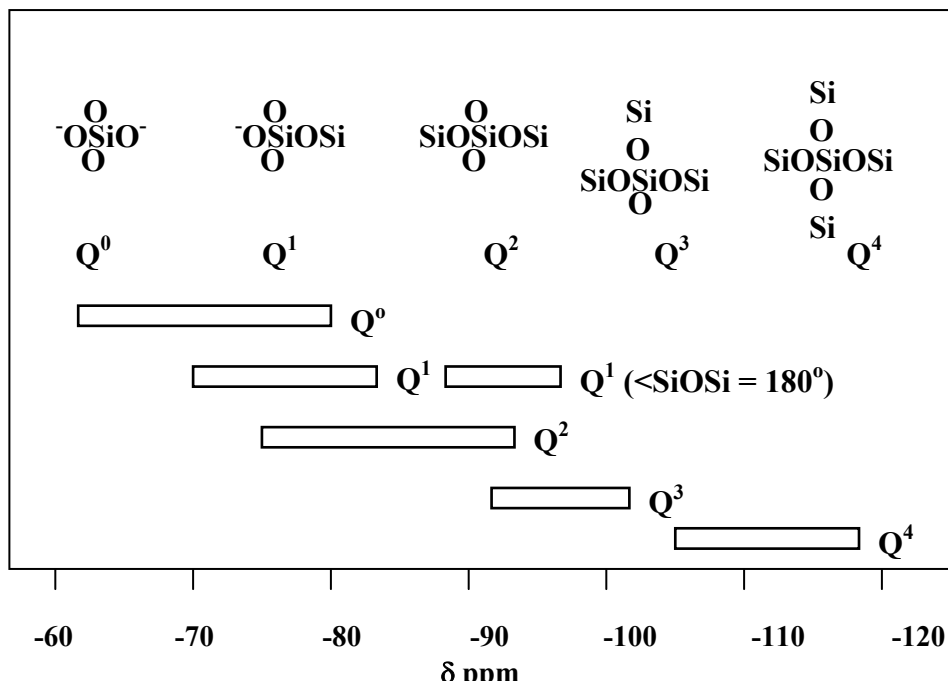


Figure 2.8: Range of ^{29}Si chemical shifts of Q^n in solid silicate

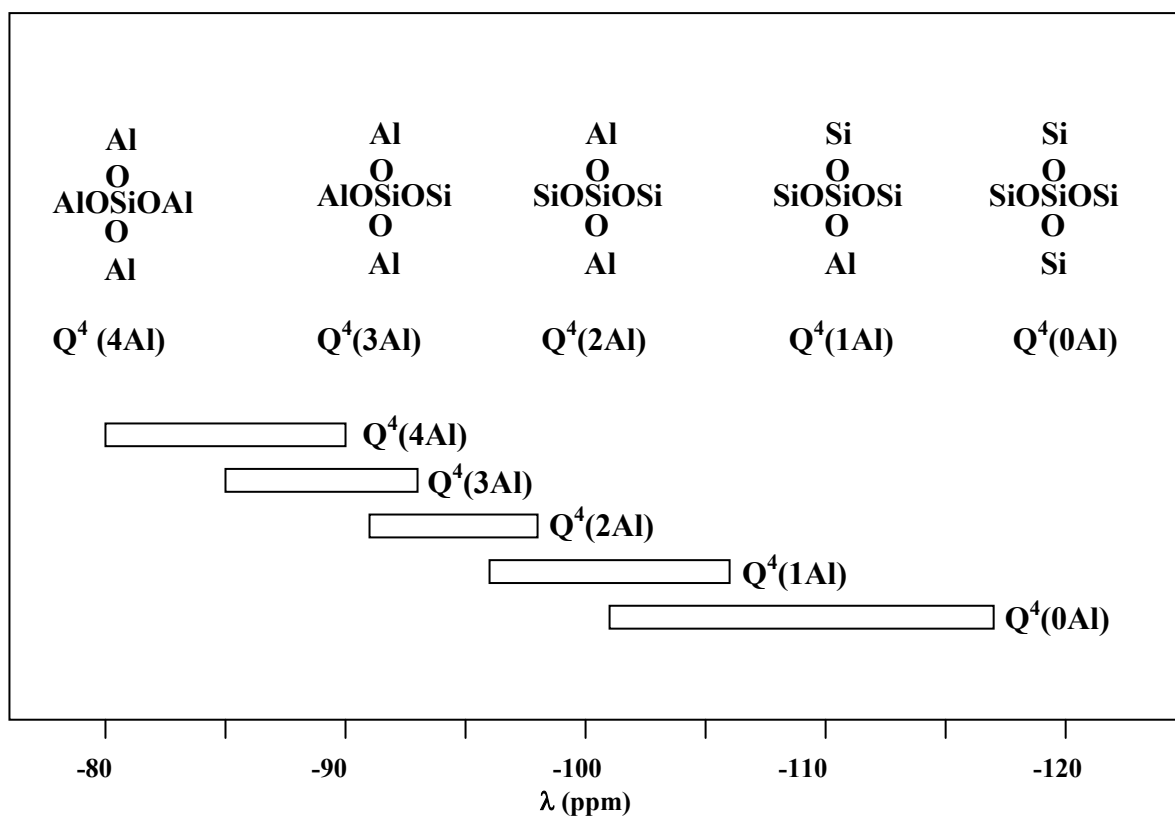


Figure 2.9: Range of ^{29}Si chemical shifts of $Q^4(m\text{Al})$ units in aluminosilicates

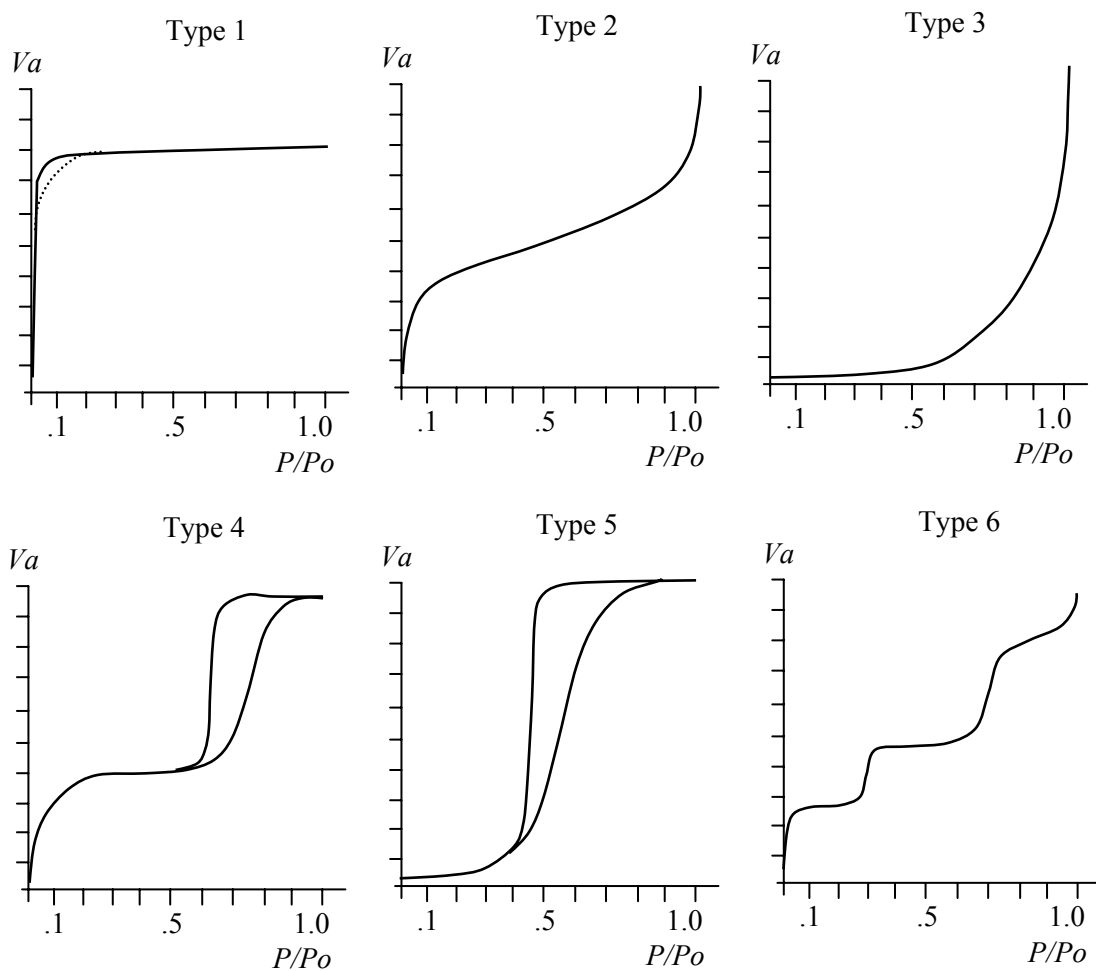


Figure 2.10: Six types of adsorption isotherm and adsorption and desorption isotherm for mesoporous and microporous materials.

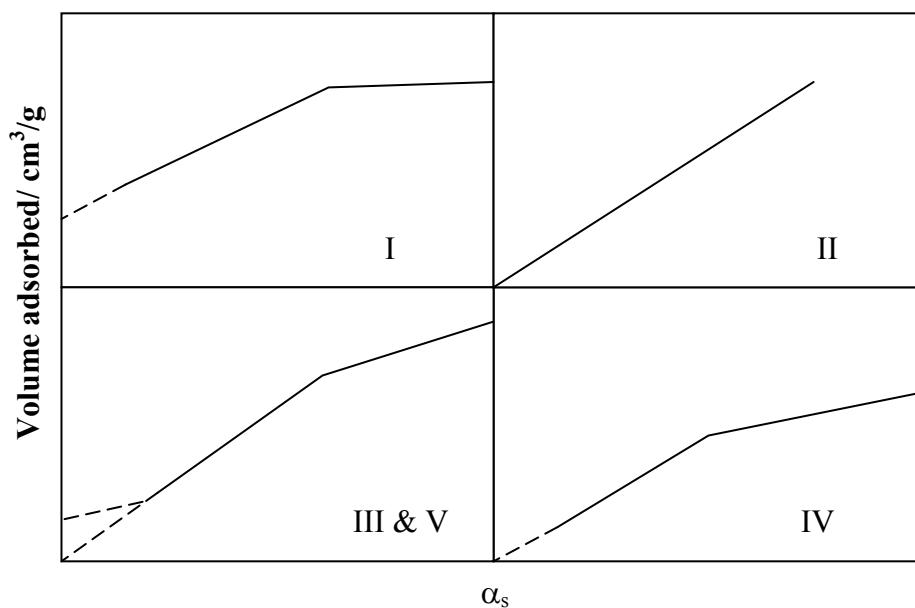


Figure 2.11: The α_s plot that determined the type of adsorption isotherms

CHAPTER 3

EXPERIMENTAL

3.1 Synthesis of Ferrierite

3.1.1 Chemicals

The rice husk ash which was employed as silica sources were either obtained from Kilang Padi BERNAS, Banting Selangor or burning of rice husk at 700°C for 3 hours. The chemical compositions of rice husk ash are listed in Table 3.1. The ashes were used directly without further treatment as main silica sources in this study. Other chemicals that were employed for the synthesis of ferrierite were sodium hydroxide pellets (99% Merck), sodium aluminate (54 % Al_2O_3 ; 41 % Na_2O w/w, Merck), pyrrolidine (99%, Merck), piperidine (99%, Merck), glycerol (99%, Merck), ethylenediamine (99%, Merck), fume silica (Fluka) and distilled water.

For acidity study, pyridine (99%, Aldrich) was used as adsorbate. As for catalytic testing, the propionic anhydride (99%, Fluka Chimika), acetic anhydride (98%, Fluka Chimika) and anisole (99%, Merck) were used directly as reactant in the Friedel-Crafts acylation. Toluene (99% Merck) and n-hexane (96%, Merck) were used as the internal standard for gas chromatograph.

Table 3.1: The oxides composition of rice husk ash (Chen *et al.* 1992)

Compound	Percentage ,%
SiO ₂	95.12
Al ₂ O ₃	0.19
Fe ₂ O ₃	0.07
CaO	0.32
MgO	0.51
Na ₂ O	0.01
K ₂ O	1.64
LOI	2.14
Total	100.0

LOI = Loss on Ignition

3.1.2 Synthesis of Ferrierite from Rice Husk Ash

Ferrierite was synthesized from rice husk ash by using different type of templates and methods by the previous researchers. Pyrrolidine, piperidine, ethylenediamine and glycerol were used as templates for preparing of ferrierite. The initial oxides gel compositions were varied for each synthesis is listed in Table 3.2. The crystalline phase of the rice husk ash was determined using X-Ray Diffractogram (XRD) technique. Only rice husk ash in amorphous form will be used in the preparing of ferrierite. Hydrothermal synthesis of ferrierite was carried out in stainless autoclave with total volume of gel is 50 g.

Generally, synthesis of zeolites involves preparation of silicates mixture which consist rice husk ash and sodium hydroxide. Rice husk ash (4.89 g) was added into sodium hydroxide solution (0.17 g dissolved in 10 g distilled water). The mixture was vigorously stirred in Teflon beaker for an hour using homogenous stirrer. Pyrrolidine (3.24 ml) was gradually added into the silicate mixture and was stirred further for another one hour. In other container, aluminate solution was

prepared by mixing sodium aluminate (1.11 g) with distilled water (30 ml) and stirred using magnetic stirrer until dissolved. The sodium aluminate solutions obtained was then added to the silicate mixture containing the template (pyrrolidine) and the mixture was further stirred for 2 hours. The gel mixture was left without stirring overnight and continued stirring for another one hour before removing into the autoclave. Crystallization of ferrierite was carried out by placing the autoclave in air oven at 200°C for 12 days. At the end of crystallization period, the autoclave was quenched with water to stop the reaction. The product was filtered and washed with distilled water until pH of the filtrate become neutral. The solid product obtained was then dried in air oven at 100°C overnight followed by calcination in a furnace at 550°C for 6 hours with the increase temperature rate is 1°C per minute. The solid product was denoted as Fer-12.

Ferrierite was also prepared by using commercial fume silica with the same initial composition as have been carried out for sample Fer-12. This sample was labeled as Fer-12-FS. The same procedure was employed for preparation of Fer-12-FS.

To study the effect of the different organic templates for ferrierite synthesis, the same experiment was carried out at different oxides composition as shown in Table 3.2. Rice husk ash was employed as silica source for every reaction.

Table 3.2: Molar oxides composition for synthesis ferrierite using various type of template

Sample	Na ₂ O	Al ₂ O ₃	SiO ₂	Template	H ₂ O
Fer-1-Gly	11.97	1	30	198.7 (glycerol) ¹	158
Fer-2-En	1.85	1	15.2	19.7 (ethylenediamine) ²	592
Fer-12-Py	1.3	1	12	6.67 (pyrrolidine)	410
Fer-7-Pn	6.78	1	22.69	8.99 (piperidine)	368
Fer-8-PnGly	6.78	1	22.69	4.5 (pyrrolidine) 50.3 (glycerol)	368
Fer-12-Py-FS*	1.3	1	12	6.67	410

* fume silica as silica source

¹Sanyuang *et al.* 1997, ²Jongkind *et al.* 1997,

3.1.3 Optimization Synthesis of Ferrierite from Rice Husk Ash

To study the capability of rice husk ash to form ferrierite at different oxide ratios, the appropriate amount of silica rice husk ash, with pyrrolidine as structure directing agent and sodium hydroxide was varied based on initial gel mixture of sample Fer-12. The initial gel mixture that was used for optimization synthesis of ferrierite was listed in Table 4.2 in Chapter four. The solid products obtained were further characterized using XRD and FTIR techniques.

3.1.4 Method to Study the Transformation of Rice Husk Ash to Ferrierite

The transformation of rice husk ash to ferrierite was investigated by using sample Fer-12. Synthesis was carried out at different crystallization period; 6 hours, 12 hours, 1, 2, 3, 4, 7, 9 and 12 days. Each sample was labelled as Fer-12-0.25, Fer-12-0.5, Fer-12-1, Fer-12-2, Fer-12-3, Fer-12-4, Fer-12-7, Fer-12-9 and Fer-12-12. At the end of the each crystallization period, the solid product was filtered, washed, dried and weighted (W_1). The solid product was then characterized using XRD, FTIR, N_2 adsorption, ^{29}Si MAS NMR and SEM in order to study the formation of ferrierite phase.

The percentage of solid weight obtained was indicated by using the following procedure; 0.3 g of sample was calcined at $550^{\circ}C$ to eliminate all trapped volatile compound, as well as the template. The sample was dried at room temperature and weight (W_2) again. The amount of the initial rice husk ash used in the synthesis was denoted as W_0 . The percentage of solid product weighted over initial amount of rice husk ash was calculated according to the following equation;

Weight ratio, % (weight product / weight rice husk ash) =

$$\left(\frac{W_1 \times W_2}{0.3} \times \frac{1}{W_o} \right) \times 100 \% \quad (3.1)$$

3.2 Characterization of Solid Product

The solid product obtained for each synthesis was characterized by X-ray Diffraction (XRD), Fourier Transformation Infrared (FTIR), ^{29}Si MAS NMR, N_2 adsorption and also Scanning Electron Microscopy (SEM). All these techniques are important in order to study the transformation of rice husk ash into ferrierite phase.

3.2.1 X-ray Diffraction (XRD)

X-ray Diffraction technique is the most important tool for indications of solid phase, crystallinity and also the purity of solid samples. This measurement was carried out using Siemens D5000 powder instrument with Cu K_α radiation ($\lambda = 1.5418 \text{ \AA}$, $kV = 40$, $mA = 40$). Samples were saturated over concentrated NH_4Cl solution in desiccator to ensure complete dehydration before recording the XRD pattern as this can affect the lattice parameter. 1g of Grounded solid samples was mounting into sample holder and lightly pressed using slide glass to get smooth surface of thin layer. X-ray Diffractogram was recorded in the 2θ scale of 2° to 50° . Scanning was carried out in a step interval 0.02° with counting time of 1 second per step. X-ray Diffractogram obtained was compared with standard ferrierite diffractogram from IZA to ensure the phase of solid the produced. In order to determine the crystallinity of ferrierite, the intensity of one particular peak or a

number of peaks is compared with the intensity of the same peak of a standard (Bekkum *et al.* 1991) sample as given by following equation:

$$\text{X-ray crystallinity} = \frac{\text{intensity of peak } hkl \text{ of sample}}{\text{intensity of peak } hkl \text{ of standard}} \times 100\% \quad (3.2)$$

3.2.2 Fourier Transformed Infrared Spectroscopy

FTIR spectra were measured at room temperature using Shimadzu 8300 spectrometer by using KBr disc technique. KBr disc was prepared by mixing and grinding a mixture of solid samples and KBr (ratio of sample to KBr is 0.25 mg / 300 mg). Approximately 50 mg of the mixture were placed in a die and pressed at 10 kPa under vacuum for one minute. For structural characterization, FTIR spectra were recorded in the range of wavenumber between 1400 cm^{-1} to 400 cm^{-1} . The measurement was employed at ambient temperature to remain the hydration state of the zeolite and to minimize any structural changes.

3.2.3 ^{29}Si MAS NMR

The ^{29}Si MAS NMR measurement was measured at spectral frequency of 79.5 MHz using 4 mm zirconia double bearing rotor with a relaxation time delay of 600 s and spinning rate of 10kHz with 45° pulses. The NMR spectrum was recorded using Bruker Ultrashield 400 instrument. Chemical shifts are quoted in ppm from external tetramethylsilane (TMS).

3.2.4 N₂ Adsorption

Nitrogen adsorption analysis was carried out in order to get the information of the types of pores, BET surface area and pore volume. This measurement was performed on Micrometecs ASAP 2010 volumetric adsorption analyzer. Nitrogen was used as an adsorbate at 77 K. Before measurement was performed, 0.5 g sample was dehydrated at 200°C for 3 hours. Dehydrated sample was weighted automatically and the samples were then evacuated to 10⁻² Torr and immersed in liquid nitrogen. Data was recorded and calculated from nitrogen adsorption data with the linear part of BET plot to get BET surface area of samples using Equation xx

3.2.5 Scanning Electron Microscopy

This measurement was performed on electron microscope Philip XL40 under vacuum condition at 5 bar pressure. Scanning Electron Microscopy was carried out in order to determine the morphology of the sample and the crystal size. Before the measurement, samples were mounted over sample holder (stubs) using double sided tape. The sample was further coated with gold using Bio Rad Coating System at 10⁻¹ mbar with current flow 30 mA for 75 seconds. Sample was then placed into SEM instruments for scanning. Tungsten filament was used as electron sources and SEM micrograph was recorded with 10 kV resolutions to obtain 5000x enlargement.

3.3 Acidity measurement

3.3.1 Ammonium ion-exchange method

The calcined sample of ferrierite obtained from the synthesis was ion-exchanged using ammonium nitrate solution to replace Na cations with ammonium and followed by further heating to decompose the ammonium ion which left sample in the form of hydrogen ferrierite. Sample Fer-12, Fer-20 and Fer-30 which contain Na^+ cations (5 g), were added into ammonium nitrate solution (50 ml, 1 M) each, and stirred at 80°C for 4 hours. The solid was filtered and washed using deionised water and dried overnight at 110°C. The ion-exchange process was repeated three times to complete the process and samples in NH_4 -ferrierite formed were calcined at 400°C. All samples were denoted as H-Fer 12, H-Fer 20 and H-Fer 30.

3.3.2 Pyridine Adsorption

The amount of Brønsted acid sites and Lewis acid sites and the hydroxyl groups were determined using FTIR spectroscopy technique. Pyridine was used as probe base in order to measure the Brønsted and Lewis acid sites in H-ferrierite. Experimental setup for the acidity study is schematically shown in Figure 3.1. The system consists of an IR cell, vacuum line and pyridine adsorbate. 10 mg of samples was grinded and pressured less than 5 tonne for 3 minutes in order to obtain wafer disc with diameter of 13 mm. Afterwards, the wafer disc was placed in a steel holder and mounted in a quartz cell equipped with CaF_2 windows. The quartz cell was connected to the vacuum pump and put into a tube furnace.

Sample H-ferrierite was degassed under vacuum at 400°C for over night to evacuate all trapped water and released surface group which could interfere with the adsorption pyridine. Sample was cooled into room temperature and FTIR spectrum was recorded in the region ranged from 4000 cm^{-1} to 1400 cm^{-1} . The pyridine was adsorbed onto the sample for 1 minutes and desorbed under vacuum ($P = 1 \times 10^{-2}$

mbar) for 1 hour at room temperature, 150°C and 400°C. The FTIR spectrum for the sample at each desorption temperature were recorded.

3.3.3 Temperature-Programmed Desorption Ammonia

The experiment for Temperature Programmed Desorption (TPD) ammonia was carried out in a flow apparatus with nitrogen as the carrier gas. TPD measurements were performed on TPDRO 1100 of Thermoquest. For each experiment, about 150-200 mg samples were used. At first, the samples were flushed with nitrogen gas at the flow of 15°C/min to 450°C for 3 hours. The sample that was cooled to 100°C within an hour followed by reheating the sample at 600°C with the flow of ammonia. The desorption of ammonia from samples were employed by continuous heating of samples in a flow of nitrogen. The desorbed amount of ammonia was recorded continuously using a thermal conductivity detector.

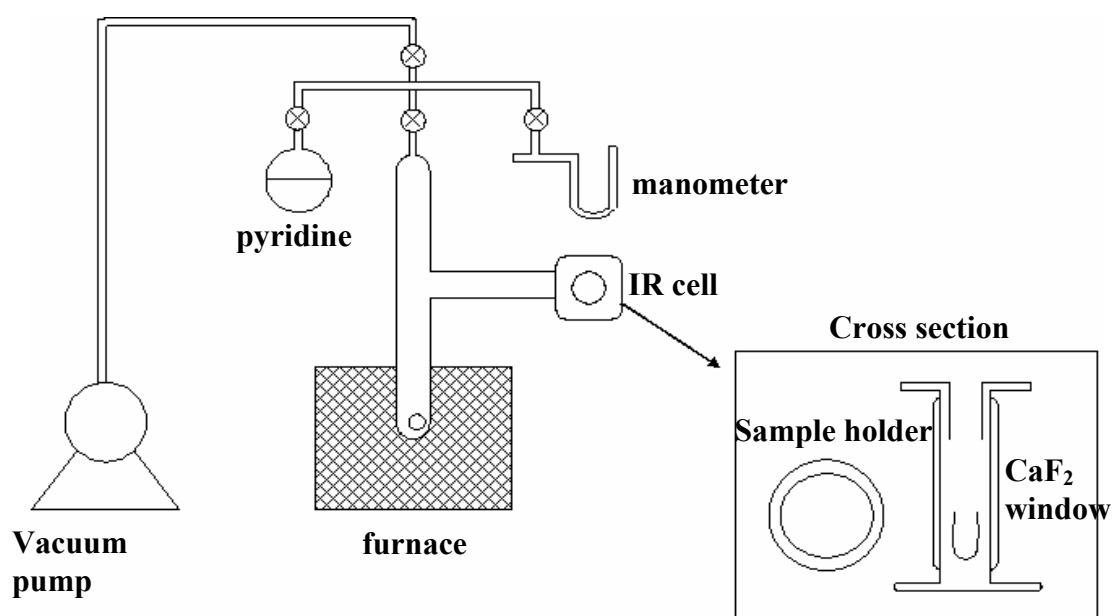


Figure 3.1: Experimental setup for acidity measurement.

3.4 Catalytic Activity Testing

The catalyst (0.03 g) which is in the hydrogen form was placed in a quartz crucible and activated at 500°C for three hours using air furnace before reaction begins. The activated catalysts were immediately put into the round bottle flask containing anisole (3.28 ml) and propionic anhydride (3.87 ml) as reactants. Three main studies were carried out in this reaction, the effect of SiO₂/Al₂O₃ ratio of catalyst, the effect of reaction time and the effect of reaction temperature. All reactions were carried out using the batch reactor.

In order to study the potential of H-Ferrierite as catalysts in Friedel-Crafts acylation, the reaction between anisole and propionic anhydride was employed as a model reaction. The reaction was carried out using 50 ml two necked round bottle flask equipped with condenser. The round bottle flask was placed in oil bath at 120°C with magnetic stirrer and the reaction was carried out at 120°C for 24 hours. At the end of reaction period, the organic liquid yield obtained was separated from catalysts and placed in glass vial for further characterization using GCMS and GC.

To determine the equilibrium of the reaction, the reaction was repeated but the product was sampled at 0, 15 min, 45 min, 1.5 h, 2 h, 2.5 h, 4 h, 8 h and 24 h. For the effect of reaction temperature, H-Fer 12 was used as catalysts and the reaction was repeated and carried out at 90°C, 100°C, 110°C, 120°C and 130°C.

3.4.1 Gas Chromatography

All the samples were analysed using GC to verify the amount of obtained product. Gas chromatograph Hewlett Packard 5890 series II with FID detector and Hewlett Packard 3396 series II integrator were used and equipped with Phase AT-WAX column (0.25 mm x 0.2µm x 30m). 100 µL of yield was added with 100 ppm of internal standard (100ppm of toluene in hexane). 0.1 µL of those samples was injected to GC using 10 µL syringes at initial temperature 50°C for one minute, with

the rate of temperature increased 15°C/min until 200°C, and hold for 35 minutes. The percentage of reacted anisole (% A) and the selectivity of yield (*p*-methoxypropiophenone) (% yield) were measured using the following equation.

$$\% A = \frac{\text{initial area} - \text{initial final}}{\text{initial area}} \times 100\% \quad (3.3)$$

$$\% \text{ Yield} = \frac{\text{p-methoxypropiophenone area}}{\text{total yield area}} \times 100\% \quad (3.4)$$

3.4.2 Gas Chromatography-Mass Spectroscopy Detector

Identification of the compounds in the liquid yield was characterized by GCMSD using Agilent 6890N-5973 Network Mass Selective Detector model equipped with HP-5MS column (30 m x 0.251 mm x 0.25µm), diffusion pump and turbomolecular pump. Sample was analyzed on splitless method with Helium as the carrier gas. The oven-programmed setup is shown in Table 3.3.

Table 3.3: The oven-programmed setup for GCMS

Ramp	Rate, °C/min	Next, °C	Hold, min	Runtime, min
Initial	-	50	2	2
Ramp 1	10	200	5	25
Post	-	-	-	27

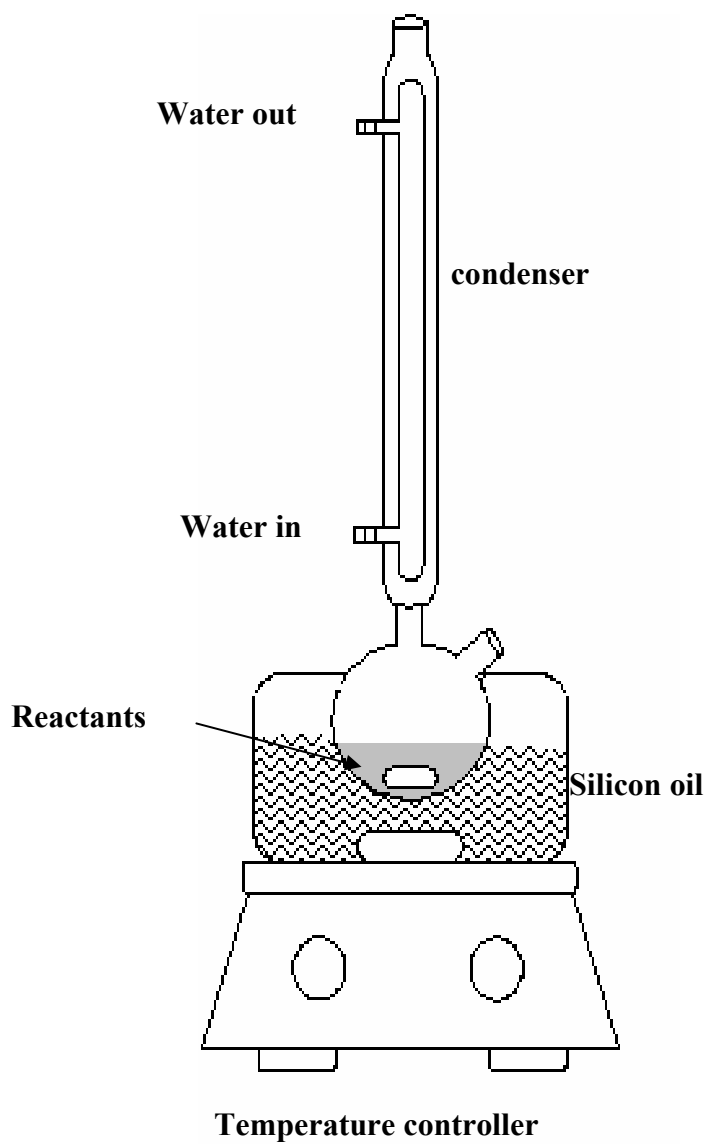


Figure 3.2: Heterogeneous batch reaction apparatus

CHAPTER 4

RESULTS AND DISCUSSION

4.1 Synthesis of zeolite ferrierite with different initial oxides compositions

Zeolites ferrierite was synthesized using rice husk ash as silica source with different organic templates such as pyrrolidine, piperidine, ethylenediamine and glycerol in different initial gel composition. All samples are white solids which were characterized using X-ray Diffraction and Fourier Transform Infrared Spectroscopy techniques.

4.1.1 Effect of different template

4.1.1.1 X-ray Diffractogram Study

In this study, the efforts to produce ferrierite from rice husk ash have been carried out using different type of template. Ferrierite has been synthesis using rice husk ash with pyrrolidine as the organic template and structure directing agent. The attempt in using other templates such as piperidine, glycerol and ethylenediamine failed to produce ferrierite. These templates have been produce ferrierite when using commercial silica as silica sources. A lot of studies have been carried out by many researchers in order to produce ferrierite using pyrrolidine as the structure directing agent. Pyrrolidine was already recognized as a good template for synthesis of

ferrierite due to its unique properties. The fact that only pyrrolidine can be used to direct the formation of ferrierite from rice husk ash shows the uniqueness properties of this template. It has been shown that the size of pyrrolidine is the best fit in the pore of ferrierite compared to another template [Rollmann *et al.*, 2000].

The X-Ray Diffraction pattern for samples Fer-12-Py, Fer-1-Gly, Fer-2-En, Fer-7-Pn and Fer-8-PnGly which were synthesized using rice husk ash are shown in Figure 4.1. For comparison, sample Fer-12-Py(FS) was prepared using commercial fume silica as the silica source and the XRD diffractogram of commercial ferrierite were recorded and labeled as Fer-STD. Samples Fer-12-Py and Fer-12-Py-FS were synthesized using the same initial molar reaction mixture $1.31 \text{ Na}_2\text{O} : \text{Al}_2\text{O}_3 : 12 \text{ SiO}_2 : 6.67 \text{ Py} : 410 \text{ H}_2\text{O}$. In this study, commercial fume silica was used as silica source for sample Fer-12-Py-FS and rice husk ash as silica source for sample Fer-12-Py with pyrrolidine as template under hydrothermal synthesis. X-ray diffractogram of the Fer-12-Py and Fer-12-Py-FS samples showed similar diffractogram pattern to the reference ferrierite (Fer-STD) indicating the samples are ferrierite type zeolite. The x-ray diffractogram for sample Fer-12-Py in Figure 4.1 clearly show that ferrierite has been formed based on the existence of the very intense peaks at 2θ 9.5° , 17.28° , 13.4° , 22.4° , 23.5° , 24.3° , 25.1° and 25.6° . The XRD diffractogram for sample Fer-12-Py is similar to the XRD pattern of ferrierite that was synthesized by Ahedi *et al.* (2001) and Tae *et al.* (1996) and also from JCPDS data. This further proves that ferrierite has been successfully formed from rice husk ash as the silica source while pyrrolidine was employed as structure directing agent.

Fer-1-Gly was prepared according to previous method in which the glycerol was used as template while other synthesis parameters were kept constant [Sanyuang *et al.*, 1997]. However, the XRD diffractogram for sample Fer-1-Gly reveals the formation of mordenite phase zeolite instead of ferrierite. The diffraction peaks of the sample exist at 2θ 9.77° , 13.84° , 22.27° , 25.67° , 26.27° , 26.64° and 27.71° which were assigned to mordenite phase [Dutta *et al.*, 1994]. Previous study has reported that ferrierite was produced when commercial Ludox 30 was used as silica source with the same initial reaction mixture as the Fer-1-Gly. The difference in results between these two experiments might be due to the different sources of silica used.

Breck [1974] has indicated that when the reaction mixture are prepared using amorphous silica as the silica source, the products that are formed can be different from those crystallized from the homogeneous sodium aluminosilicate gel. The reason is attributed to the difference in the solubilization of the silicate anions and the resulting interaction with the aluminate ions present in the solution. Silica sol such as Ludox contains sodium silicate in solution, with the remaining silica as silica gel. In the experiment that involved silica from rice husk ash, the silica is in polymeric SiO_2 , which require higher alkalinity solution in order to dissolve the polymeric silica to become polymeric silicates anions. Further more, ferrierite require higher alkaline solution as compared to mordenite. It is suggested that when rice husk ash was used, the alkalinity of the solution decreases, which gives a proper condition to facilitate the crystallization of mordenite. Besides this factor, mordenite that is well-known as silica rich and large pore zeolite can be formed easily even without the organic template present or in template-free systems. For example, by adding a small amount of hexamethylene imine, high silica to alumina ratio (25.8) of mordenite can be produced [Jongkind *et al.*, 1997].

Another experiment was carried out using ethylenediamine as template (sample Fer-2-En). It was found that pure ZSM-5 was formed instead of ferrierite. It has been reported that zeolite ZSM-5 can be obtained using ethylenediamine as template [Jacobs *et al.* 1987]. Normally, in the preparation of ZSM-5 through hydrothermal synthesis, tetrapropylammonium cation was employed as a structure directing agent, which is relatively expensive compared to the ethylenediamine. However, the formation of ZSM-5 instead of ferrierite in this experiment was expected since ZSM-5 was already known as a competitor for ferrierite crystal growth. In addition, ZSM-5 is also easily formed even in a free template system [Tae *et al.*, 1996, Neil *et al.*, 1995]. From this finding, template ethylenediamine could be used as an alternative template in the synthesis of ZSM-5 instead of TPABr due to its low cost and simple method of preparation.

Another method of synthesis has been carried out by applying piperidine and a mix-template technique of piperidine and glycerol to promote ferrierite from the mixture of silicate and sodium aluminate solutions. However, in both cases it failed

to form ferrierite. X-ray diffraction patterns for samples Fer-7-Pn and Fer-8-PnGly in Figure 4.1 show that analcime was produced in both cases.

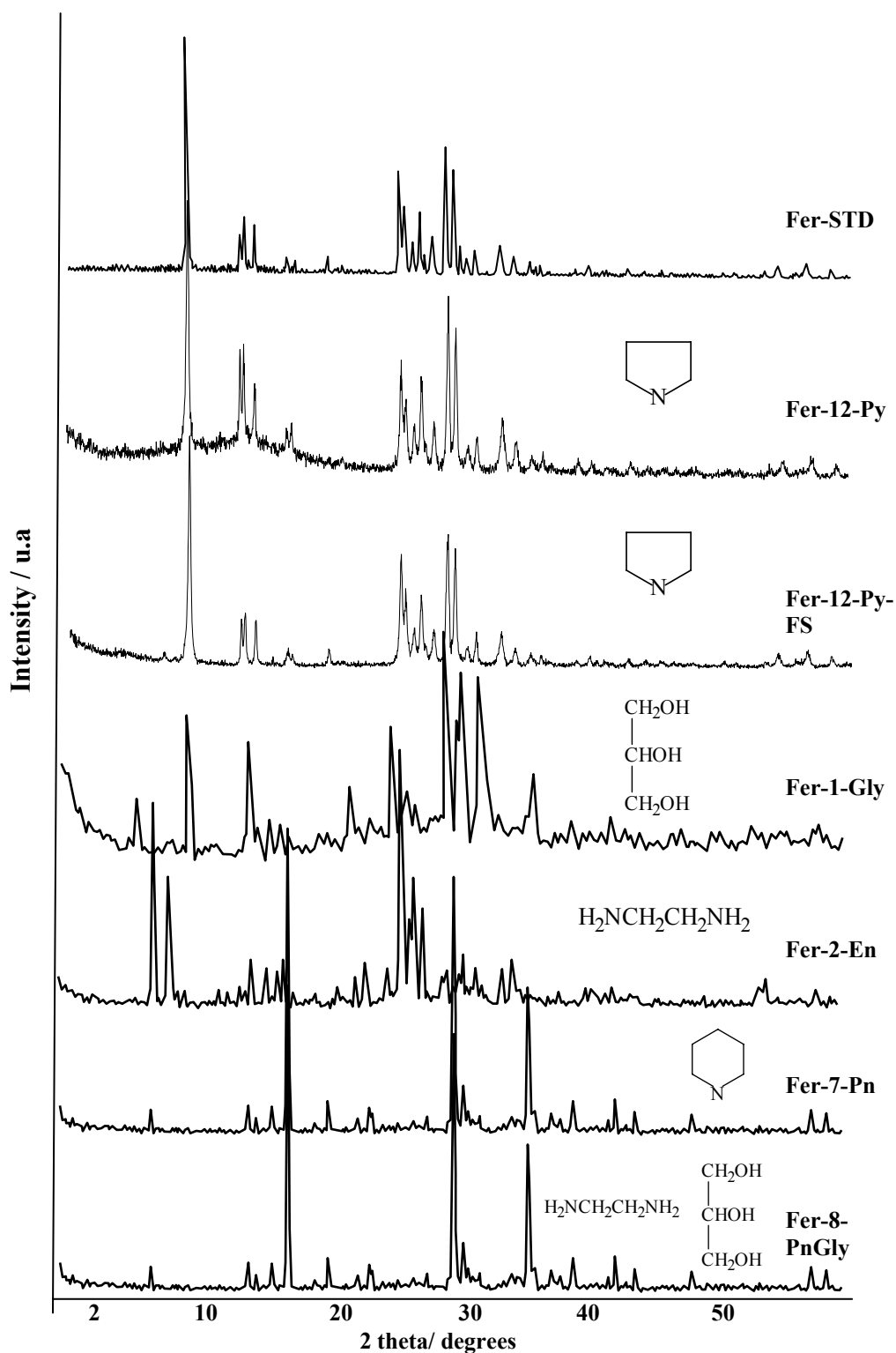


Figure 4.1: X-Ray Diffractogram for sample Fer-STD, Fer-12-Py, Fer-12-Py-FS, Fer-1-Gly, Fer-2-En, Fer-7-Pn and Fer-8-PnGly; Effect of different template and silica sources

Table 4.1: Comparison of lattice spacing, d between commercial ferrierite with Fer-12-Py and Fer-12-Py-FS samples

Angle (2-Theta)	d, spacing (Å)		
	Commercial FER	Fer-12-Py-RHA	Fer-12-Py-FS
9.35	9.38	9.48	9.44
12.82	6.89	6.96	6.89
22.35	3.96	3.97	3.97
23.59	3.75	3.77	3.76
25.18	3.52	3.53	3.53
25.65	3.45	3.47	3.46

Comparison between lattice spacing of as-synthesized ferrierite (Fer-12-Py and Fer-12-Py-FS) with that of commercial ferrierite is illustrated in Table 4.1. Both synthesis samples gave similar lattice spacing with the commercial ferrierite. It shows that pure ferrierite is obtained from the synthesis regardless of the type of silica source used. However, both samples differ in crystallinity. Fer-12-Py-Fs gives a higher crystallinity 73.74 % compared to sample Fer-12-Py that gives only 57.21% crystallinity relative to commercial ferrierite as the standard.

4.1.1.2 Fourier Transform Infrared Study

Each zeolite species has a typical infrared pattern for structural vibration which consists of four main peaks; the asymmetric and symmetric peaks of TO_4 (T = Al, Si) at $1250 - 1000 \text{ cm}^{-1}$ and $750 - 650 \text{ cm}^{-1}$ respectively and T-O bending at $500 - 400 \text{ cm}^{-1}$. The IR spectra of the samples are shown in Figure 4.2. The structure of ferrierite was characterized by the appearance of peaks at $441 \text{ cm}^{-1} - 462 \text{ cm}^{-1}$

(doublet), 527 cm^{-1} , 584 cm^{-1} , 702 cm^{-1} , 796 cm^{-1} , 1070 cm^{-1} and 1234 cm^{-1} [Khomane *et al.* 2000]. All bands that corresponded to the IR spectra of ferrierite are observed in the IR spectra of samples Fer-12-Py and Fer-12-Py-FS. It is further confirmed that sample Fer-12-py is ferrierite that has been successfully synthesized from rice husk ash. The absorption bands around $441\text{ cm}^{-1} - 462\text{ cm}^{-1}$ (doublet), 702 cm^{-1} and 1070 cm^{-1} are assigned to the internal vibration of tetrahedral SiO_2 in which these bands can also be observed in silica or quartz samples [Jacobs *et al.*, 1981].

For sample Fer-2-En, it shows the vibrations at 1220 cm^{-1} and 1078 cm^{-1} both assigned to asymmetric stretching for TO_4 , 788 cm^{-1} that was assigned to the symmetric stretching for TO_4 , 538 cm^{-1} that was assigned to double ring of ZSM-5 and 443 cm^{-1} that was assigned to TO_4 bending. This FTIR spectrum proved that ZSM-5 has been produced instead of ferrierite.

Sample Fer-1-Gly shows a characteristic vibration for mordenite. The band observed at 1225 cm^{-1} shows an external asymmetric stretching for mordenite while the band at 1050 cm^{-1} corresponds to the internal asymmetric stretching for mordenite framework. Another two bands observed for symmetric stretching of mordenite at 800 cm^{-1} and 720 cm^{-1} which were both assigned to external and internal symmetric stretching. The band which appeared at 580 cm^{-1} and 560 cm^{-1} are both assigned to the vibration of double ring. A sharp band at 480 cm^{-1} is assigned to the T-O bending of mordenite framework (Hincapie *et al.* 2004).

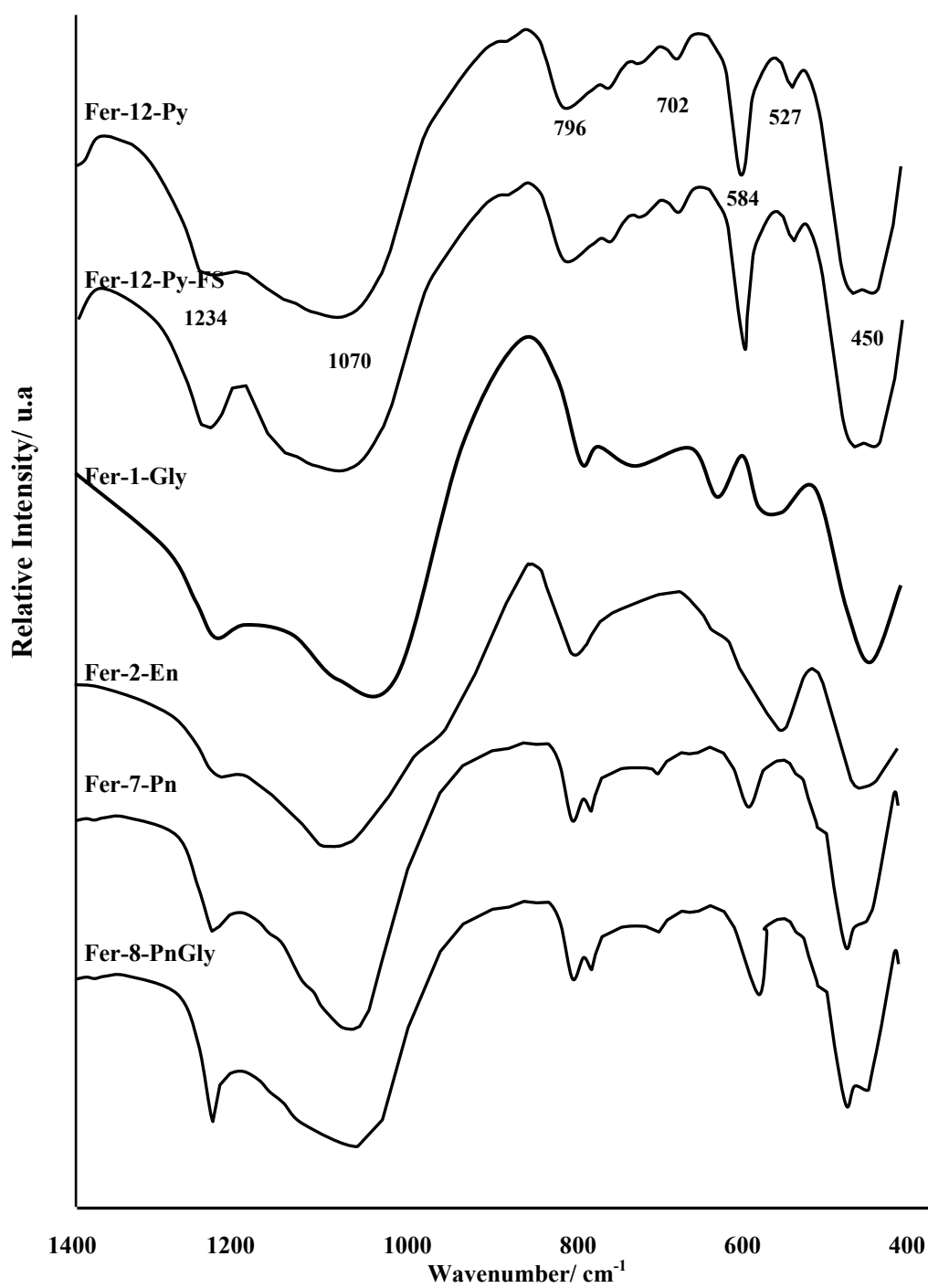


Figure 4.2: FTIR spectra for sample Fer- 12-Py, Fer-12-Py-FS, Fer-1-Gly, Fer-2-En, Fer-7-Pn and Fer-8-PnGly

4.1.2 Effects of different molar composition of the initial gel

The study of the effects of different molar composition of the initial gel was carried out to investigate the influence of each component in the formation of ferrierite. The $\text{SiO}_2/\text{Al}_2\text{O}_3$, $\text{Py}/\text{Al}_2\text{O}_3$ and SiO_2/Py molar ratios were varied in this study as listed in table 4.2 and 4.3. The effect of silica to alumina ratios was investigated by varying $\text{SiO}_2/\text{Al}_2\text{O}_3$ within 10 to 50 mole ratios with pyrrolidine being used as organic template and structure directing agent (Table 4.2). Figure 4.3 reveals the x-ray diffractogram of each sample obtained from the difference of the initial gel silica to alumina ratio.

The diffractogram pattern of rice husk ash that has been used in this study is amorphous as shown in Figure 4.3. It has been reported that the amorphous phase of rice husk ash is the most active silica source compared to crystalline and quartz phase in zeolite synthesis [Hamdan *et al.* 1997]. The pure phase of ferrierite was successfully formed when the $\text{SiO}_2/\text{Al}_2\text{O}_3$ ratios of initial reaction mixture is within 10 to 30. Diffraction peaks of ferrierite obviously appeared at 2θ 9.5° , 17.28° , 13.4° , 22.4° , 23.5° , 24.3° , 25.1° and 25.6° . Sample Fer-12-Py was chosen as a reference sample. In this section, Fer-12-Py is denoted as Fer-12 in which the $\text{SiO}_2/\text{Al}_2\text{O}_3$ ratio of the sample is 12. The initial amount of each sample was modified by expanding the range of $\text{SiO}_2/\text{Al}_2\text{O}_3$ ratios from 10 to 50. It is observed that when the $\text{SiO}_2/\text{Al}_2\text{O}_3$ ratio was raised to 20, the pure phase of ferrierite was obtained (Figure 4.3; Fer-12 and Fer-20). However the intensity of ferrierite in sample Fer-20 is relatively low compared to Fer-12, but when the amount of silica was increased up to 50 as in samples Si-30, Si-40 and Si-50, only the diffraction peaks that correspond to quartz were observed in which the intensity increased with the increase of silica content. Peaks corresponding to quartz were observed at 2θ 22° and 28° . Sample Si-30 shows a small peak of quartz at 2θ 27.3° and some amorphous patterns. It reveals that only a small amount of rice husk ash has been transformed into quartz phase. The increase in the $\text{SiO}_2/\text{Al}_2\text{O}_3$ ratios up to 40 and 50 (Si-40 and Si-50), results in the increase of the total peak intensities of quartz with the disappearance of amorphous pattern. From this observation, it is indicated that the crystallization for ferrierite was not favored in the high concentration of silica to alumina ratio. This might be due to the

low concentrations of alkaline medium to enable dissolution of silica. The increasing of $\text{SiO}_2/\text{Al}_2\text{O}_3$ ratios while other reactants were kept constant will indirectly reduce the alkalinity of the medium which at the same time decreases the dissolution of silica. Murayama *et al.* [2002] investigated the effects of alkalinity of the initial reaction mixture solution to produce zeolite P from coal fly ash. They reported that the high Na^+ content is necessary in order to neutralize the negative charge on aluminate in zeolite structure when zeolite crystal is formed. The low Na^+ concentration might be the reason for the low crystallinity of ferrierite produced in sample Fer-20 and the formation of quartz instead of ferrierite in samples Si-30, Si-40 and Si-50.

The failure to obtain ferrierite in high $\text{SiO}_2/\text{Al}_2\text{O}_3$ ratios was prompted to synthesis ferrierite by changing the amount of pyrrolidine and Na_2O as listed in Table 4.3. Sample Si-30,N-5,Py-3 was prepared by increasing Na_2O (N) content with reduced amount of pyrrolidine (P) while the $\text{SiO}_2/\text{Al}_2\text{O}_3$ ratio is kept at 30. The XRD diffractogram of the samples shows that the rice husk ash has been transformed into quartz phase. This finding suggests that, the high amount of Na^+ does not facilitate the transformation of silica of rice husk ash to ferrierite when the amount of pyrrolidine is low. At low pH solution, the amorphous silica will dissolve and become polymeric silicate anion in which at this stage the pyrrolidine as a template will direct the formation of ferrierite. Rollmann *et al.* [2000] reported that pyrrolidine also played a pore-directing role for the formation of ferrierite, in which the size of pyrrolidine fits with the molecular shape within the pores of ferrierite zeolite. It is suggested that the failure to obtain ferrierite even in high alkali medium is due to the lack of concentration of structure directing agent i.e. the pyrrolidine in this case.

Another sample with $\text{SiO}_2/\text{Al}_2\text{O}_3$ ratio 30 was synthesized with increased amount of pyrrolidine concentrations while the amount of Na_2O remained the same as in sample Si-30. The sample was denoted as Fer-30,Py-10 and its XRD diffractogram in Figure 4.3 corresponds to ferrierite phase. This finding proved that the template is crucial to form ferrierite. Pyrrolidine in this case not only functions as structure directing agent but also as a pH-stabilizer [Rollmann *et al.* 1999]. The increased amount of pyrrolidine will increase the pH solution to facilitate the

solubility of silica. To further prove that the role of pyrrolidine as the pH-stabilizer of the gel mixture, the $\text{SiO}_2/\text{Al}_2\text{O}_3$ ratio of the initial gel was increased to 40 (sample Si-40,Py-10). Based on the XRD diffractogram of Si-40,Py-10 in Figure 4.3, it shows that pure analcime phase was obtained with high intensity. Analcime peak appeared at 2θ 15.8, 25.9 and 30.7 [Treacy *et al.* 1996]. Analcime is the type of zeolite that is easily formed in two different conditions either in low $\text{SiO}_2/\text{Al}_2\text{O}_3$ content with the high alkaline gel mixture [Barrer, 1982] or in the high $\text{SiO}_2/\text{Al}_2\text{O}_3$ content with low alkaline solution [Joshi *et al.* 1991]. It is further confirmed that by increasing $\text{SiO}_2/\text{Al}_2\text{O}_3$ ratio, it will decrease the pH of the gel in which the composition was not suitable for the formation of ferrierite.

Table 4.2: Initial reaction mixture for samples at different $\text{SiO}_2/\text{Al}_2\text{O}_3$ mole ratios while other component remain same

Sample	Na ₂ O	Al ₂ O ₃	SiO ₂	Py	H ₂ O	Product
Fer-12	1.31	1	12	6.67	410	FER
Fer-20	1.31	1	20	6.67	410	FER
Si-30	1.31	1	30	6.67	410	QUARTZ
Si-40	1.31	1	40	6.67	410	QUARTZ
Si-50	1.31	1	50	6.67	410	QUARTZ

Table 4.3: Initial reaction mixture for modified samples with different SiO_2 , Na₂O and Py ratio.

Sample	Na ₂ O	Al ₂ O ₃	SiO ₂	Py	H ₂ O	Product
Si-10	4.02	1	10	6	410	FER
Si-14	2	1	14	4	410	FER
Si-30,Py-5, N-3	5	1	30	3	410	QUARTZ
Fer-30,Py-10	1.31	1	30	10	410	FER
Si-40,Py-10	1.31	1	40	10	410	ANALCIME

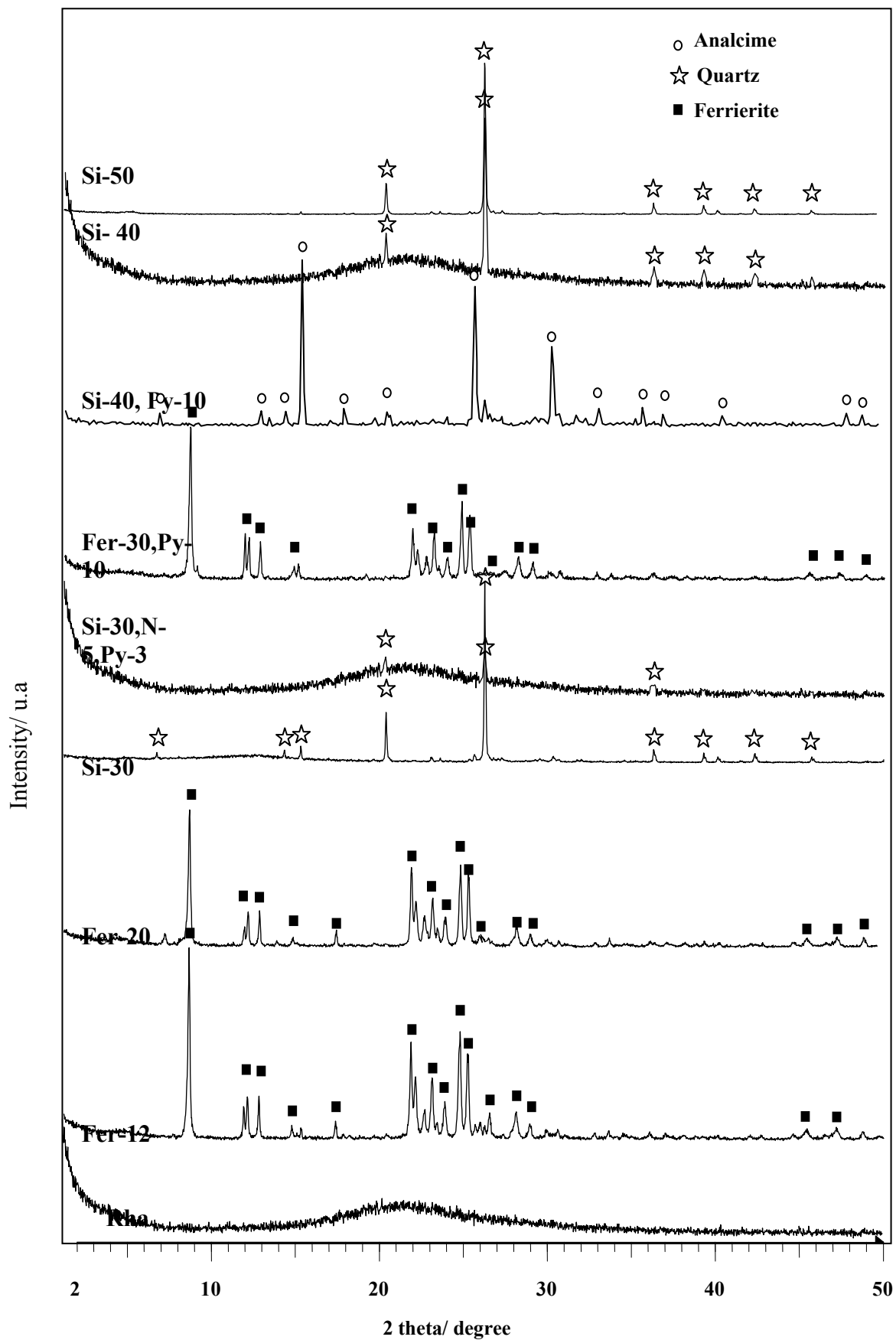


Figure 4.3: XRD diffractograms of samples at different $\text{SiO}_2/\text{Al}_2\text{O}_3$ mole ratio

In order to investigate the capability of ferrierite crystal, grow from rice husk ash in a different amount of organic template pyrrolidine, a study has been conducted using 1.31 Na₂O : Al₂O₃ : 12 SiO₂ : X Py : 410 H₂O oxides molar ratios in which X was varied from 3 to 10 while other synthesis conditions were kept constant. The X-ray diffraction patterns given in Figure 4.4 reveal that ferrierite with a high crystallinity can be prepared with the Py/Al₂O₃ ratio of the reaction mixture as low as 4. When the Py/Al₂O₃ ratio of the reaction mixture is lower than 4, it will produce quartz instead of ferrierite as shown in Figure 4.4 due to lack of pyrrolidine amount in gel mixture.

In order to monitor the effects of silica to pyrrolidine (SiO₂/Py) content that was employed for ferrierite synthesis at different Na₂O/Al₂O₃ ratios in each initial gel mixture, the Na₂O/Al₂O₃ ratio vs. SiO₂/Py ratio in each sample was plotted. From Figure 4.5, there are three types of crystalline phases that were produced when the amount of SiO₂/Py and Na₂O/Al₂O₃ was varied. It is noted that with increasing SiO₂/Py ratio in the initial gel composition, different types of product were produced. The phase of zeolite was found to change along the SiO₂/Py axis while in the Na₂O/Al₂O₃ axis no clear significant changes were observed; suggesting that the amount of Na₂O/Al₂O₃ ratio does not directly affect the formation of ferrierite crystal. Ferrierite phase will only be obtained when the range of SiO₂/Py ratios are between 2 to 4. For SiO₂/Py ratios above 4, analcime type zeolite (classified into small pore zeolite) will be formed. Novotna et al. [2003] reported that analcime can be formed even in a free template system. Analcime also was found as a competitor in ZSM-5 template free synthesis. The gel composition having SiO₂/Al₂O₃ ratios which were more than 70, yielded impurities phases consisted of quartz and analcime [Aiello *et al.* 1987]. It can be suggested that the low pyrrolidine amount in high silica content of initial gel mixture is not sufficient to direct the formation of ferrierite framework. Analcime phase zeolite is produced instead in the small quantity of pyrrolidine template.

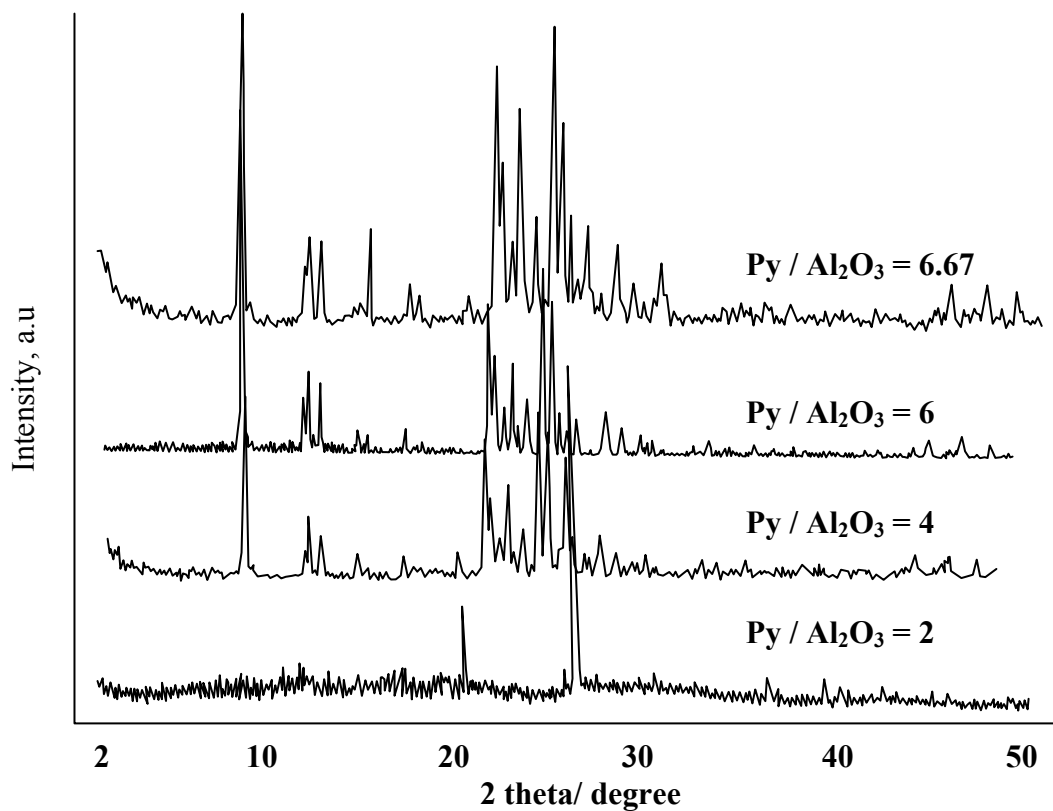


Figure 4.4: XRD patterns of ferrierite synthesized with different concentrations of pyrrolidine.

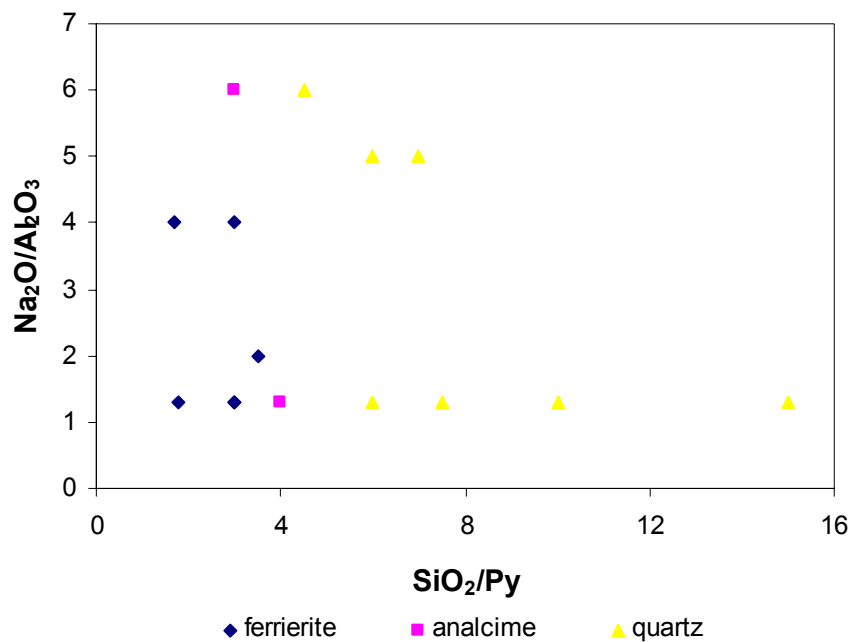


Figure 4.5: The distribution of formation of zeolite phase along the range of SiO₂/Py ratio and Na₂O/Al₂O₃ ratio

The solid product obtained differs when the SiO_2/Py ratios were further increased. XRD diffractogram confirmed that quartz was produced. Quartz is polymorphs of silicon dioxide and belongs to an informal group called the silica group. Quartz is usually obtained from rice husk ash when the ashes were burnt at a temperature more than 1000°C with prolonged time [James *et al.* 1986]. In this case, the small amount of pyrrolidine has little effect in the formation of zeolite framework; instead with the presence of concentrated polymeric silicate anion without structure directing agent will facilitate the formation of quartz.

Figure 4.6 shows the phase diagram of ferrierite and quartz phases obtained in each gel mixture when the SiO_2 , Py and Na_2O were varied within the ranges of 10-50 SiO_2 : 2-10 Py : 1.31-6 Na_2O . It is noted that for the formation of ferrierite, the mole percent of SiO_2 should vary from 48% to 75% and for pyrrolidine from 20% to 40% and for Na_2O it is around 1% to 25% only. As the $\text{SiO}_2/\text{Al}_2\text{O}_3$ ratio increases while other components remain the same, the quartz phase will be produced instead of ferrierite. From previous discussion, this circumstance is most probably due to the lack of OH^- in the gel mixture that will distort the solubility of rice husk ash and also the low amounts of template pyrrolidine to direct the formation of the structure of ferrierite.

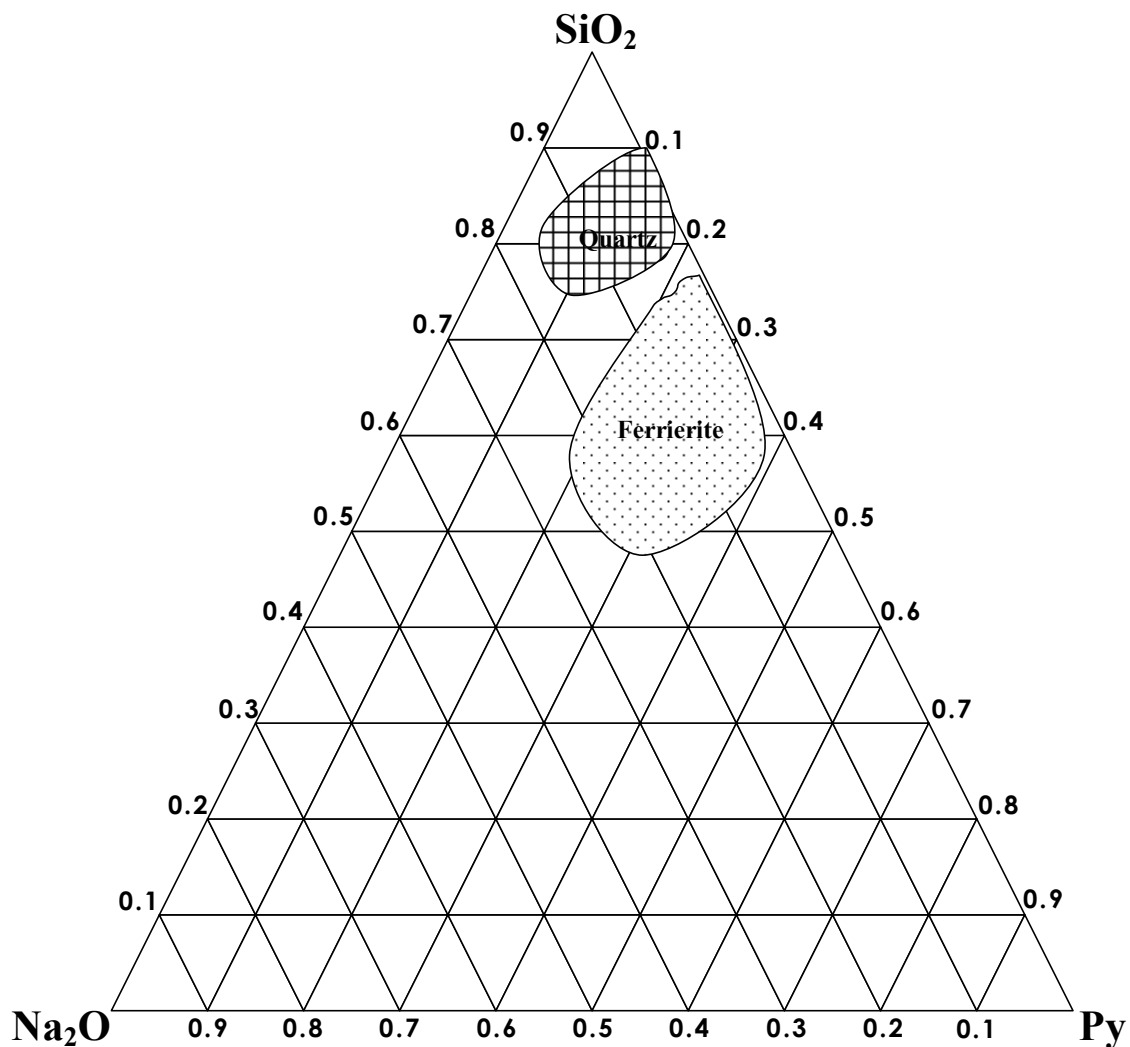


Figure 4.6: Phase diagram showing the ferrierite and quartz phase produced when the reaction mixture compositions of $\text{SiO}_2/\text{Py}/\text{Na}_2\text{O}$ were varied within the range of 10-50 SiO_2 : 2-10 Py : 1.31-6 Na_2O

* analcime was omitted in this diagram

4.2 Transformation of rice husk ash to ferrierite type zeolite

To study the transformation of rice husk ash to ferrierite, the synthesis was carried out at several crystallization periods i.e. 0.25, 0.5, 1, 2, 3, 4, 7, 9 and 12 days using initial molar oxides composition of sample Fer-12. The temperature was kept constant at 200°C. The transformation of rice husk ash to ferrierite was monitored using X-Ray Diffraction Technique (XRD), FTIR, ²⁹Si MAS NMR, nitrogen adsorption and Scanning Electron Microscopy (SEM).

4.2.1 X-ray Diffraction Study

The XRD pattern for each sample that was produced at different crystallization periods is presented in Figure 4.7. At 0.25 day, the solid product was found unchanged in an amorphous phase since no diffraction peaks was observed in the XRD pattern. The XRD diffractogram of the sample at 0.25 day illustrates a pattern similar to that of rice husk ash as the initial silica source. When the crystallization was prolonged to 0.5 day, a few small peaks appeared at 2θ 9.5° and 24.3 and 25.1° which correspond to the earlier formation of ferrierite phase. The amorphous phase was still the dominant phase in this solid product. It suggests that during this period, the gel continued to dissolve and transform into the ferrierite phase. This stage that is called “reaching of supersaturation state” occurs when the solution contains more dissolved solid than it does at its equilibrium state then followed by nucleation. During the transformation, no other crystalline phase was observed beside the ferrierite. After 1 day of crystallization, some intense peaks appeared at 2θ 9.5, 17.28, 13.4, 22.4, 23.5, 24.3, 25.1 and 25.6, and corresponds to the peaks for ferrierite. The fact that only ferrierite phase is formed showed that the dissolution of the amorphous gel, followed by the nucleation of ferrierite took place only within 1 day of crystallization. The ferrierite nucleus that was formed in 0.5 day crystallization in this case acted as seeds that play an important role in the growth of ferrierite crystals. The nucleation of ferrierite particles was then followed by the growth of ferrierite crystals.

As the crystallization period was extended to 12 days, the unstable crystallinity was observed in the sample. It indicated that even though the transformation of rice husk ash into ferrierite phase occurs within one day, the crystallization processes in which the ordering and rearrangement of precursor species on the growing crystal phase still occurs. This phenomenon will affect the crystallization rate and also at the same time will dissolve the crystal faster than the growth itself.

The percentage of crystallinity of zeolite ferrierite with time of crystallization is shown on Table 4.4. It is clearly observed that formation of ferrierite from rice husk ash increased drastically in the first day of crystallization. When the crystallization period was extended to 1 day, the crystallinity of ferrierite increased significantly up to 95.87%. The lowering of the crystallinity between 1 to 9 days proved that some rearrangement and ordering of the crystals occurred. The crystallinity has reached maximum stabilization in 9 days and remains constant until 12 days of crystallization. Based on these findings, it is suggested that the optimum crystallization period for the transformation of rice husk ash to ferrierite should taken as 9 days in order to allow the stabilization of the ferrierite structure formed earlier.

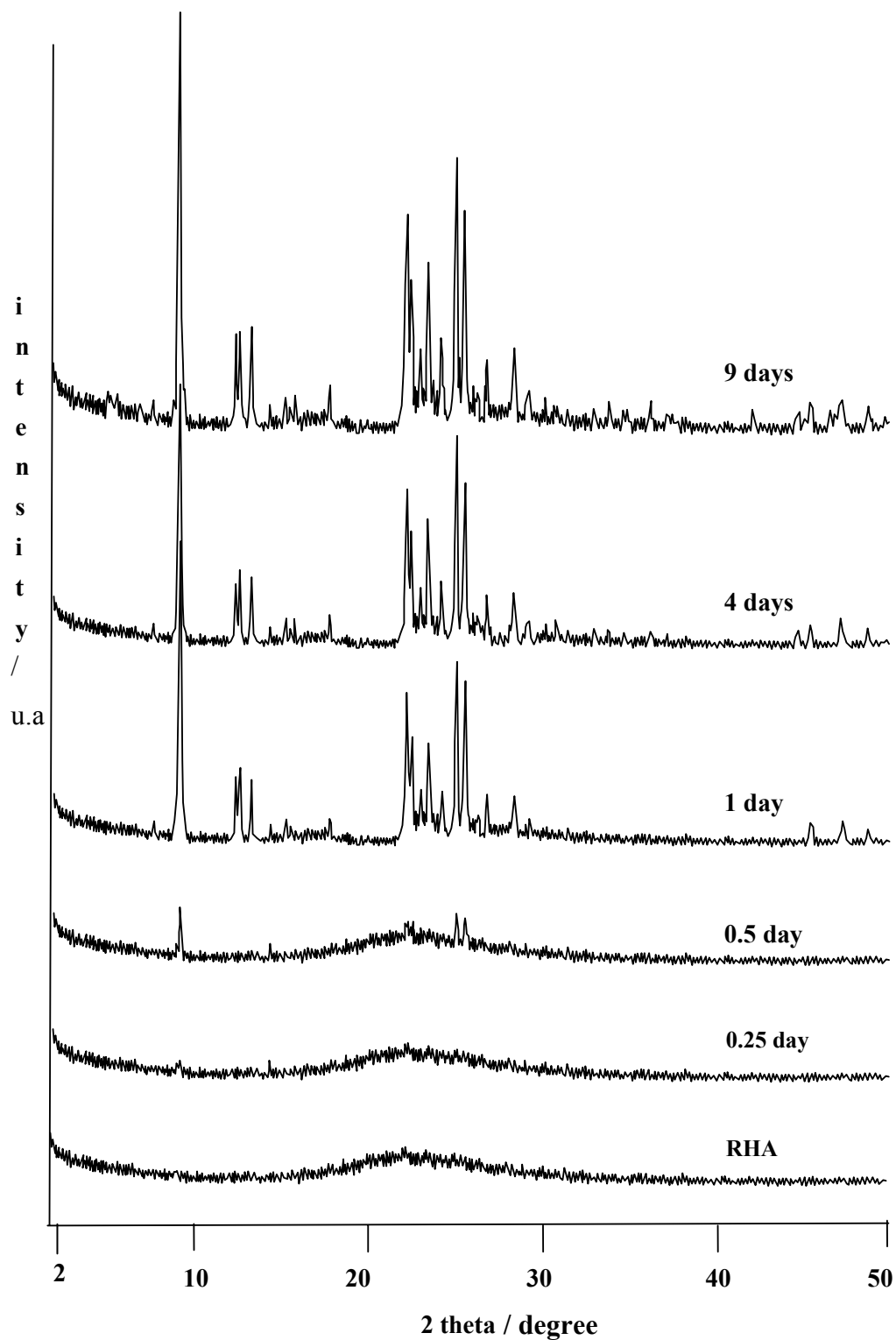


Figure 4.7: X-ray diffractogram pattern for sample Fer-12 under various crystallization periods.

Table 4.4: The influence of crystallization period on the solid weight of the products for the formation of ferrierite

Sample	Time, day	Phase product	Solid weight/RHA, %	% of crystallinity
RHA	0	Amorphous silica	95.5	0
Fer-4-0.25	0.25	Amorphous silica	77.27	0
Fer-4-0.5	0.5	Amorphous silica + FER	78.68	26.31
FER-4-1	1	FER	78.4	95.87
FER-4-2	2	FER	82.7	93.75
FER-4-3	3	FER	83.51	89.97
FER-4-4	4	FER	85.94	88.9
FER-4-7	7	FER	87.8	92.68
FER-4-9	9	FER	90.93	100
FER-4-12	12	FER	92.91	99.45

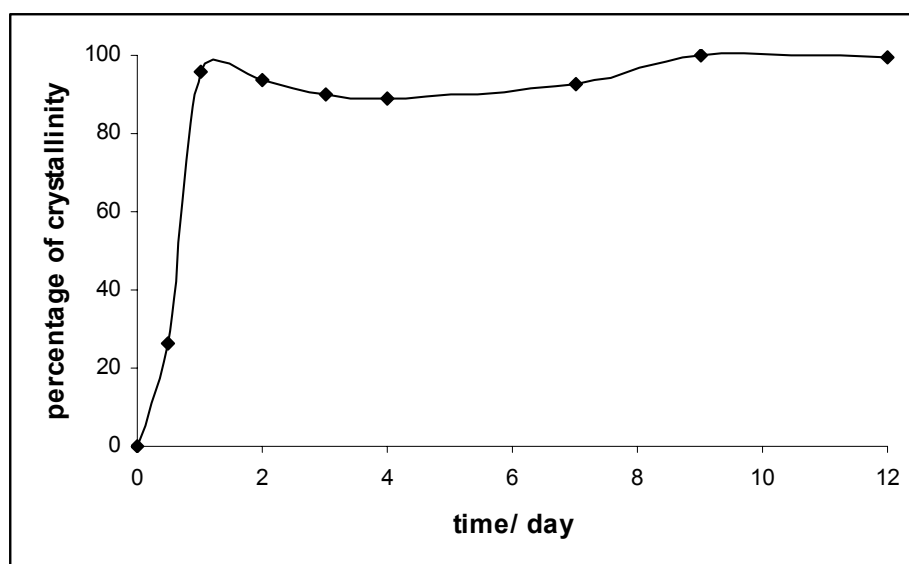


Figure 4.8: Crystallization curve for ferrierite from rice husk ash in sample Fer-12

4.2.2 The solid weight

The transformation of rice husk ash to ferrierite is also monitored by measuring the weight of the product formed with the time of crystallization. Solid product which was prepared at different crystallization period was dried and calcined at 550°C for at least 6 hours to remove all templates and any volatile compounds. The temperature that was used in calcination was set at 550°C to ensure all templates that were trapped in the framework (pore of ferrierite) were removed sufficiently. Table 4.4 reveals the percentage of solid product weight to rice husk ash as a function of the crystallization period. Solid that was obtained before the crystallization process begins gave 95 % wt. It decreases to 77 % wt. at 0.25 day crystallization which is a 21 % decrease from the initial gel mixture. After 0.50 day crystallization, the percentage of solid product increases slightly up to 79 %. The amounts of solid weight continuously increased gradually with time until 12 days crystallization. During the preparation of the gel mixture, only 5% of the gel was dissolved because the gel containing amorphous phase of silica rice husk ash has low solubility at room temperature. When the gel mixture was kept at 200°C within 0.25 day, the amount of solid product decreased, indicating that the solubility of the amorphous gel increased. Barrer reported that the solubility of amorphous silica gel increased up to 6.2×10^{-2} g for each 100 g of silica at 200°C [Barrer, 1982]. In addition, the solubility of silica increases in the presence of OH⁻ that might facilitate the formation of polymeric silica anions. Besides that, Scott [1996] reported that, high alkaline solution will decrease the production of colloidal particles of silica in which will facilitate the formation of polymeric silicate anions due to the sufficiency of charge compensation. This gradually facilitates the dispersion of amorphous gel and turns it into ferrierite crystal in the presence of template. This finding is consistent with the XRD diffractogram of the sample at 0.25 day (Figure 4.7), which reveals the existence of amorphous pattern in the solid product. After 0.25 day, the percentage of solid weight increases gradually up to 12 days of crystallization in which the formation of ferrierite crystal started to grow at 0.5 day.

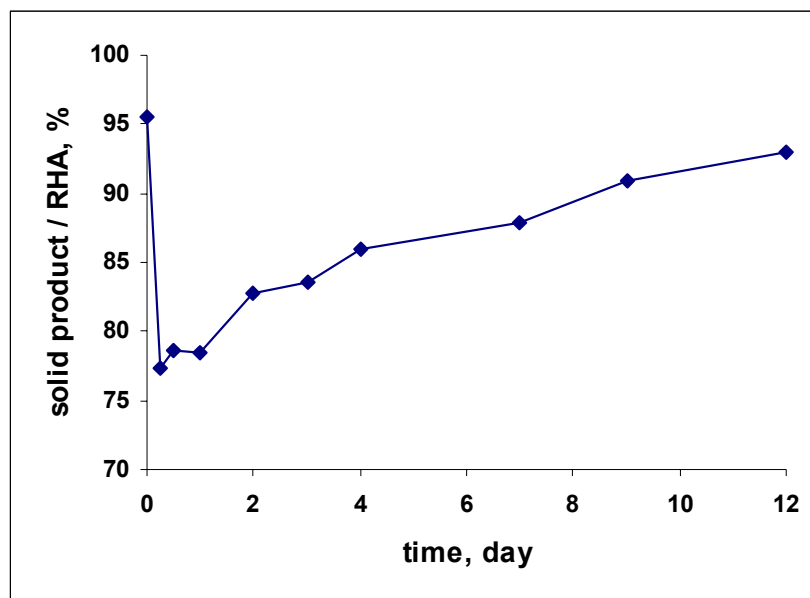


Figure 4.9: The percentage of solid products obtained over the initial rice husk ash with time of crystallization

4.2.3 Fourier Transform Infra Red Study

Transformation of rice husk ash to ferrierite was monitored using FTIR which focuses on the changes of the intensities of bands at $1080\text{-}1060\text{ cm}^{-1}$, 790 cm^{-1} and $470\text{-}430\text{ cm}^{-1}$. Figure 4.10 shows the FTIR spectra for samples Fer-12 at various crystallization periods. The FTIR spectra of rice husk ash in Figure 4.9 (RHA) shows the vibration patterns of the silica rice husk ash used. A broad peak at 1103 cm^{-1} corresponded to the asymmetric stretching for SiO_4 tetrahedron, and very intense peaks at 801 cm^{-1} and 461 cm^{-1} , both assigned to symmetric stretching for SiO_4 tetrahedron and Si-O bending for silica in rice husk ash. These three peaks can be assigned to the internal vibration of tetrahedral SiO_4 and are normally observed in silica or zeolite type materials.

Sample at 0.25 day crystallization shows similar spectrum to that of the RHA. However, the asymmetric stretching band for SiO_4 has shifted to lower wavenumber, from 1103 cm^{-1} in rice husk ash to 1075 cm^{-1} in the solid product. The same observation was found for symmetric stretching of TO_4 and Si-O bending in which each band shifted to the lower wavenumbers. This indicates that silica bonding in rice husk ash has been replaced by Al atoms that are responsible for the shifting of the wavenumber of the major vibrations bands.

After 12 hours of crystallization (half day), two new bands appeared in the spectrum of sample 0.5 day (Figure 4.9; 0.5) at 1228 cm^{-1} and 581 cm^{-1} . These two bands are recognized as the typical characteristics bands for zeolite phase. The first new peak appears at 1228 cm^{-1} which was assigned to the asymmetric stretching mode of the external TO_4 linkages. This band that was classified under the structure sensitive for zeolite vibrations occurs with the change of topology and building unit of zeolite framework [Flanigen *et al.*, 1971]. The second band observed at 581 cm^{-1} with only a small intensity, is corresponding to the vibration of double ring of ferrierite framework. The appearance of the band for asymmetric stretching and double ring vibrations proved that at this stage, the nucleation of ferrierite framework has started in the gel solution. This observation is parallel with the XRD finding which further proved that the framework buildings for ferrierite started to form at 0.5 day crystallization. The shifting of the band to the lower wavenumber proved that the incorporation of aluminium into the tetrahedral SiO_4 has taken place and it is the starting of the crystallization process to form ferrierite framework.

For sample synthesized within 1 day crystallization period, the FTIR spectrum shows that several new peaks appeared at 527 cm^{-1} and 439 cm^{-1} in which each was assigned for double ring vibration and T-O bending for zeolite framework. One interesting feature that was observed in this sample is the increase of the intensity for double ring vibration for ferrierite at 585 cm^{-1} . This intense peak explained the increase in the crystallinity of the ferrierite crystal, which is a good agreement with the XRD results. As the crystallization period was extended to 12 days, the FTIR spectra for each sample show the enhancement of vibration intensities and the shifting of several peaks towards lower wavenumbers. The increase of the peak intensity was clearly observed for the double ring vibration at 582 cm^{-1} and for

asymmetric stretching at 1063 cm^{-1} to become broader with the extension of the crystallization period. These results might be due to the increasing ferrierite crystallinity.

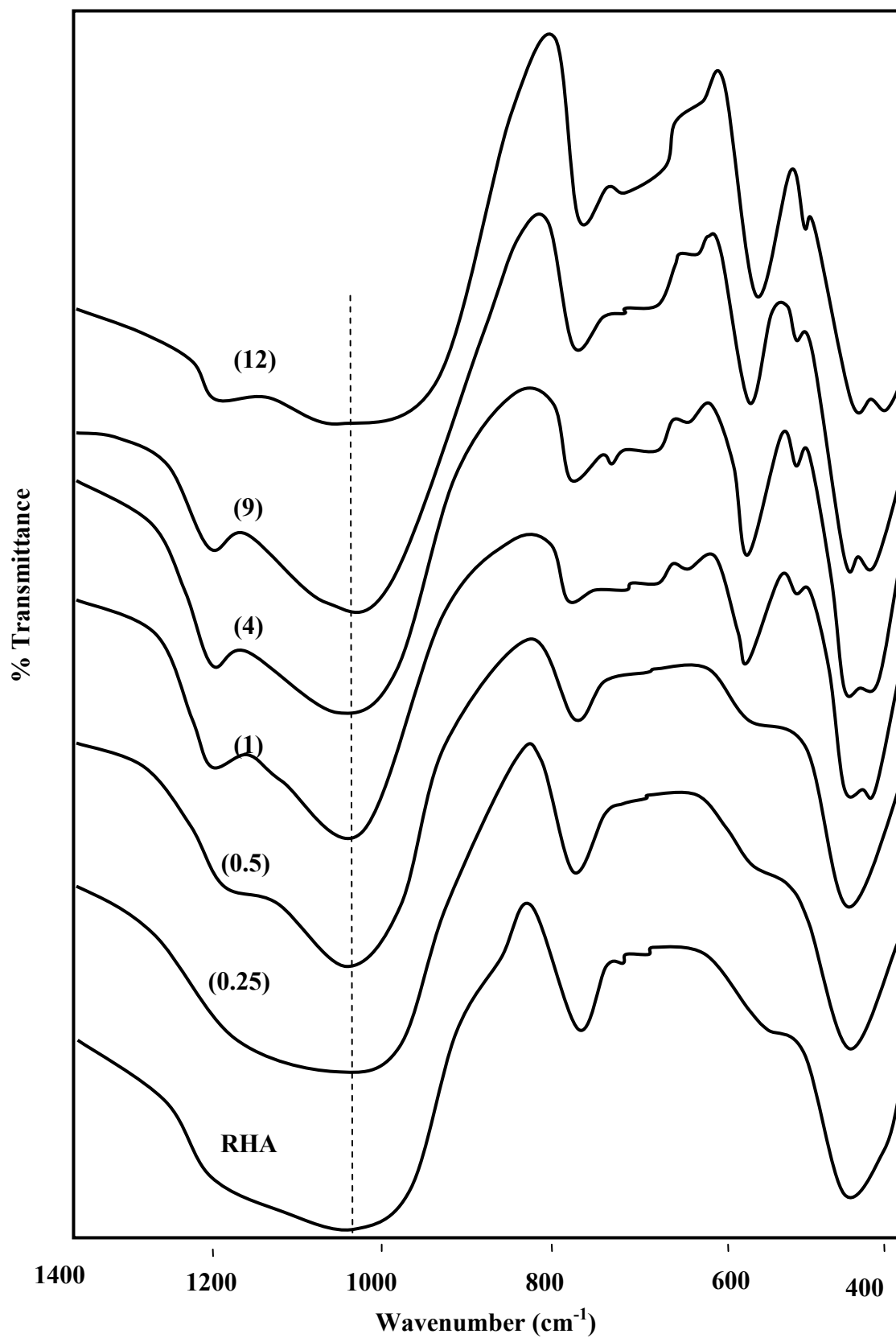
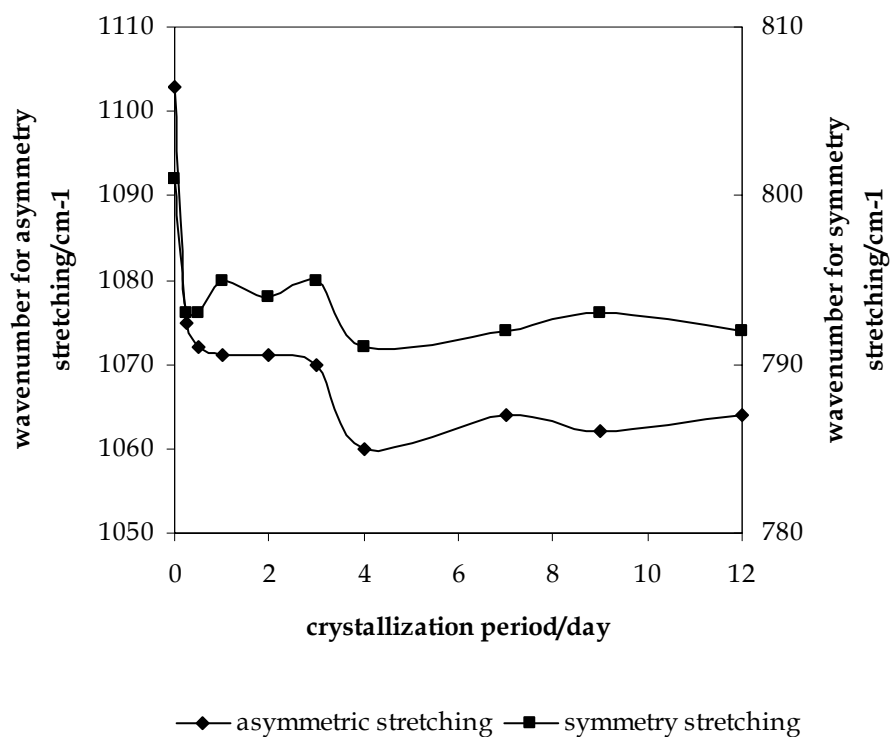


Figure 4.10: FTIR spectra for sample FER-12 at various crystallization period

Table 4.5: FTIR wavenumbers observed for each sample

Sample	TO ₄ Stretching (T= Si, Al)			Double Ring, cm ⁻¹		T-O Bending, cm ⁻¹	
	Asymmetry,		Symmetry, cm ⁻¹				
	cm ⁻¹	cm ⁻¹		cm ⁻¹			
RHA	-	1103	801	-	-	467	
0.25	-	1075	793	-	-	463	-
0.5	1228	1072	793	581	-	462	-
1	1235	1071	795	585	527	462	439
2	1241	1071	794	585	526	462	436
3	1236	1070	795	585	526	462	438
4	1235	1060	791	508	523	462	431
7	1233	1064	792	582	524	463	435
9	1235	1062	793	582	524	462	435
12	1235	1064	792	582	524	463	434

**Figure 4.11:** The changes of asymmetric and symmetric stretching for TO₄ bending with crystallization periods

Closed observation towards the shifted asymmetric and symmetric stretching for TO_4 bending was illustrated in Figure 4.11. The wavenumber of each sample shifted to the lower frequency with the extended crystallization period. By focusing to the asymmetric stretching of TO_4 at 1103 cm^{-1} to 1060 cm^{-1} region, it clearly shows that the shifting increased as early as 0.25 day crystallization. Though the ferrierite framework was not formed yet at 0.25 day, the incorporation of aluminium into the tetrahedral framework has already occurred as shown by the right shifting of vibration from 1103 cm^{-1} to 1075 cm^{-1} and 801 cm^{-1} to 793 cm^{-1} . It can be suggested that at this stage, the silicate anion of rice husk ash and aluminium (III) began to react to form aluminosilicate gels. It should be noted that, the solids samples studied were not the aluminosilicate solutions, but the solid gel samples obtained after the filtering and drying of the aluminosilicate gels [Scott, 1996]. The shifted of vibration to lower frequency was continuously observed until the fourth day of crystallization. The shifted wavenumber of asymmetric stretching for TO_4 shows that the incorporation of aluminium into ferrierite framework slowly occurs with the growth of ferrierite crystals. Figure 4.8 shows the optimum crystallization process which can be achieved at 4 days crystallization.

4.2.4 Nitrogen Adsorption Study

The calcined solid samples obtained at different crystallization period were further characterized with nitrogen adsorption technique to verify the sorption properties and pores system. Zeolites are classified as microporous materials, in such that ferrierite is expected to give the adsorption isotherm of type I compared to rice husk ash that is known as nonporous materials. The nitrogen adsorption isotherms of the calcined samples are illustrated in Figure 4.12. It can be seen that the significant changes of adsorption isotherm occurred from type II for rice husk ash to type I for sample at 9 days crystallization and it was explained that the amount of nitrogen adsorption increased with the increasing crystallinity. The XRD and FTIR results are parallel which explains that ferrierite crystals began to grow as early as 0.5 day and it was further proven by isotherm adsorption for sample at 0.5 day crystallization. Rice

husk ash and samples at 0.25 day crystallization show similar isotherm type II which show signs of nonporous materials. This clearly indicates that the solid sample at the early stage of crystallization does not contain ferrierite materials; the main component might be the amorphous aluminosilicate gel.

For samples at 12 hours crystallization period, it was clearly seen that the changes of adsorption isotherm has started to show Type I isotherm which is the characteristic of microporous materials. The similar isotherm was observed for samples at long crystallization period. However, the total volume of nitrogen adsorption for this sample is still relatively low showing that the solid is not fully crystallized. The adsorption isotherm for sample at 1 day as well as 9 days crystallization occurs at similar adsorption volume which means that the ferrierite crystals grow as early as 12 hours crystallization and completely form at one day crystallization. However, at the end of relative pressure, the plot for sample at 0.5, 1 and 9 days of crystallization was slightly increased which is turn to Type II isotherm. This is due to the monolayer adsorption and condensation capillary process occurred during the measurement. In order to prove that solid obtain are microporous material, the α_s method are employed. The α_s value was determined using the Equation 3.3 and α_s plot for each sample as shown in Figure 4.13. Samples at 0.5, 1 and 9 days of crystallization, shows the α_s plot that correspond to type I isotherm which was further prove that samples are microporous materials [Bhambani, 1972].

The BET surface area of the calcined samples synthesized at different crystallization period shows that the surface area increased drastically when the crystallization period was extended to 1 day crystallization. Table 4.5 shows the surface area for sample at 0.25 day crystallization as $7.81 \text{ m}^2/\text{g}$ which is nearly the same as the surface area of rice husk ash. The surface area increased continuously up to 1 day crystallization where it became constant up to 9 day crystallization ($299.62 \text{ m}^2/\text{g}$). Figure 4.14 illustrates the correlation between surface areas, pore diameter and pore volume of each sample at various crystallization periods. Other than the surface area, the pore volume of sample also increases from $0.034 \text{ cm}^3/\text{g}$ at 0.25 day to $0.18 \text{ cm}^3/\text{g}$ at 9 days crystallization. Rice husk ash which is a nonporous material

gives high pore diameter and had been transferred into microporous material, namely ferrierite. The curve of pore diameter presented in Figure 4.14 reveals that the average diameter size of pore decreased from 153.28 Å at 0.25 day to 26.59 Å when the crystallization was prolonged to 9 days of crystallization. This further consolidates that ferrierite has been successfully formed from rice husk ash as early as 12 hours and completed as early as 1 day crystallization.

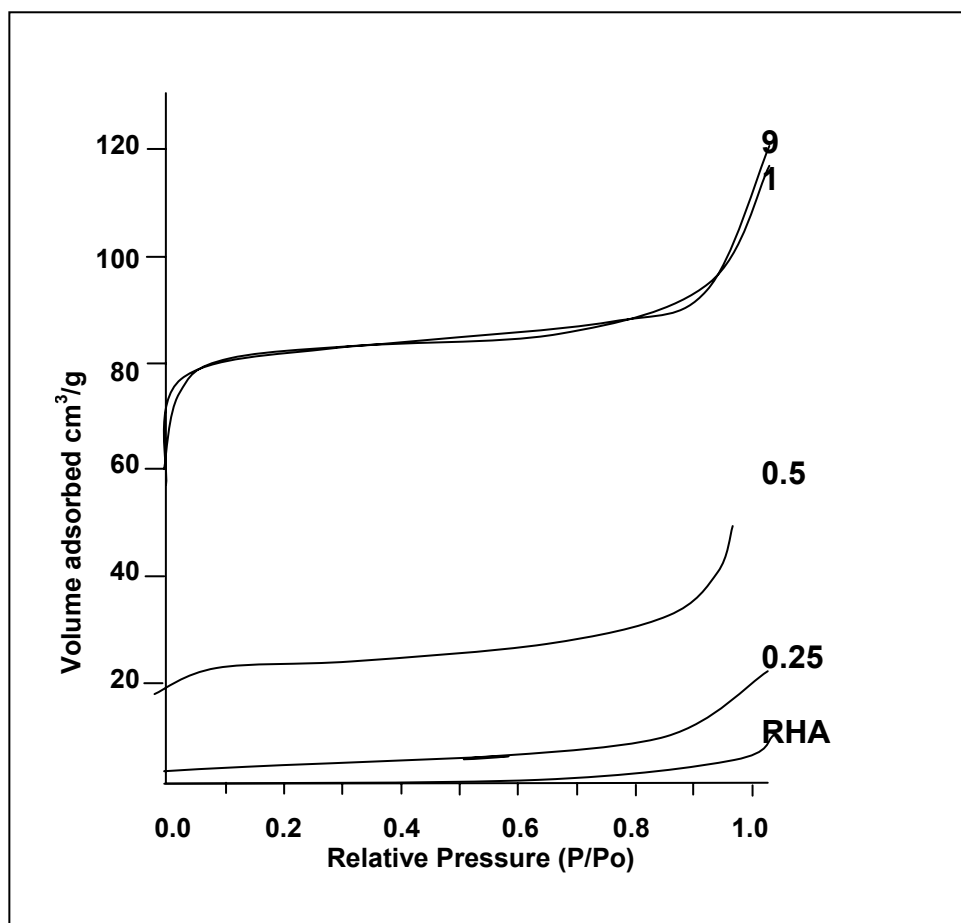


Figure 4.12: N₂ adsorption isotherm of calcined samples at various crystallization period

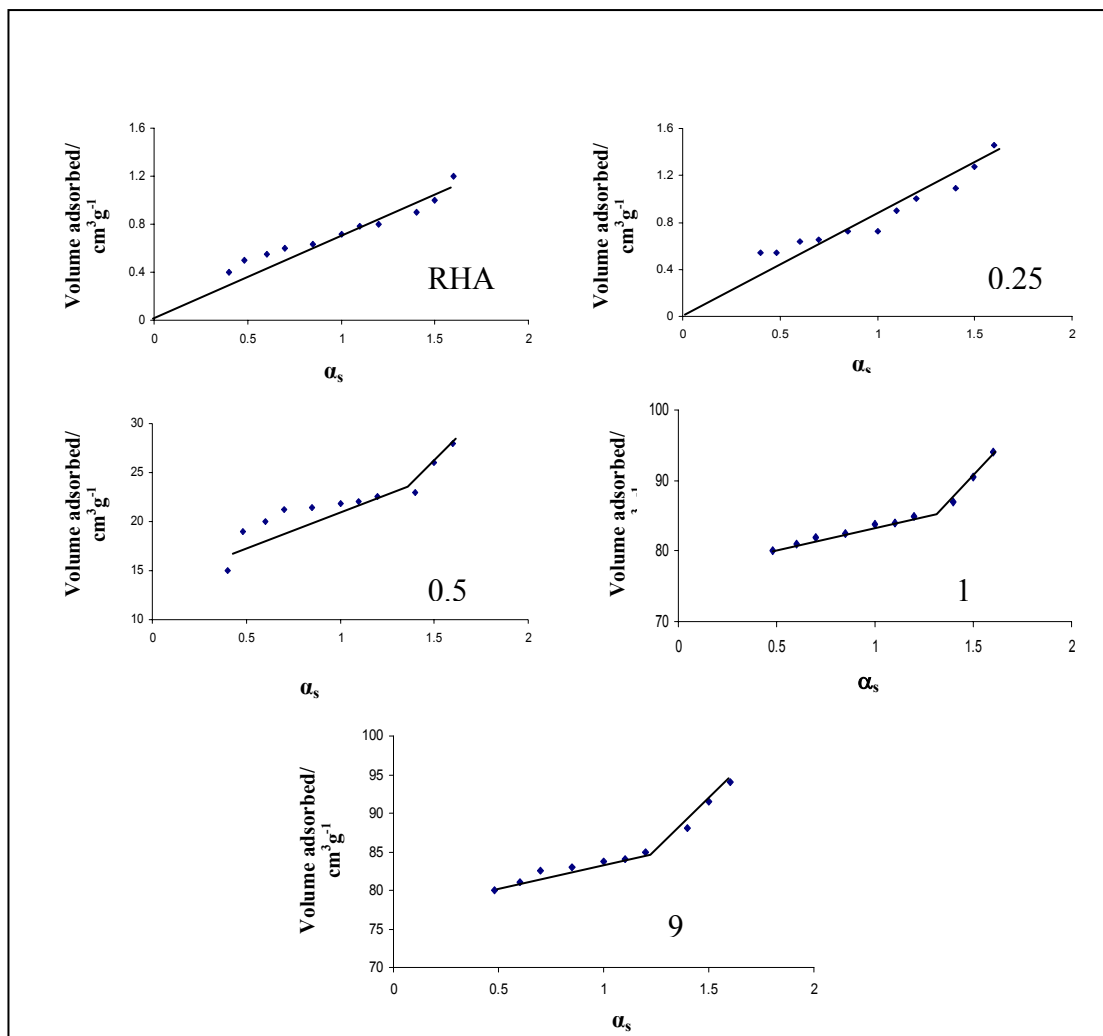


Figure 4.13: α_s plot for sample at different crystallization period

Table 4.6: The BET surface area, average pore diameter and pore volume of sample Fer-4-Py crystallized at different periods.

Sample	BET surface area / m ² /g	Average Pore Diameter/ Å	Pore volume / cm ³ /g
RHA	4.00	153.00	0.034
Fer-4-0.25	7.00	153.00	0.034
Fer-4-0.5	59.00	45.00	0.067
Fer-4-1	299.00	24.00	0.059
Fer-4-9	280.00	26.00	0.18

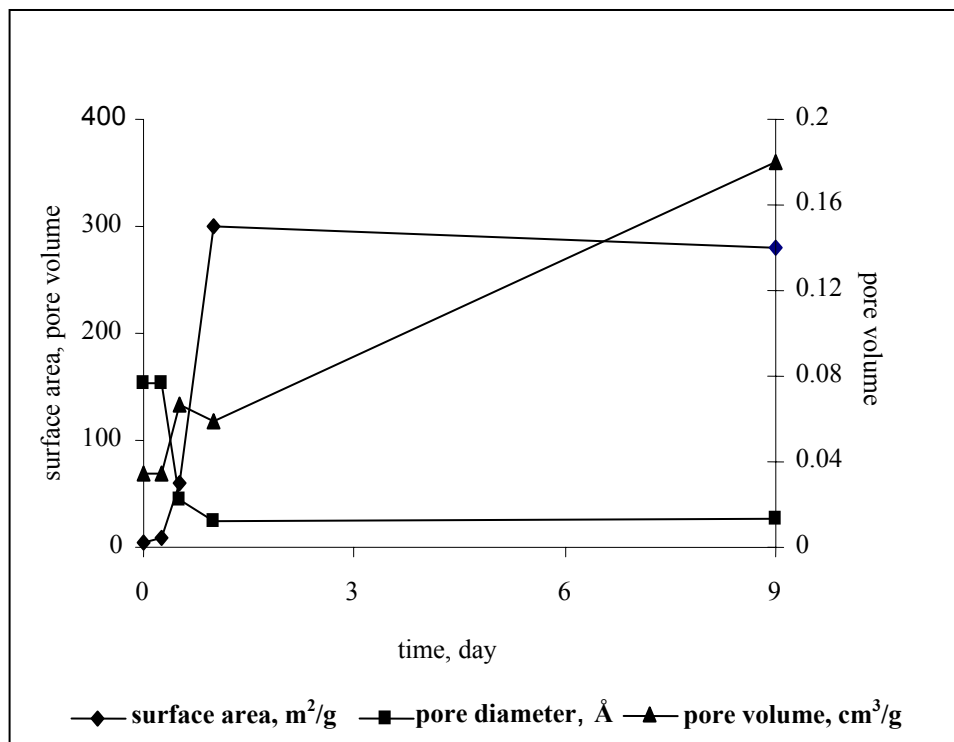


Figure 4.14: Correlation between surface areas, pore diameter and pore volume of sample Fer-12 at different crystallization period

4.2.5 ²⁹Si MAS NMR Spectroscopy Study

White solid samples obtained at various crystallization periods were further characterized using the powerful ²⁹Si MAS NMR technique. This technique was employed for measurement of local environment of tetrahedral SiO₄. Figure 4.15 illustrates the ²⁹Si MAS NMR spectrum for solid samples obtained at various crystallization periods. In general observations, it shows that the reallocation of NMR signals towards higher ppm occur with extended crystallization time. At 6 hours crystallization, a broad signal appeared with the maximum centered at -105 ppm. This indicates the existence of SiO₄ tetrahedron (3Si,1Al). This broad peak indicates that the aluminium has been incorporated into silicon tetrahedron which is further confirmed by the XRD studies. With the extension of crystallization period to

12 hours, the signals which comprised of two broad peaks that overlap at -100 ppm and -108 ppm have slightly shifted towards the higher field. The broad peak becomes narrower and the maximum signal appeared at -108 ppm which slightly shifted to the higher field. The existence of the shoulder at -100 ppm which corresponds to the signal of $\text{Si}(\text{OSi})_3(\text{O}^-)$ in solid silicate explains that at this stage, the solid silicate still contains the amorphous silica that is not totally transformed into ferrierite phase [Prabir *et al.* 1994]. The shift of NMR signal at 12 hours crystallization from -105 ppm to -108 ppm indicated the changes of local environment occurring for $\text{SiO}_4(3\text{Si},1\text{Al})$.

After one day crystallization, the signal in lower field reduced with the increment of the signal in higher field. The NMR spectrum reveals an overlapping of three peaks centered at -105 ppm, -109 ppm and a new peak at -111 ppm. The signal at both -105 ppm and -109 ppm is assigned to $3\text{Si},1\text{Al}$ with different environment. A new peak at -111 ppm corresponds to the signal of tetrahedron $\text{SiO}_4(4\text{Si},0\text{Al})$ from aluminosilicate solid. With the appearance of these peaks, it is concluded that the characteristic spectral features for ferrierite which appeared in the one day crystallization is in agreement with XRD data [Datka *et al.* 2003]. The signal at -100 ppm is totally diminished, which explained that amorphous gel was totally transformed into SiO_4 tetrahedron ($3\text{Si},1\text{Al}$) in agreement with XRD data. As time of crystallization increased until 9 days, the signals become narrower which reflects the increasing crystallinity for each sample.

From ^{29}Si MAS NMR, the change of tetrahedron silica from solid silicate to solid aluminosilicate is clearly seen. The process begins with the dissolution of rice husk ash to form solid silicate $\{\text{Si}(\text{OSi})(\text{O}^-)\}$. Within 1 day of crystallization, the incorporation of aluminium into sodium silicate takes part to form aluminosilicate. The process of aluminium incorporation continuously occurred with the broadness of signal.

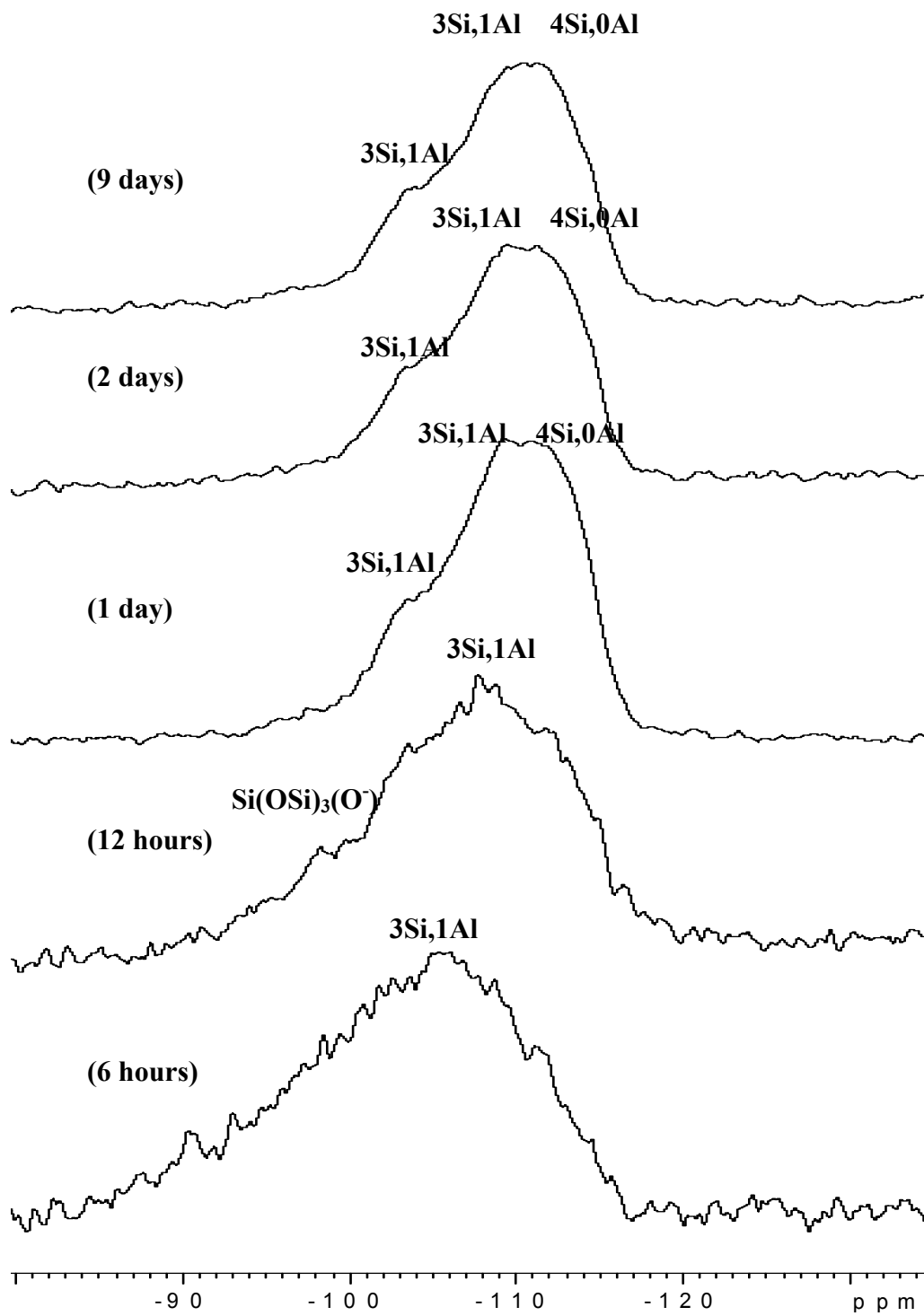


Figure 4.15: ^{29}Si MAS NMR spectrum for samples at various crystallization periods

4.2.6 Surface Morphology

The scanning electron micrographs (Figure 4.16) for the solids crystal obtained at different crystallization time reveal characteristic patterns of sizes. The morphology of the ferrierite crystals clearly indicated that the crystal size is strongly influenced by the crystallization period. In general, all samples gave a similar morphology of the crystal but with a difference in size. As the crystallization period was extended to 5 days, a mixture of the star-shaped particulates with small needles was formed (Figure 4.16b). A well-developed ferrierite crystal after 12 days of synthesis in association with star-shaped particle without small needles is presented in Figure 4.16d.

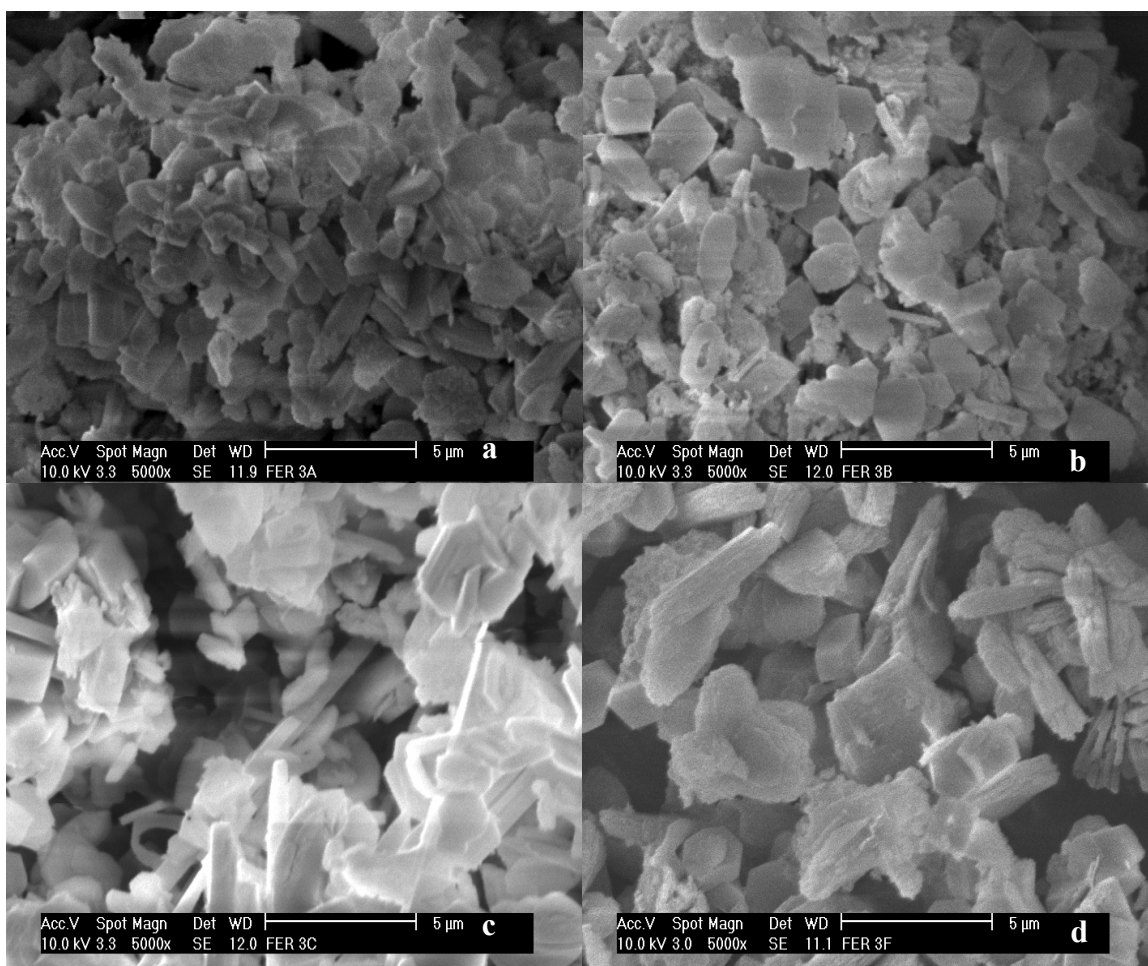


Figure 4.16: Scanning electron micrograph for ferrierite at different crystallization period (a) 1 day (b) 5 days (c) 9 days (d) 12 days

4.4 Acidity Study

4.4.1 ^{29}Si MAS NMR for H-ferrierite

The effects of the $\text{SiO}_2/\text{Al}_2\text{O}_3$ ratio towards the environment of silicon in ferrierite framework can be determined using ^{29}Si MAS NMR. Figure 4.17 shows the ^{29}Si MAS NMR spectra for each sample. The ^{29}Si MAS NMR spectrum of H-Fer 12, H-Fer 20 and H-Fer 30 contains two main peaks at -113 ppm and -106 ppm which were assigned for the Si(0Al) and Si(1Al) respectively. Figure 4.17 reveals the chemical shifting of samples that have been shifted to higher ppm and the spectrum became broader from H-Fer 12 to H-Fer 30 and followed by H-Fer 20. It shows that the silica content in ferrierite framework increased from H-Fer 12 to H-Fer 30 and H-Fer 20. This is in agreement with the Si/Al ratios of each sample which is represented in Table 4.7. The data was indicated by using equation 2.1 towards the deconvolution spectrum of ^{29}Si MAS NMR.

Generally, increasing the $\text{SiO}_2/\text{Al}_2\text{O}_3$ ratio in the initial gel of reaction will increase the Si/Al ratio in the framework. From Table 4.7, it is shown that the Si/Al ratio increased from H-Fer 12 (5.4) to H-Fer 20 (7.8) but decreased in H-Fer 30 (6.9). Samples H-Fer 12 and H-Fer 20 were synthesized using the same gel ratio but with the increase of $\text{SiO}_2/\text{Al}_2\text{O}_3$ ratios from 12 to 20. However, for H-Fer 30, it was synthesized using the different $\text{SiO}_2/\text{Al}_2\text{O}_3$ ratio (30) and Py/ Al_2O_3 ratio (10) while other parameters remain same. The insignificant finding might come from the different initial ratios that have been used in synthesis. H-Fer 30 with initial $\text{SiO}_2/\text{Al}_2\text{O}_3$ ratio 30 is difficult to obtain based on the Si-rich ferrierite which has a Si/Al ratio of 10.4 [Engelhardt, 1987]. It is suggested that only a half amount of initial silica take part in the formation of ferrierite framework, whereas the rest is still in the form of silicate solution. Besides that, the amount of Si/Al ratio obtained from NMR for H-Fer 30 is close to the amount of H-Fer 20. By comparing the SiO_2/Py ratios for both compositions, it is found that the ratio is nearly the same which is 3. This observation explains that the amount of Si/Al ratio obtained also depends on the amount of SiO_2/Py ratio in the initial composition.

The results obtained from NMR explain the insignificant finding observed in FTIR pyridine adsorption study and TPD NH_3 study. With the increasing $\text{SiO}_2/\text{Al}_2\text{O}_3$ ratio (Si/Al ratio), the number of acid sites will decrease due to the decrement of aluminium in zeolite framework. Similar observations have been found by Derouane which used H-Beta at different Si/Al ratios. With the increasing Si/Al ratio, the amount of yield decreased due to the low amounts of aluminium in framework. The low Si/Al ratio provided the higher polarity which enhances the competitive adsorption of polar molecules in particular that of the nitrogen and pyridine in these cases [Derouane *et al.* 2000]. H-Fer 30 which failed to give high Si/Al ratio as expected gives the amount of adsorbed NH_3 as well as pyridine in between with the amount obtained for H-Fer 12 and H-Fer 20. Results obtained by Peixoto *et al.* (2003) show that with the increasing Si/Al ratio of H-ferrierite from 8.2 to 15.9, the amount of NH_3 desorbed from TPD was decreased. This finding further proved that the high Si/Al will decrease the amount of acid sites.

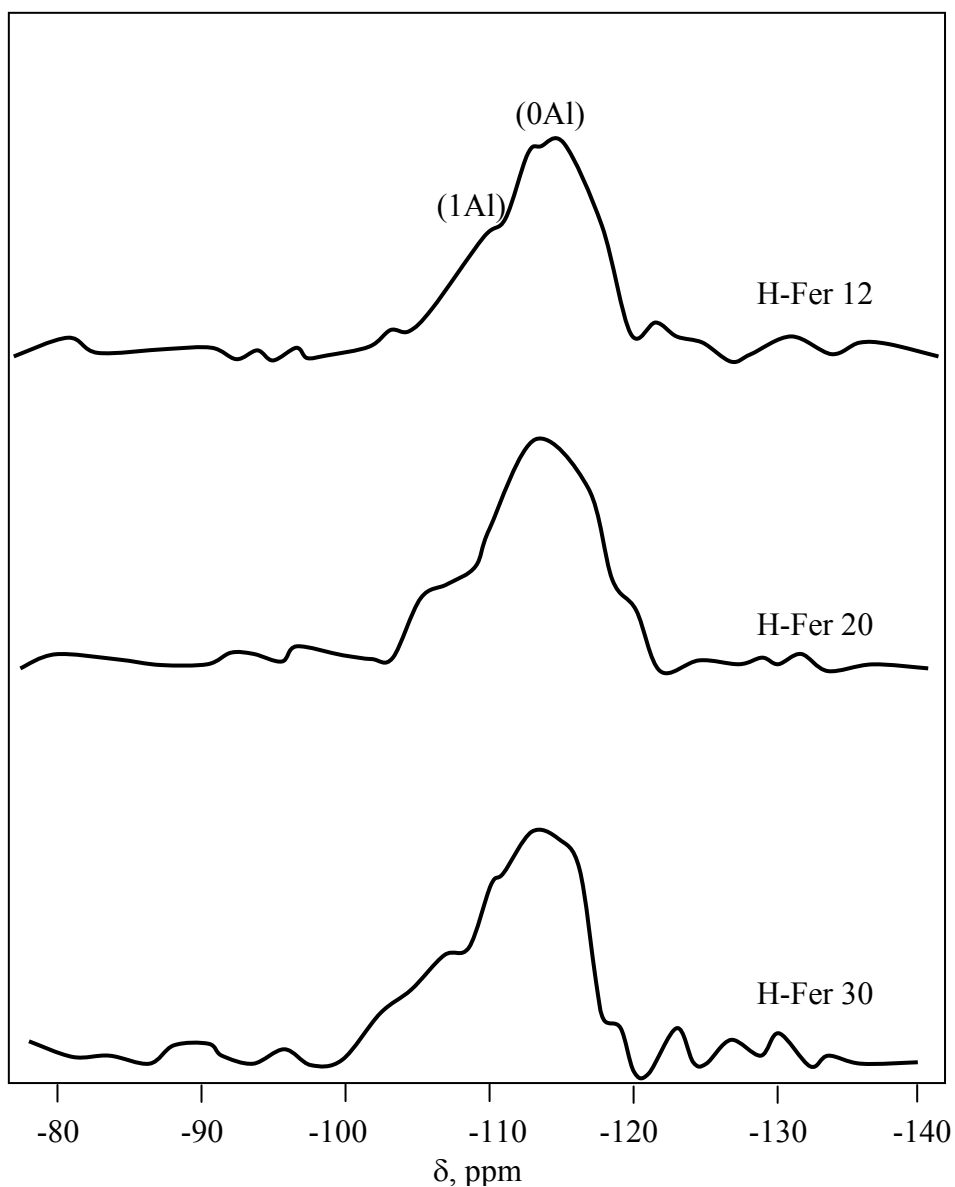


Figure 4.17: ^{29}Si MAS NMR spectra for sample H-ferrite at different $\text{SiO}_2/\text{Al}_2\text{O}_3$ ratios

Table 4.7: The chemical shifting and Si/Al ratio of samples H-ferrite

Sample	Chemical shifting, ppm (relative intensity)		Si/Al ratio
	SiO_4 , (3Si, 1Al)	SiO_4 , (4Si, 0Al)	
H-Fer 12	-106	-114	5.4
H-Fer 20	-107	-116	7.8
H-Fer 30	-106	-114	6.9

4.3.2 Infrared Spectroscopy of Pyridine Adsorption

The determination of acid sites is important in order to understand the function and performance of acidic catalysts in the synthesis or transformation of hydrocarbons. The reactivity of zeolite depends on the strength and the number of acid sites in the framework. Active sites in zeolite are classified according to the types of Brønsted and Lewis acids. Brønsted acid site in zeolite occurs when the cations balancing of the anionic framework charge are protons, H^+ , which can be defined as a proton-donor-acidity [Szoastak, 1989]. Lewis acids arise at the electron deficient sites that can accept a pair of electron. In the case of zeolite, it usually acts as electron acceptor acidity. Generally, to determine the acid sites in zeolite, the characteristics vibration of silanol (OH) groups and the adsorption of base-molecules such as pyridine and ammonia are employed with the aim of using their spectral features. Pyridine as a strong base was chosen as the probe base due to its ability to interact with a wide scale of acid strength and it can also differentiate between the Brønsted and Lewis sites.

The *in situ* infrared spectroscopy of pyridine adsorption is employed to determine the type of acid sites that exists in H-ferrierite, which has been synthesized from rice husk ash. Interaction between pyridine and Brønsted acid sites in zeolites leads to the formation of pyridinium ion ($C_5H_4NH^+$) in zeolites framework as shown in Figure 4.18. For Lewis acid sites, the accessible aluminium cations in zeolites which play the role as electron pair acceptor will interact with the nitrogen lone pair in pyridine molecules.

The *in situ* FTIR spectra obtained for H-Fer 12 before and after pyridine adsorption are shown in Figure 4.19. Normally, in the hydroxyl region between 2500 cm^{-1} to 4000 cm^{-1} three bands were observed in the dehydrated H-zeolite samples, that was individually assigned for the vibration of bridging OH groups (3604 cm^{-1}), terminal silanol (SiO-H) groups (3745 cm^{-1}) and for AlO-H groups (3650 cm^{-1}) [Lercher *et al.*, 1996]. Figure 4.19a depicts IR spectrum of H-Fer 12 after dehydration at 400°C showing two bands at 3641 cm^{-1} and 3600 cm^{-1} where both were assigned to the vibration of Al-OH groups and bridging OH groups [Xu *et al.*

1996] and a shoulder at 3570 cm^{-1} which was assigned to hydroxyl group stretching band [Armaroli *et al.*, 2001]. No band was observed in the region of terminal silanol (SiO-H) groups which indicated that the samples content has no defect sites in the framework.

After adsorption with pyridine at room temperature, peak that was assigned for bridging OH group at 3604 cm^{-1} disappeared followed by the appearance of new peaks at 1542 and 1487 cm^{-1} in the pyridine region. According to the study by Wihcterlova, all these are due to the interaction of pyridine ($\text{C}_5\text{H}_5\text{N}$) with proton of the bridging OH groups [1998]. Another sharp band at 1637 cm^{-1} and shoulder at 1622 cm^{-1} are both assigned to the characteristics properties of pyridinium ion stretching that bind to Brønsted acid sites and to Lewis acid sites [Pais da Silva *et al.* 2002]. There are no peaks observed in the region of 1450 cm^{-1} to 1460 cm^{-1} where bands usually occur by the interaction of pyridinium ion with aluminium extraframework that was recognized as Lewis acid sites [Gabriella *et al.* 2000].

Pyridine was desorbed at 150°C and 400°C to measure the strength of Brønsted acid and Lewis acid for sample H-Fer 12. The intensity of pyridine peak relatively decreased with the increasing desorption temperature. Upon heating at 150°C , the intensity of the band at 1545 cm^{-1} decreased slightly in parallel to the reappearance of bridging OH group band at 3604 cm^{-1} . This proved the existence of Brønsted acid sites in H-Fer 12 framework. When the sample was further heated at 400°C , the band at 1545 cm^{-1} still remained with further decrease in intensity. Meanwhile, the bands in the region between 3700 cm^{-1} to 3400 cm^{-1} reappeared, similar to the pyridine adsorption before.

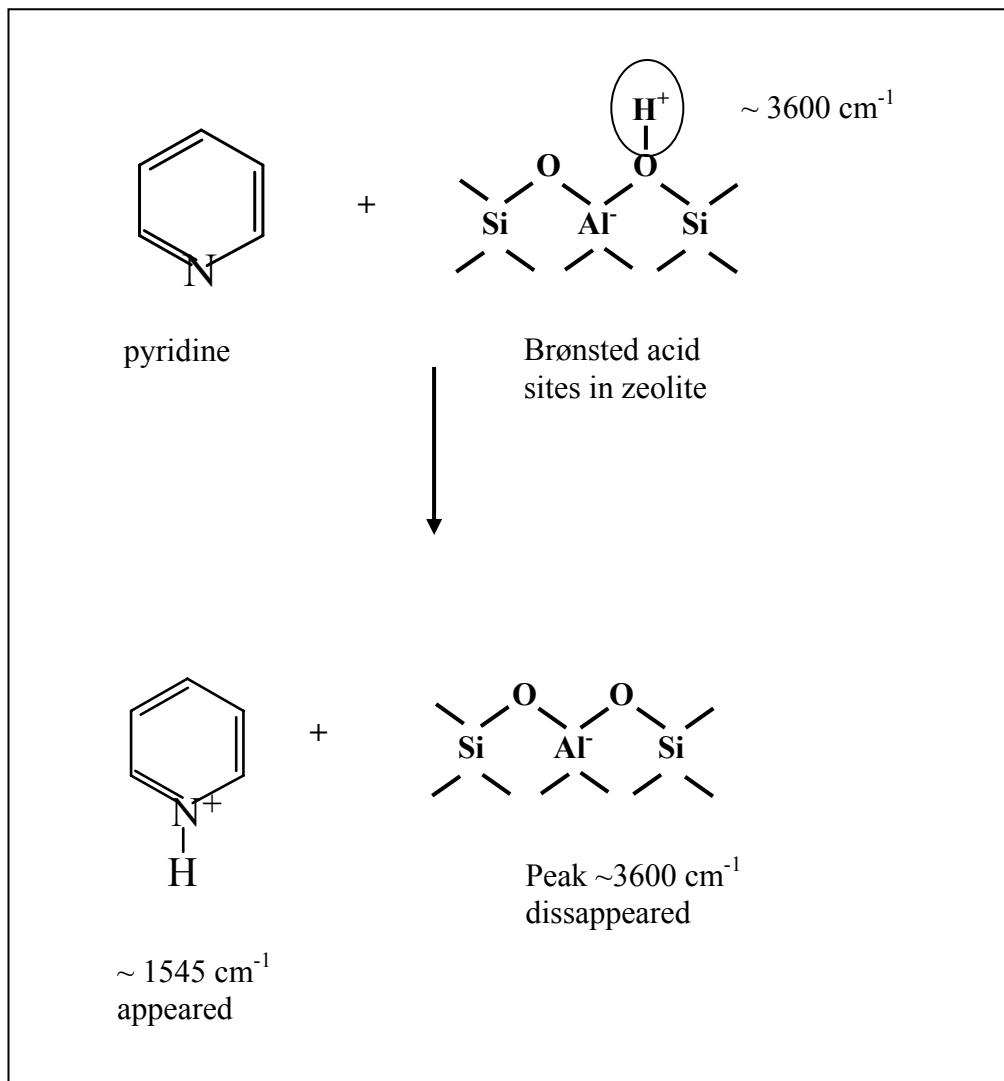


Figure 4.18: Proposed mechanism of interaction between pyridine molecules with Brønsted acid sites in zeolite.

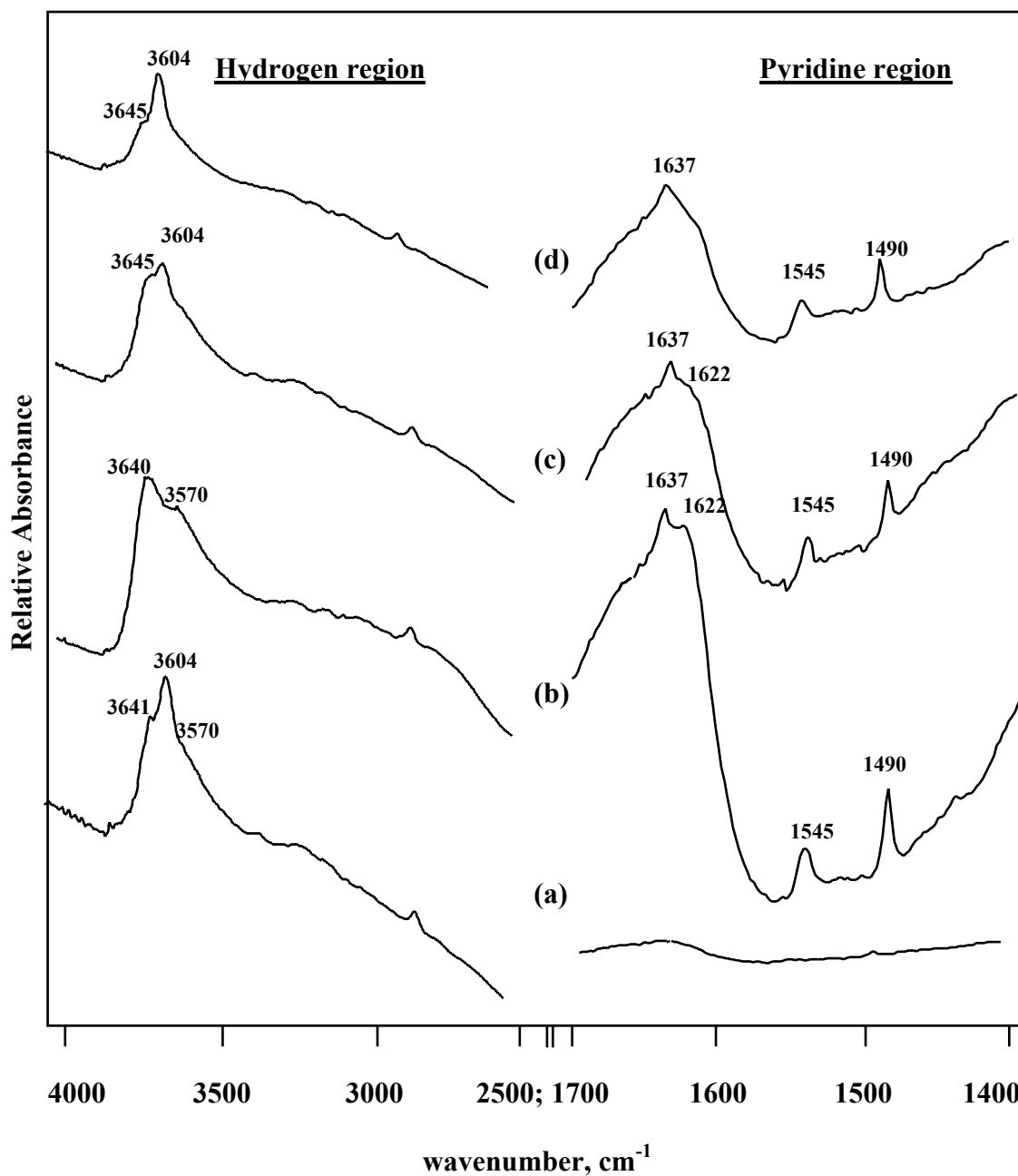


Figure 4.19: FTIR spectra of H-Fer 12 after (a) heated at 400°C, following thermal treatment of (b) pyridine desorbed at room temperature, (c) pyridine desorbed at 150°C and (d) pyridine desorbed at 400°C

Figure 4.20 shows the pyridine desorption FTIR spectra for sample H-Fer 12, H-Fer 20 and H-Fer 30 that were heated at 150°C. The calculated amount of Brønsted and Lewis acid sites are summarized in Table 4.8. It is noted that all samples have mainly Brønsted acid sites and are present only in a small quantity of Lewis acid sites. Similar observations were reported by Silva et al. [2002]. However, each sample has different peak intensity. The amount of acid sites present in catalysts was calculated using the equation reported from previous researcher [Ramli, 1995].

From Table 4.8, it shows the amount of acid sites in H-ferrierite framework increased with the decreasing Si/Al ratio obtained from ^{29}Si MAS NMR measurement. However, the amount of Lewis acid sites was not show significant changes with the decreasing or increasing $\text{SiO}_2/\text{Al}_2\text{O}_3$ ratio due to small amount of Lewis acid sites contain in catalysts. H-Fer 12 gives high amount of Brønsted acid sites and Lewis acid sites compared to other catalysts. For H-Fer 20, the amount of Brønsted acid sites is relatively lower than H-Fer 30 which is due to the higher amount of the Si/Al ratio in framework. These results are in agreement with the quantitative TPD NH_3 analysis showing that H-Fer 20 gives low amounts of adsorbed pyridine and ammonia and low amounts of acid sites.

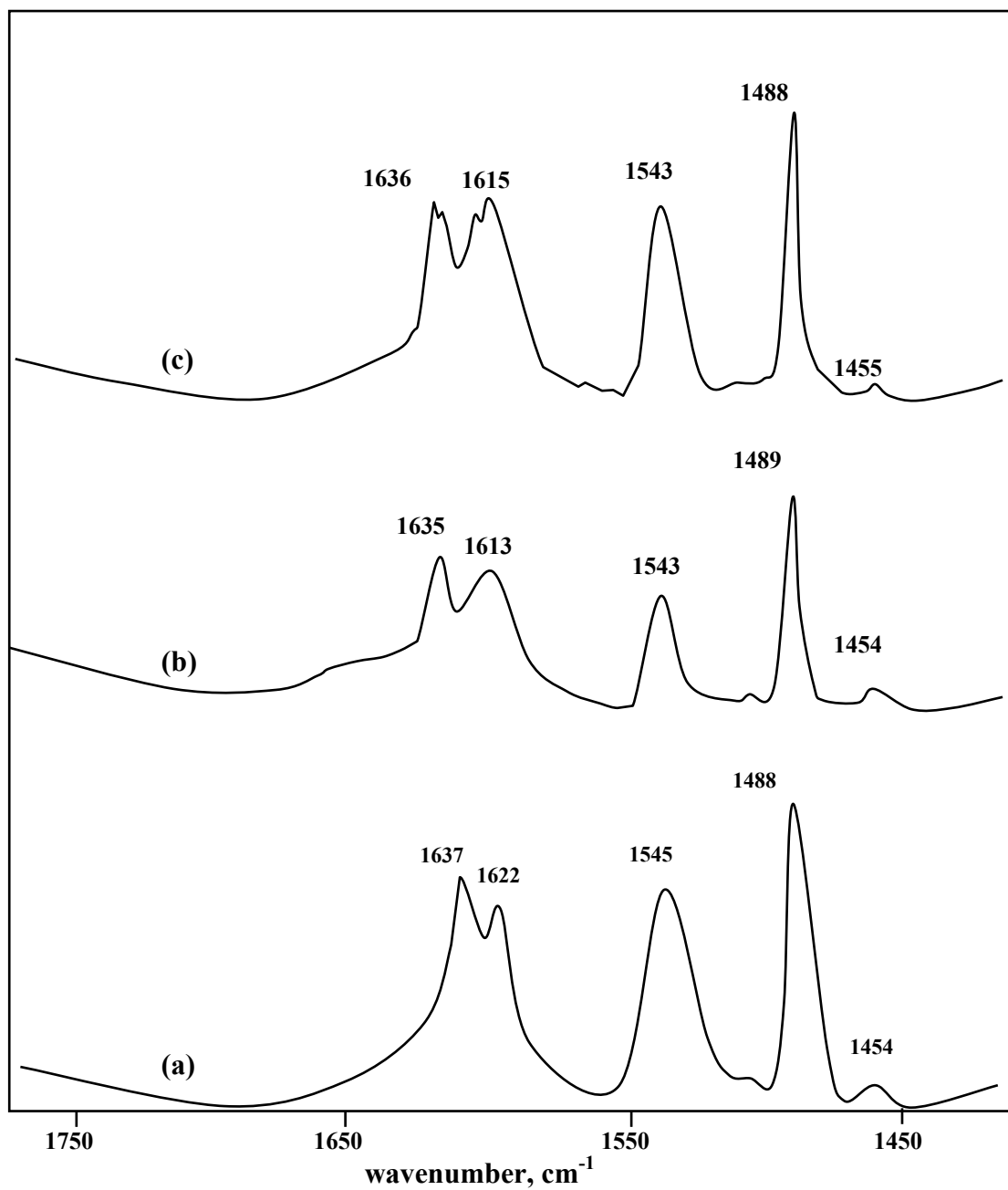


Figure 4.20: Infrared spectra of pyridine adsorbed at 150°C on H-ferrierite with various $\text{SiO}_2/\text{Al}_2\text{O}_3$ ratios; (a) H-Fer 12, (b) H-Fer 20 and (c) H-Fer 30

Table 4.8: The amount of Brønsted and Lewis acid sites in catalysts

Sample	Si/Al	Peak Area (cm ⁻¹)		Amount of Adsorbed Pyridine (mmol/g)	
		Brønsted	Lewis	Brønsted	Lewis
H-Fer 12	5.4	45.68	0.56	1.18	0.012
H-Fer 20	7.8	17.29	0.12	0.44	0.004
H-Fer 30	6.9	27.08	0.12	0.70	0.003

4.3.3 Temperature-Programmed Desorption (TPD) of Ammonia

Temperature-Programmed Desorption of ammonia has been carried out on the hydrogen formed of ferrierite at various SiO₂/Al₂O₃ ratios to measure the acid strength and the total amount of acid sites in the catalysts. Figure 4.21 shows the ammonia desorption profile of all catalysts. The desorbed amounts of ammonia are summarized in Table 4.9. From Figure 4.21, it is noted that H-Fer 12 and H-Fer 30 give two humps at 270°C region and 540°C region whereas H-Fer 20 also give two humps but at a lower region than H-Fer 12 and H-Fer 30. The first region is corresponding to the low strength acid sites whereas the upper region for moderate to high strength of acid sites. At low region of acid sites consists of the physically bonded ammonia to the surface of catalysts which is called physisorbed and at higher region of acid sites, consists of the chemically bonding of ammonia with the catalyst which is called chemisorbed [Bagnasco *et al.* 1996]. Sample H-Fer 12 having the lowest SiO₂/Al₂O₃ ratio or the highest aluminium content among all samples shows the most intense peak signal in low temperature region followed by H-Fer 30 and H-Fer 20.

Sample H-Fer 20 gives very low peak signals compared to both H-Fer 30 and H-Fer 12. At high temperature region, the peak for H-Fer 30 and H-Fer 12 show

comparatively similar intensity. H-Fer 20 shows different behavior in which both the lower and upper region arise at lower temperature than H-Fer 12 and H-Fer 30. The similar observation observed with the pyridine adsorption measurement in which H-Fer 20 gives the lowest amount of acid sites compared to H-Fer 12 and H-Fer 30. The first peak for H-Fer 20 appeared at 170°C and the second peak at around 370°C. Though the second peak appeared at a lower temperature, the amount of desorbed ammonia is relatively higher than other samples as shown in Table 4.9.

Table 4.9 shows the amount of desorbed ammonia and the maximum temperature for each sample. At low temperature region (1st peak), it is noted that H-Fer 12 give the highest amount of desorbed ammonia followed by the H-Fer 30 and H-Fer 20. On the other hand, for high temperature region (2nd peak), H-Fer 30 gives relatively higher amounts of desorbed ammonia rather than H-Fer 12. (This observation does not include H-Fer 20 due to the 2nd peak appeared at lower temperature). According to Hunger et al. as the amount of SiO₂/Al₂O₃ ratios increased, the amount of desorbed ammonia relatively decreased [2002]. However, the total amount of desorbed ammonia obtained in each sample only give a little distinction in which H-Fer 20 gives slightly higher amount followed by H-Fer 30 and H-Fer 12.

The maximum temperature achieved for the desorbed ammonia in the samples explains the strength of acid sites whereas the total amount of desorbed ammonia represents the total acid sites in samples. It can be seen that both H-Fer 12 and H-Fer 30 have relatively similar amount of the desorbed ammonia and the maximum temperature which explained that both samples having a similar reactivity.

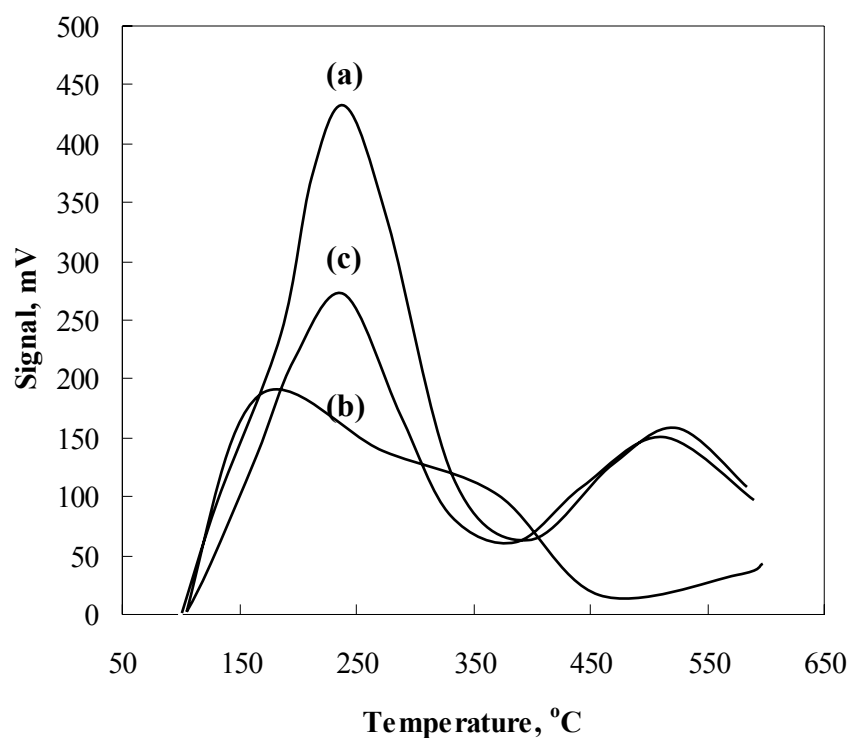


Figure 4.21: TPD of ammonia thermogram of H-Ferrierite with various $\text{SiO}_2/\text{Al}_2\text{O}_3$ ratios denoted as (a) H-Fer 12, (b) H-Fer 20 and (c) H-Fer 30

Table 4.9: Quantitative results of H-Ferrierite at different $\text{SiO}_2/\text{Al}_2\text{O}_3$ ratio from the TPD analysis

Catalysts	Si/Al ratio	Desorbed NH_3 amount (mmol/g)			T_{max} ($^{\circ}\text{C}$)	
		1 st peak	2 nd peak	Total	1 st peak	2 nd peak
H-Fer 12	5.4	1.58	0.35	1.93	240	520
H-Fer 20	7.8	1.38	0.69	2.07	170	370
H-Fer 30	6.9	1.49	0.49	1.98	240	520

4.5 Friedel Crafts acylation of anisole and acid anhydrides

From pyridine adsorption measurement and Temperature Program Desorption of ammonia, ferrierite shows the potential as a catalyst for Friedel-Crafts reaction due to the presence of both Lewis acid sites and Bronsted acid sites which are necessary to catalyze the reaction. The reactivity of ferrierite was tested in Friedel-Crafts acylation of anisole and both acetic anhydride and propionic anhydride. The study was carried out based on the effects of $\text{SiO}_2/\text{Al}_2\text{O}_3$ ratios of ferrierite, effects of reaction time and also the effects of reaction temperature. Ferrierite was classified under medium pore zeolite which generally expects to give higher selectivity for the product. To investigate the effects of acylating agent size towards Friedel-Crafts acylations, another reaction was carried out using acetic anhydride as substrate instead of propionic anhydride.

Figure 4.23 and 4.24 show the gas chromatogram and GCMS chromatogram of the liquid yield obtained from the reaction between propionic anhydride and anisole. This reaction was carried out at 120°C for 24 hours using H-Fer 12 as the catalyst. The chromatogram eluted 6 peaks at different retention time, $t_{\text{R}} = 2.47, 5.46, 9.09, 9.69, 10.72$ and 22.65 . Theoretically, the reaction of anisole with propionic anhydride will produce two main products which are *p*-methoxypropionophenone and propionic acid as shown in Figure 4.22 [Smith, 1994]. This is in comparison with the same reaction carried out using H-Beta as catalyst which produced the variety of product [Didik, 2001].

From these six peaks observed, two of them belong to the reactants which show the retention time $t_{\text{R}} = 9.11$ and 10.77 , both being identified as anisole and propionic anhydride respectively. From GCMS (Figure 4.23) chromatogram, it is clearly seen that only two products were obtained which are propionic acid and *p*-methoxypropionophenone with the percent of probability is 95%.

p-methoxypropionophenone is the preferred desired product for Friedel-Crafts acylation of anisole with propionic anhydride. Anisole has an active *ortho* and *para* direction due to the presence of hydroxyl and methyl substitution in benzene ring.

However, the *ortho* isomer might be produced in certain cases due to the isomer selectivity between *para*, *ortho* and *meta* is 31: 1 (*para* : *ortho* and *meta*) [Smith, 1994]. Identification using GCMS chromatograph, proved that only *para* isomer was produced in this reaction

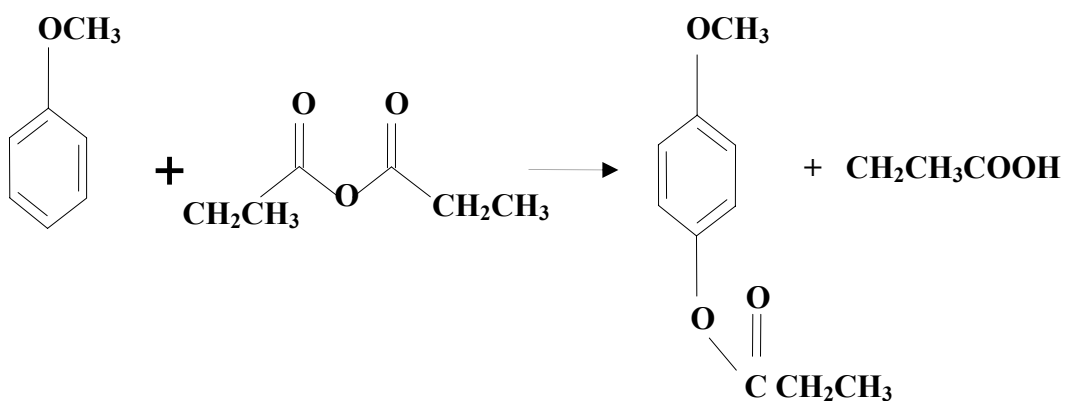


Figure 4.22: Friedel-Crafts acylation between anisole and propionic anhydride

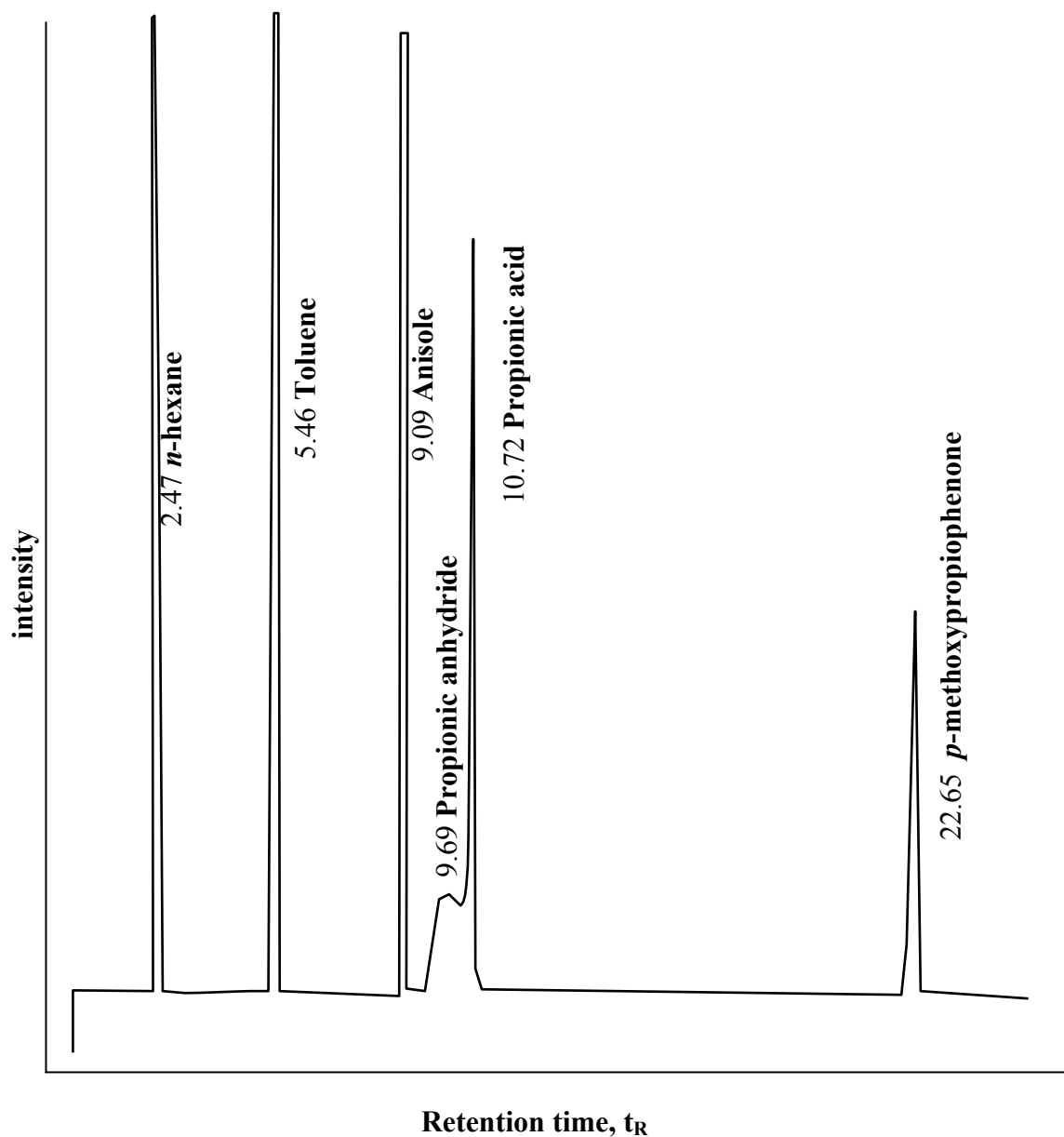


Figure 4.23: GC chromatogram of yield product over acylation of anisole using H-Fer 12 as catalyst

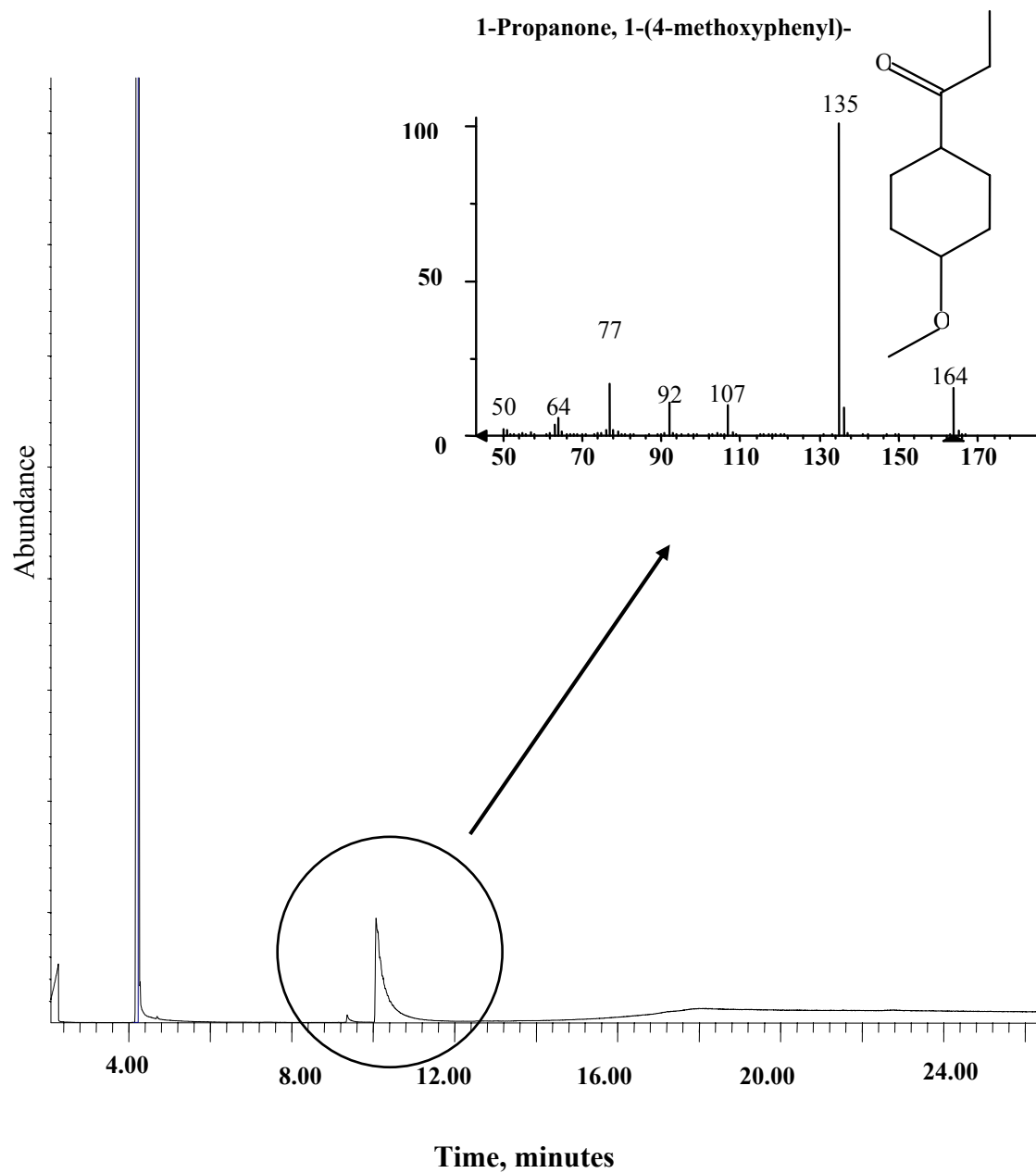


Figure 4.24: GCMS spectra of yield product for acylation of anisole with propionic anhydride over H-Fer 12 catalysts.

4.4.1 Effect of SiO₂/Al₂O₃ ratios

Ferrierite prepared at different SiO₂/Al₂O₃ ratios (12, 20, and 30) was ion-exchanged with ammonium nitrate solution to transform the ferrierite into H-ferrierite. The effects of SiO₂/Al₂O₃ ratios of ferrierite towards acylation reaction of anisole was carried out using the same parameter but with different catalyst. Figure 4.25 shows the calibration curve for anisole containing internal standard of toluene in hexane (100 ppm). This calibration curve was used in order to measure the amount of anisole in liquid solution before and after the reaction. All the catalysts at different SiO₂/Al₂O₃ ratios show a similar pattern of chromatogram. An internal standard solution containing toluene in hexane was added to liquid yield in which they appeared at retention time $t_R = 2.47$ for hexane and 5.46 for toluene.

Figure 4.26 reveals the percentage of anisole conversion and percentage of product selectivity towards *p*-methoxypropionophenone for each catalyst. It is observed that the conversion of anisole increase with the decrease of Si/Al ratio obtained from ²⁹Si MAS NMR. H-Fer 12 as having Si/Al ratio 5.4 can be seen giving 63 % of anisole conversion which is higher than the other. The conversion of anisole for catalyst H-Fer 30 was slightly higher than H-Fer 20 but lower than H-Fer 12.

However, no trend observed in the product selectivity with the increase in SiO₂/Al₂O₃ ratio of the catalysts. It can be seen that H-Fer 12 (Si/Al = 5.4) gives 80%, H-Fer 20 (Si/Al = 7.8) gives 50 % and H-Fer 30 (Si/Al = 6.9) gives 20 % of selectivity.

In this study, sample H-Fer 12 is the most reactive catalyst compared to other catalysts with the highest selectivity as well as conversion. Based on this, H-Fer 12 is used as the catalyst to study other effects on the Friedel-Crafts acylation of anisole with propionic anhydride. Further study was carried out using H-Fer 12 as catalyst in order to investigate the effects of H-ferrierite as catalysts at different temperatures and reaction times.

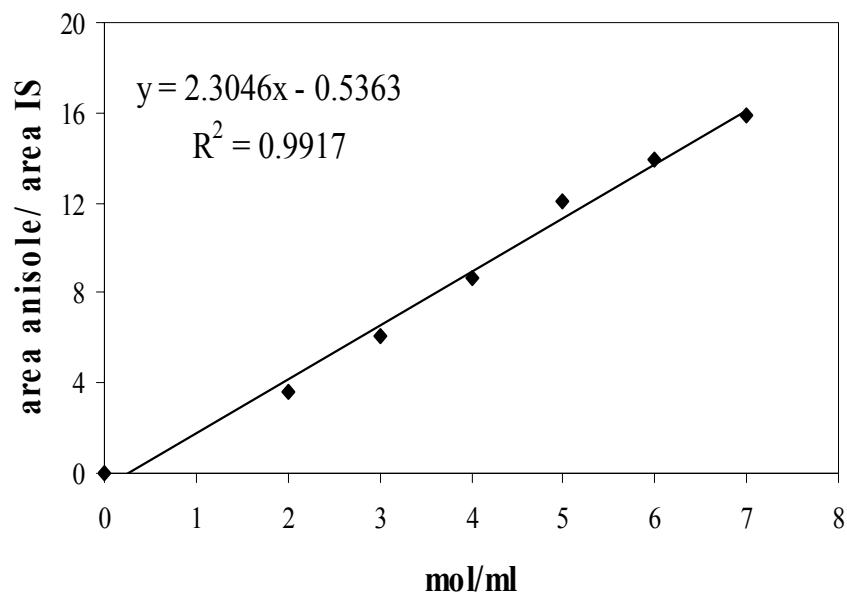


Figure 4.25: Quantitative calibration plot of anisole contain internal standard (IS) as analysed by Gas Chromatograph

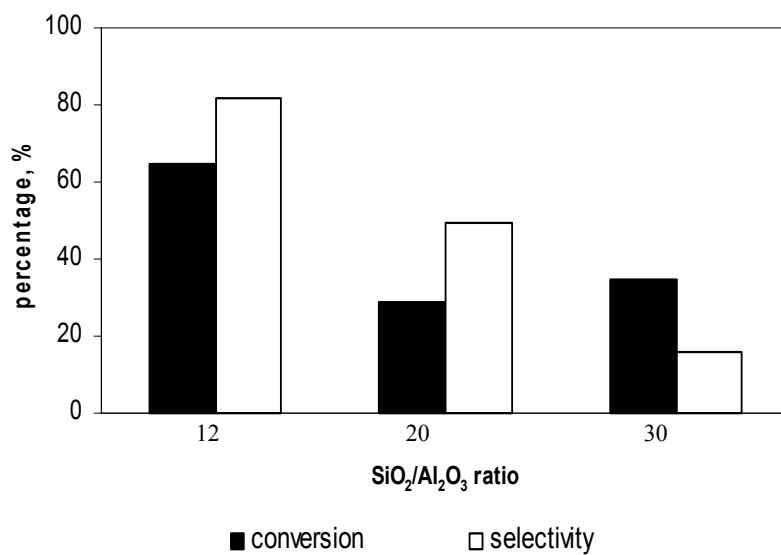


Figure 4.26: Effect of SiO₂/Al₂O₃ ratios of H-ferrierite on the conversion and selectivity of products.

4.4.2 Effect of reaction times

The reaction was carried out using H-Fer 12 as the catalyst with other parameters in which temperature was kept constant except at the time of reaction. In order to study the effects of reaction time for acylation of anisole with propionic anhydride, the liquid yield was taken at 0, 15 min, 45 min, 1.5 h, 2 h, 2.5 h, 4 h, 8 h and 24 h at 120°C (refer to sec. 4.4.3). Figure 4.27 illustrates the percentage of selectivity and conversion proportional vs. reaction time. Generally, in the initial period the percentage of both anisole conversion and product selectivity increased significantly within 2 hours of reaction, achieved equilibrium at 4 hours and increased slowly until 24 hours of reaction.

Along with *p*-methoxypropiophenone, propionic acid is also produced in this reaction. However, the existence of propionic acid was already found in liquid mixture before the reaction begins. The formations of propionic acids easily occur through nucleophilic substitution of propionic anhydride. The substitution may happen with the interaction of propionic anhydride with moisture in air which is called self-hydrolyzed. This organic acid is less active for Friedel-Crafts acylation than propionic anhydride. The amount of propionic acid increased with time as a side product of reaction. It was reported that propionic acid may be involved in acylation of anisole [Chiche *et al.* 1998]. However the increasing amount of propionic acid with time in this study explained that this might not happened.

Figure 4.28 reveals the percentage of concentrations for each compound in liquid yield versus time. The percentage of anisole concentration decreased significantly in the first 45 minutes. The concentration of anisole continues to decrease slowly until four hours of reaction in which after this time, the decrease in the concentrations of anisole become constant. From this finding, the optimum reaction period for anisole is taken to be around 4 hours. The same results were obtained by using H-Beta in which the optimum reaction time is 4 hours [Didik, 2001].

It is noted that the concentrations of *p*-methoxypropiofenone and propionic acid were increased significantly with the extension of reaction period. The enhancement of propionic acid concentrations with time indicates that propionic acid does not take part in acylation of anisole. With the increase of reaction time, the amount of the acid keeps increasing as a side product of *p*-methoxypropiofenone.

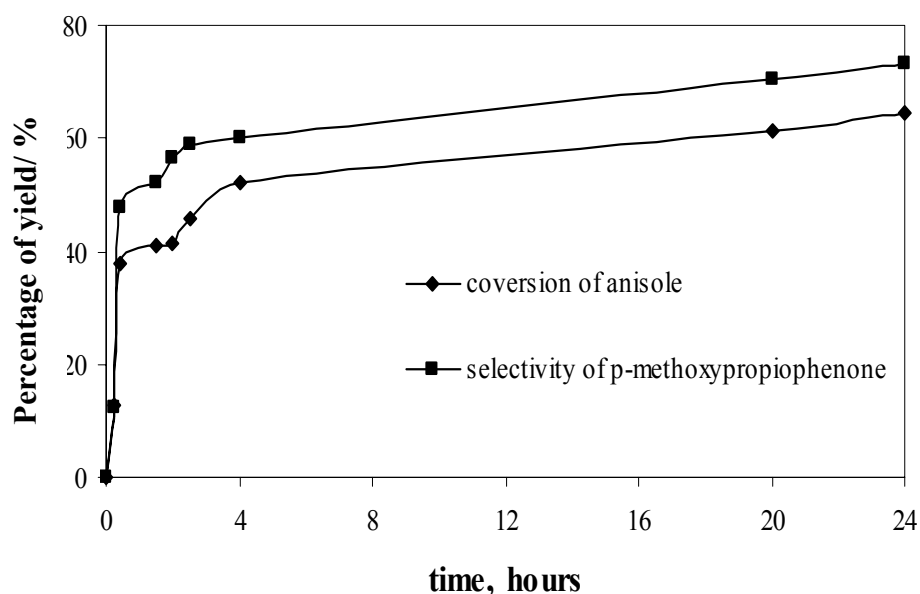


Figure 4.27: The reactivity of H-Fer 12 in Friedel-Crafts acylation of anisole with time

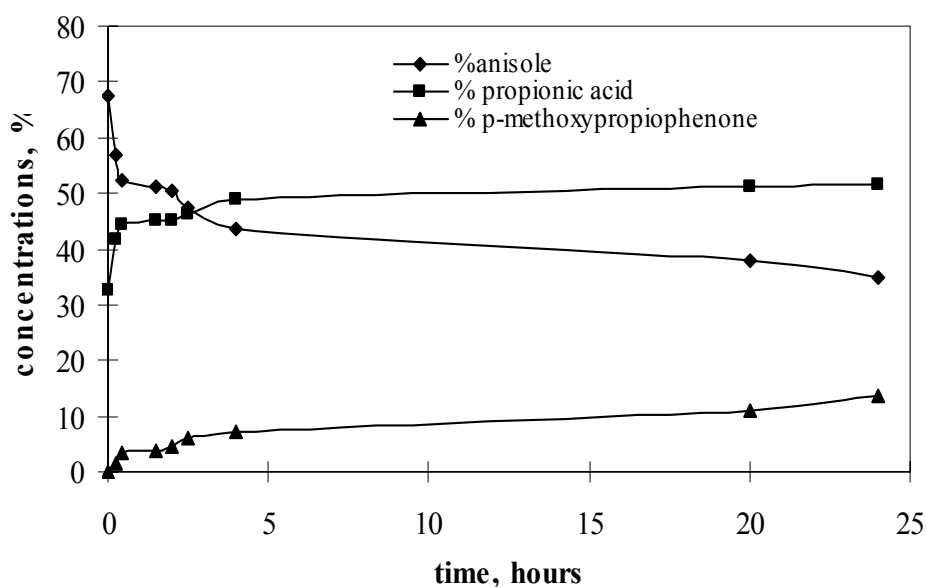


Figure 4.28: The percentage of concentrations for every compound in organic yield

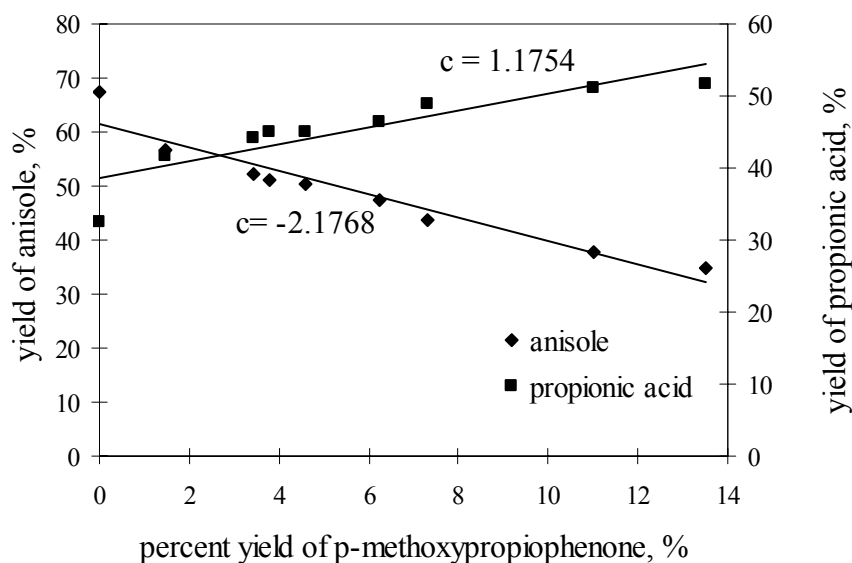


Figure 4.29: Correlation between the concentrations of anisole and propionic acid with the concentrations of *p*-methoxypropiofenone.

Figure 4.29 reveals the amount of anisole and propionic acid that exist in liquid product with correlation between the amounts of *p*-methoxypropiofenone. The amount of anisole in liquid yield decreased in proportion with the increase of *p*-methoxypropiofenone. On the other hand, the concentration of propionic acid increased in proportion to the amount of desired product *p*-methoxypropiofenone. However, by focusing on the modulus slope value for each curve, it is revealed that the value of anisole concentrations with desired product is relatively higher than the value of propionic acid produced. Theoretically, the modulus slope value of anisole used and propionic acid produced with the production of *p*-methoxypropiofenone is relatively comparable due to acylation of anisole with propionic anhydride is 1 to 1 reaction. Furthermore, the modulus slope value of propionic acid production might be greater than anisole used due to the ability of propionic anhydride to self-hydrolyze. It is suggested that propionic acid may take a slight part as electrophile that will further react with anisole to produce a desired product.

4.4.3 Effect of reaction temperature

The effect of reaction temperature for acylation of anisole was investigated using H-Fer 12 as catalysts at temperature within 90°C to 130°C for 4 hours. Figure 4.30 reveals that further increase in temperature will enhance the anisole conversion up to 120°C. However, when the temperature was further increased to 130°C, conversion was slightly decreased. Results show that H-Fer 12 is not active at 90°C as catalysts in acylation of anisole. The activity is likely to increase up to 110°C, which is about 20 % of conversion increased. However, when the reaction temperature is increased to 120°C, the anisole conversion increased almost 35% to give 58% of conversion.

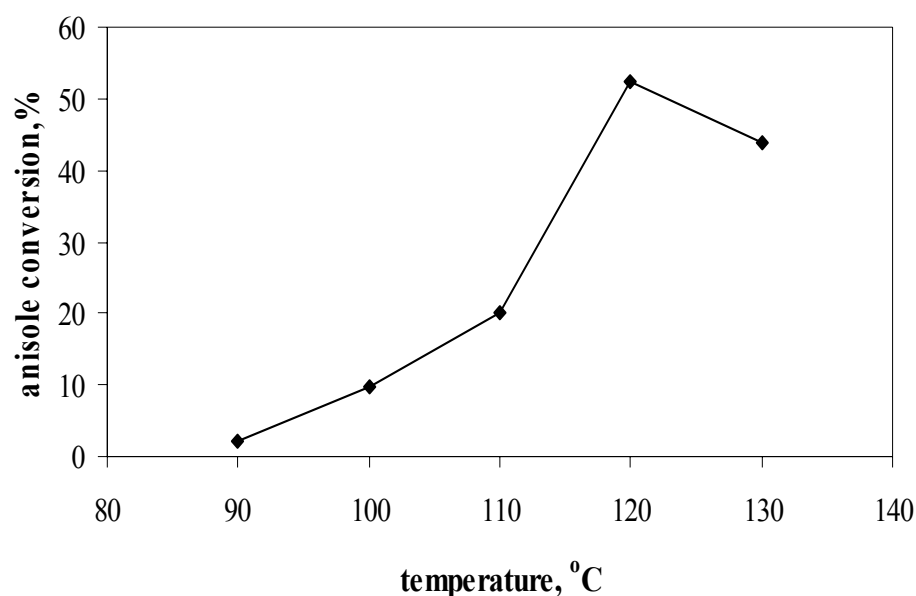


Figure 4.30: Effect of reaction temperature on the conversion of anisole as substrate with using H-Fer 12 as catalysts in the Friedel Crafts acylation of anisole with propionic anhydride

4.4.4 Effects of the size of acylating agent

In order to study the effects of the size of acylating agent towards the reactivity of H-ferrierite as selective catalysts for Friedel-Crafts acylation, another reaction was carried out between anisole and acetic anhydride as the acylating agent which having less carbon atom. The reaction was carried at 120°C for 4 hours in batch reactor. Anisole will mainly transformed into *p*-methoxyacetophenone with acetic acid as a side product. From GC and GCMSD results, it shows that only two products are obtained which are identified as *p*-methoxyacetophenone and acetic acid.

Figure 4.31 reveals the percentage of conversion and selectivity of product. The reaction between anisole and acetic anhydride results in 55 % of anisole conversion, slightly higher than the reaction between anisole and propionic anhydride (52 %). The selectivity of *p*-methoxyacetophenone is higher than *p*-methoxypropiofenone which is 98 % compared to only 60 % for *p*-methoxypropiofenone. The reason attributed to this finding might be due to the difference in the sizes of the reactants. The small size of acetic anhydride ($M_r = 102.09$), rather than propionic anhydride ($M_r = 130.15$) shows that acetic anhydride penetrates to the pores and reached the active sites in the pores easily in H-ferrierite. The size of pore opening for ferrierite is relatively smaller for propionic anhydride rather than acetic anhydride that can slightly prohibit the penetration of propionic anhydride into ferrierite pores. Besides that, the possibility that can occur is the preservation of product within the pore of ferrierite. *p*-methoxypropiofenone which has larger molecular size than *p*-methoxyacetophenone, has a high possibility to be retained in the pore of ferrierite, which is difficult to penetrate out from the pores. The retention of product in the pore will decrease the selectivity of product which explains why the selectivity of *p*-methoxypropiofenone is lower than *p*-acetophenone.

The selectivity of catalyst towards the formation of *para* substitution product obtained in both reactions either using propionic anhydride or acetic anhydride as an acylating agent, shows that H-Ferrierite is a good selective catalyst for *para*

orientation products. The formation of product from acylation of anisole is explained by aromatic electrophilic substitution which involves the attack of pi electron from anisole ring to electrophil ($R-CO^+$), whereby the course of action is facilitated by acid sites in H-ferrierite.

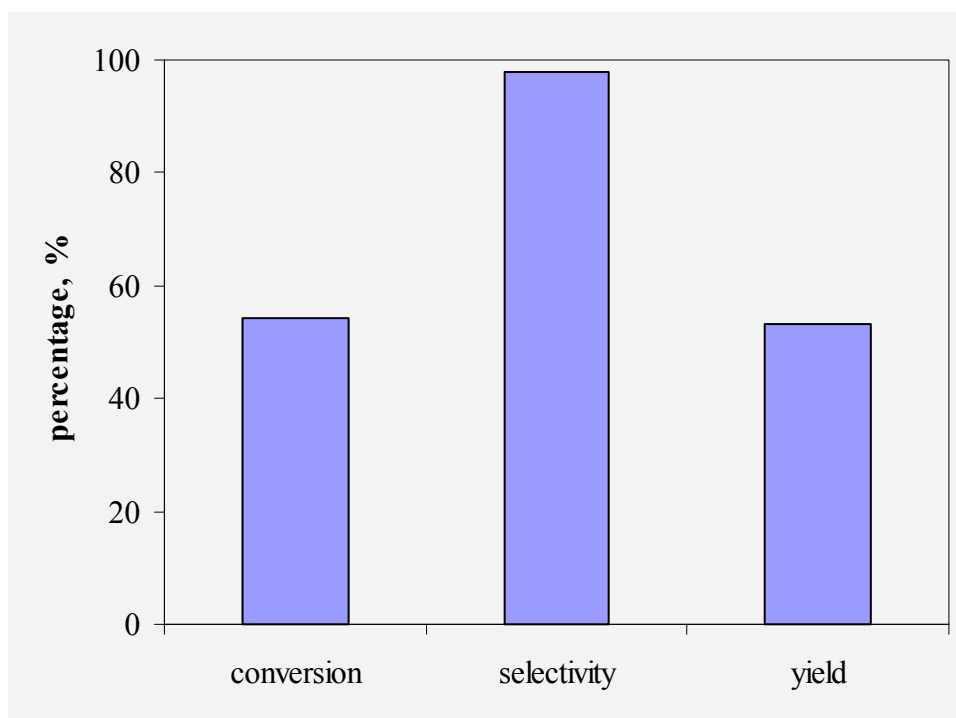


Figure 4.31: The percentage of conversion, selectivity and yield for reaction of anisole with acetic anhydride.

4.4.5 Correlations between the reactivity of catalysts with their acidity

The conversion and selectivity of desired product is mainly influenced by the strength, amount and types of acid sites in the catalysts and also the pore size of the catalysts. Ferrierite having a medium pore size of $4.2 \times 5.4 \text{ \AA}$ in the diameter played a role in controlling the selectivity of desired products. As comparison with the previous study by Didik, shows that acylation of anisole using HBeta produced more than seven side products. Nevertheless, in this study only propionic acid have been generated as a side product in which the selectivity of the desired product is relatively higher than the conversion of anisole as shown in Figure 4.27. The reverse observation was found for Didik study in which the conversion was relatively higher than selectivity of product. With these results, H-ferrierite is suggested as a potential selective catalyst for medium size of product.

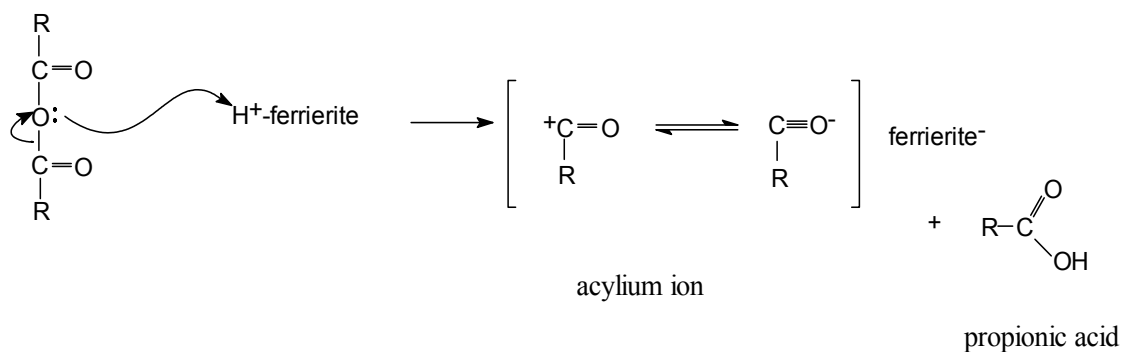
Based on the acidity study of the H-ferrierite, it reveals that all catalysts consist of higher Brønsted acid than Lewis acid sites. The amount of Brønsted acid sites is significantly increased with the decreasing $\text{SiO}_2/\text{Al}_2\text{O}_3$ content in ferrierite framework. In correlation between percentage conversions of anisole catalyzed by various H-ferrierite at different $\text{SiO}_2/\text{Al}_2\text{O}_3$ ratios which illustrates in Figure 4.26 with acidity study, it shows that high amount of acid sites is a response for the high conversion of anisole. The amount of yield produced is also influenced by the amount of Brønsted acid sites that exists in ferrierite framework. It is noted that the enrichment of Brønsted acid sites in catalysts will enhance the amount of products for the Friedel-Crafts acylation.

However, the selectivity of *p*-methoxypropiophenone shows a minor correlation with $\text{SiO}_2/\text{Al}_2\text{O}_3$ ratio, in which the selectivity increased relatively with the decreasing $\text{SiO}_2/\text{Al}_2\text{O}_3$ ratio. From studies that have been carried out with different catalysts, it was revealed that Brønsted acid sites play a main responsibility in producing high amounts of the desired product instead of Lewis acid. However, the presence of Lewis acid sites is still necessary to ensure good selectivity of product.

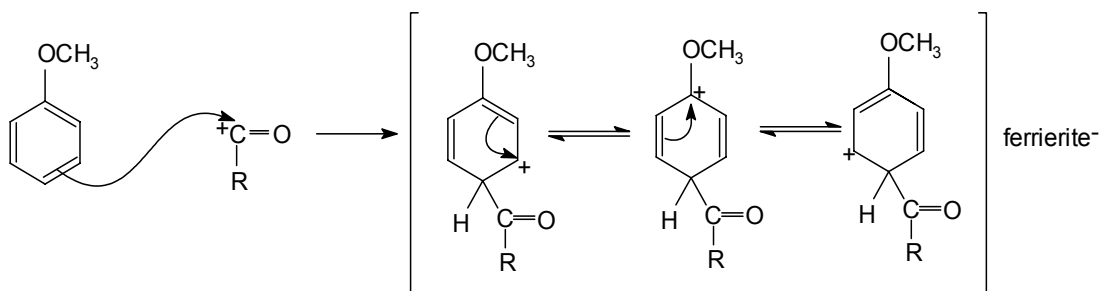
Reactions that have been employed under various periods show that the reaction reached equilibrium in the first four hours. The amount of *p*-methoxypropiofenone and propionic acid increased significantly with the reaction time. However, the ratio of anisole amount with *p*-methoxypropiofenone formed is faster than the side product which is propionic acid, suggesting that propionic acid may have taken part as an electrophil that will further react with anisole to produce desired product.

Based on all these findings, the mechanism of reaction is proposed as shown in Figure 4.31. The general mechanism for acylation of anisole involved the aromatic eletrophilic substitution. The strong acid site is necessary in order to form acylium ion for further substitution. Thus, acylium ion will act as an electrophile as shown in the proposed mechanism in Figure 4.33.

Step 1: The generation of a strong electrophile.



Step 2: A pair of electrons from the π cloud attack the electrophile



Step 3: Ferrierite⁻ as a strong base will abstract a proton from the carbon atom that received the electrophile to regenerate the aromatic ring.

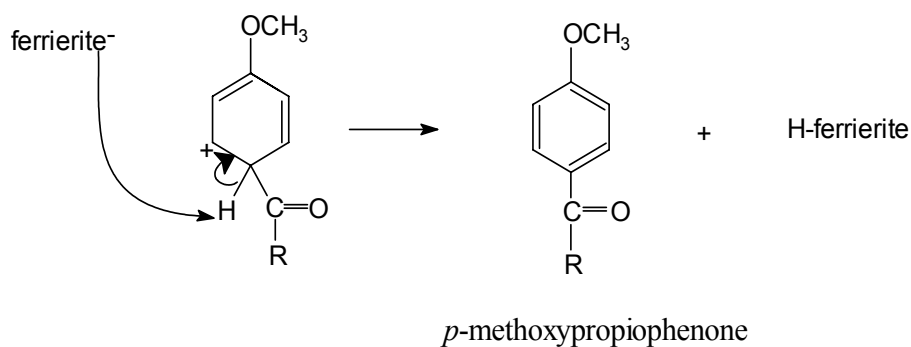


Figure 4.31: Proposed mechanism of electrophile substitution of anisole using H-ferrierite as catalyst

CHAPTER V

CONCLUSIONS AND RECOMMENDATION

5.1 Conclusions

This study has shown that rice husk ash is a potential silica source for the synthesis ferrierite. Ferrierite type zeolite has successfully been synthesized from rice husk ash only when using pyrrolidine as the organic template and structure directing agent. The ferrierite from rice husk ash was obtained under hydrothermal condition at 200°C and took only 4 days to form compared to ferrierite obtained from commercial colloidal silica which required more than 9 days.

The formation of ferrierite from rice husk ash is strongly depending on the molar oxides composition and also the type of templates. The pure ferrierite phase from rice husk ash was obtained in the range of 1.31 – 1.5 Na₂O : Al₂O₃ : 10 – 30 SiO₂ : 4.0 – 10.0 Py : 410 H₂O. The range of SiO₂/Al₂O₃ ratios for producing pure ferrierite is relatively narrow, which is from 10 to 30. For samples with SiO₂/Al₂O₃ ratio more than 30, quartz phase becomes the dominant phase rather than ferrierite. However, with the increasing of SiO₂/Al₂O₃ ratio to 30, the template pyrrolidine also need to be increased in order to form pure ferrierite. Ferrierite with high crystallinity can be prepared with the Py/Al₂O₃ ratios of the reaction mixtures as low as 4. Quartz will be formed when the ratio of Py/Al₂O₃ is lower than 4. However, the concentration of Py is limited to 10 in line with the objective of this research that is to cut the production cost of ferrierite. Ferrierite phase will only be obtained in the range of SiO₂/Py ratios between 2 to 4 and when SiO₂/Py ratios is above 4, analcime type

zeolite will be produced, followed by the quartz at higher SiO_2/Py ratios. Results showed that only pyrrolidine template plays an important role as structure directing agent for the formation of ferrierite framework and it is completely important for its existence in every gel mixture. The low amount of template concentrations will affect the formation of crystalline phase due to the lack of structure directing agent. The overall results of this study reveal that ferrierite can be successfully synthesized from rice husk ash when the reaction mixtures have the gel compositions in the range of $1.31 - 1.5 \text{ Na}_2\text{O} : \text{Al}_2\text{O}_3 : 10 - 30 \text{ SiO}_2 : 4.0 - 10.0 \text{ Py} : 410 \text{ H}_2\text{O}$.

Transformation of rice husk ash to ferrierite was monitored by XRD technique, FTIR, N_2 adsorption, SEM and ^{29}Si MAS NMR and also the changes of solid weight. Ferrierite framework formed as early as 12 hours and the silica is completely transformed into ferrierite within 1 day of crystallization. Though the ferrierite framework does not form yet at 0.25 day (6 hours), the incorporation of aluminium to tetrahedral framework has already occurred. The transformation of rice husk ash to ferrierite occurs directly without the presence of another crystalline phase. The stable structure of ferrierite was achieved in 4 days of crystallization.

^{29}Si MAS NMR measurement shows that the Si/Al ratio obtained in each ferrierite at different initial $\text{SiO}_2/\text{Al}_2\text{O}_3$ ratios increased from H-Fer 12 (Si/Al = 5.4), to H-Fer 30 (Si/Al = 6.9) and followed by H-Fer 20 (Si/Al = 7.9). An acidity study using pyridine adsorption FTIR and TPD techniques show the existence of both Brønsted and Lewis acid sites in all hydrogen form ferrierite samples (H-ferrierite). However, in each case the amount of Brønsted acid sites is higher than Lewis acid sites. The Brønsted acid sites are relatively dependent on the $\text{SiO}_2/\text{Al}_2\text{O}_3$ ratios of the ferrierite frameworks in which the higher ratio results in the low amounts of Brønsted acid sites. Meanwhile the amount of Lewis acid sites does not show any correlations with the $\text{SiO}_2/\text{Al}_2\text{O}_3$ ratios of the samples due to the small amounts of Lewis acid sites present in the ferrierite framework. These results are in agreement with the quantitative TPD NH_3 analysis showing that H-Fer 20 sample gives low amounts of desorbed ammonia and acid sites compared to both H-Fer 12 and H-Fer 30.

The activity study of H-ferrierite as catalyst in Friedel-Crafts acylation of anisole and both acid anhydride shows that H-ferrierite has a potential to be a selective *para* catalyst for producing only product with *para* orientation. All the H-ferrierite catalysts used, produced only *p*-methoxypropiophenone as a main product with propionic acid as the side product reaction. The conversion increased relatively with the decreasing SiO₂/Al₂O₃ ratios due to the increase in Brønsted acid sites in the ferrierite framework. Reactions that have been carried out under various periods show that the optimum reaction time is in the first four hours. The effect of reaction temperature study reveals that H-ferrierite gives the optimum performance when the temperature is 120°C. From this study, it is suggested that the optimum reaction conditions for acylation of anisole with propionic anhydride is at 120°C and for 4 hours. The effect of different size of acylating agent (acetic anhydride as compared with propionic anhydride) in acylation of anisole shows that the product obtained is also in *para* orientation. However, the product selectivity and the anisole conversion were 98 % and 55 %, were higher as compared to propionic anhydride. From the product obtained, we proposed that the mechanism of this reaction involved electrophile aromatic substitution which included the formation of acylium ions from the Brønsted acid sites in the catalysts.

5.2 Recommendation

The successful formation of ferrierite from rice husk ash proved the reactivity of the rice husk ash as silica source in the synthesis of zeolite ferrierite. Therefore, the study can be extended to produce ferrierite using rice husk ash with higher $\text{SiO}_2/\text{Al}_2\text{O}_3$ ratios or siliceous ferrierite. These materials are important precursor for producing mesoporous materials which are highly researched now. The modification of ferrierite from rice husk ash to mesoporous solid also can be done in order to vary the function of ferrierite as catalyst particularly for synthesizing larger organic molecules. Besides that, the study can be extended to investigate the potential of ferrierite from rice husk ash as catalysts in other reactions such as for the reduction of nitrous oxides gaseous. The utilizations of ferrierite as catalysts in the reductions of nitrous oxides gaseous have a potential to solve the problems arise while ammonia used as reducing agents. The application of ammonia is impeded by concern over safety and ammonia distribution logistics. The use of ferrierite from rice husk ash as catalysts also can be extended in the skeletal isomerization of n-alkenes which is the main potential utilization of ferrierite in the future industries.

References

- Ahedi, R.K., Kotasthane, A.N., Rao, B.S., Manna, A., and Kulkarni, B.D., (2001), Synthesis of Ferrierite-Type Zeolite in the Presence of Catalytic Amount of Pyrrolidine and Sodium Bis(2-ethylhexyl) Sulfosuccinate”, *Journal of Colloid and Interface Science*, **236**, 47-51
- Aiello, R., Crea, F., Nastro, A., and Pellegrino, C., (1987), “Zeolite Crystallization from High-Silica Mono-or Bicationic Alkali (Li, Na, or K) Gels in Presence and in Absence of TPA ions”, *Zeolites*, **7**, 549-553
- Amick, J.A., (1982), “Purifications of Rice Hulls as a Source of Solar Grade Silicon for Solar Cells”, *Journal of Electrochem Society*, **129**, 864
- Anonymous, (1996), “US Zeolites Market Set to Reach \$1 Billion in 2001, Study Says,” *Chemical Market Reporter*, **250**, New York: Schnell Publishing Company.
- Armaroli, T., Bevilacqua, M., Trombetta, M., Alejandre, A.G., Ramirez, J., and Busca, B., (2001), “An FT-IR Study of the Adsorption of Aromatic Hydrocarbons and of 2,6-lutidine on H-FER and H-ZSM-5 Zeolites”, *Applied Catalysis A: General*, **220**, 181–190
- Bagnasco G., (1996), “Improving the Selectivity of NH₃ TPD Measurements”, *Journal of Catalysis*, **159**, 249-252
- Bambani, M.R., (1972), “Analysis of Nitrogen Adsorption Isotherms on Porous and Nonporous Silicas by BET and α_s Methods”, *Journal of Colloid Interface Science*, **38**, 109-117

- Barrer, R. M (1982), "Hydrothermal Chemistry of Zeolites", London, Academic Press.
- Bekkum H. V. Flanigen E. M. and Jansen J. C. (Eds), (1991) "Introduction to Zeolite Science and Practice", *Studies of Surface Science Catalysis*, **58**, Netherlands: Elsevier.
- Bonnie, K. M. and Cormier, E. (1999) "Going Green with Zeolites", *Chemical Engineering Progress*,
- Breck. D. W. (1974) "Zeolite and Molecular Sieve, Structure, Chemistry and Use," New York: John Wiley and Sons.
- Bussmann, P. J. T. (2000) "Drying Food and Food Ingredients with Zeolite", *TNO Environment, Energy and Process Innovation*, 240
- Casagrande, M., Storaro, L., Lenarda, M., and Ganzerla, R., (2000) "Highly Selective Friedel–Crafts Acylation of 2-methoxynaphthlene Catalyzed by H-BEA Zeolite", *Applied Catalysis A: General*, **201**, 263–270
- Chen, S. S. and Yeoh A. K. (1992), "Development of Zeolite NaY from Rice Husk Ash", *Journal of Industrial Technology*, **2**, SIRIM, Malaysia
- Chiche B., Finiels A., Gauthier C., Geneste P., Graille J. and Pioch D., (1986), "Friedel-Crafts Acylation of Toluene an p-Xylene with Carboxylic acids catalyzed by Zeolites", *Journal Organic Chemistry*, **51**, 2128-2130
- Datka J., Kawalek M. and Marek K.G., (2003), "Acid Properties of NAKH-Ferrierite of Various Exchange Degrees Studied by IR Spectroscopy", *Applied Catalysis A: General*, **243**, 293-299
- Davis, M. E. (1998), "Zeolite-based Catalyst for Chemical Synthesis", *Microporous and Mesoporous Materials*, **21**, 173-182

- Dessau R. M. (1980) "Selective Sorption Properties of Zeolites, Adsorption and Ion Exchange with Synthetic Zeolite", American Chemical Society, Washington D.C
- Didik Prasetyoko (2001) "Pengoptimuman Sintesis Zeolite Beta daripada Silika Sekam Padi: Pencirian dan Tindak Balas Pemangkinan Friedel-Crafts" Universiti Teknologi Malaysia: MSc Thesis.
- Dutta P. K., Rao K.M., Kresge C.T., and Kennedy G.J., (1994), "Examination of the Growth Dynamics of Zeolites ZSM-5 and Mordenite from Inorganic Reactants Compositions", *Microporous Materials*, **3**, 17-27
- Derouane, E. G., Crehan, G., Dillon, C. J., Bethell, D., He, H., and Derouane-Abd Hamid S. B., (2000), "Zeolite Catalysts as Solid Solvents in Fine Chemicals Synthesis: 2. Competitive Adsorption of the Reactants and Products in the Friedel–Crafts Acetylations of Anisole and Toluene", *Journal of Catalysis*, **194**, 410–423
- Endang Listiorini (1995), "Zeolite ZSM-5 and Aluminophosphate Molecular Sieves as Catalyst in the Fisher-Tropsch Reaction: Synthesis, Characterization and Modification", Universiti Teknologi Malaysia: MSc Thesis
- Engelhardt, G. and Michel, D., (1987), "High-Resolution Solid-State NMR of Silicates and Zeolites", Chichester: John Wiley & Sons.
- Flanigel E.M., Khatami H., Szymanski H. A., (1971), "Infrared Structural Studies of Zeolite Framework", In: Robert F. Gould (Ed), *Advanced Chem. Series*, **101**, 201-227
- Flanigen E.M., Bennet JM, Grose J.w., Cohen J.P., Patton R.L., Kirchner R.M., Smith J.V., (1978), Silicalite, a New Hydrophobic Crystalline Silica Molecular Sieve, Nature, London
- Food and Agriculture Organization, (1998), FAOStat Database.

- Freese, U., Heinrich, F. and Roessner, F., (1999) "Acylation of Aromatic Compounds on H-Beta Zeolites", *Catalysis Today*, **49**, 237-244
- Gaare, K., Akporiayae, D., (1996), "Modified Zeolites as Catalysts in the Friedel-Crafts Acylation", *J. of Molecular Catalysis A: Chemical*, **109**, 177-187
- Gabriella P.B, Agnes S., Hermann K.B., (2000), "Solid State Recrystallization of Aluminium-Containing Kanemiite Varieties to Ferrierite". *Microporous and Mesoporous Materials*, **35-36**, 573-584
- Gabriella P. B. Hermann K. B. Yoshimichi K. and Fujio M. (1998) "Synthesis and Characterization of Ferrierite made by Recrystallization on an Aluminium-Containing Hydrated Megadiite", *Microporous and Mesoporous Materials*, **22**, 57-68
- Hamdan H., Muhid M.N.M., Endud S., Listiorini E., and Ramli Z., (1997), ^{29}Si MAS NMR, XRD and FESEM studies of Rice Husk Silica for the Synthesis of Zeolites", *Journal of Non-Crystalline Solids*, **211**, 126-131
- Hasliza Bahruji (2002), "Synthesis and Characterization of Zeolite ZSM-5 using Crystalline Rice Husk Ash as Silica Source", Universiti Teknologi Malaysia: BSc. Thesis
- Hincapie, B.O., Garces, L.J., Zhang, Q., Sacco, A., and Suib, S.L., (2004), "Synthesis of Mordenite Nanocrystals" *Microporous and Mesoporous Materials*, **67**, 19-26
- Holderich, W., Murakami, Y., Iijima, A., Ward, J.W., (Eds), (1986), "New Development in Zeolites Science and Technology, Studies in Surface Science and Catalysis", *Elsevier Amsterdam*, **28**, 827
- Hunger B., Heuchel M., Clark L. A. and Snurr R. Q., (2002), "Characterization of Acidic OH Groups in Zeolites of Different Types: An Interpretation of NH_3 -

TPD Results in the Light of Confinement Effects”, *Journal of Physical Chemistry, B.*, **106**, 3882-2889

Jacobs P. A., Bayer H. K. and Valyon J., (1981), “Properties of the End Members in the Pentasil-Family of Zeolites: Characterization as adsorbents”, *Zeolites*, **1**, 161-168

James R. and Roa M.S.,(1986), “Characterization of Silica in Rice Husk Ash”, *American Ceramic Society Bulletin*, **65**, 1177-1180

Jongkind. H., Daterma K.P., Nabuurs S., Seive A., and Stork W.H.J., (1997), “Synthesis and Characterization of Zeolites Using Saturated Cyclic Amines as Structure Directing Agents”, *Microporous Materials*, **10**, 149-161

Joshi, P.N., Thangaraj, A. and Shiralkar, V. P., (1991). “Studies on Zeolite Transformation of High Silica Gmelinite into Analcime.” *Zeolites*. **11**, 164

Kapur, T., Kandpal, T.C., and Garg, H.P., (1998), “Electricity Generate from Rice Husk in Indian Rice Mills: Potential and Financial Viability”, *Biomass Energy*, **14**, 573

Kerr G. T., (1966), “Chemistry of Crystalline Aluminosilicates. I. Factors Affecting the Formation of Zeolite A”, *Journal of Physical Chemistry*, **70**, 1047-1050

Khomane R. B., Kulkarni B.D. and Ahedi R. K., (2000), “Synthesis and Characterization of Ferrierite-Type Zeolite in the Presence of Nonionic Surfactants”, *Journal of Colloid and Interface Science*, **236**, 208-213

Kibby, C. L. Perrota A. J. and massoth F. E. (1974), “Composition and Catalytic Properties of Synthesis Ferrierite” *Journal of Catalysis*, **35**, 256-272

L. V. Robert, (2000), “Zeolites”, *U.S. Geological Survey Minerals Yearbook*, **85**, 1-5

- Lercher J. A., Gruendling C., Mirth G.E., (1996), "Infrared Studies of the Surface Acidity of Oxides and Zeolites using Adsorbed Probe Molecules", *Catalysis Today*, **27**, 353
- Li, Y., and Armor. J. (1992) "Catalytic Decomposition of N₂O" US Patent No 5, 171, 553,
- Lin, D.C., Xu, X.W., Zuo, F., and Long Y.C., (2004) "Crystallization of JBW, CAN, SOD and ABW type zeolite from transformation of meta-kaolin" *Microporous and Mesoporous Materials*, **70**, 63–70
- Matsukata M. Nishiyama N. Ueyama K. (1996), "Crystallization of FER and MFI Zeolites by a Vapor-phase Transport Method", *Microporous Materials*, **7**, 109-117
- Maurer T., Kraushaar-Czarnetki, B. (1999), "Thermodynamic and Kinetic Reaction Regimes in the Isomerization of 1-Pentene over ZSM-5", *Journal of Catalysis*, **187**, 202-208
- Meier W. M. and Moeck H. J., (1979), "The Topology of Three-Dimensional 4-Connected nets: Classification of Zeolite Framework Types Using Coordination Sequences", *Journal of Solid State Chemistry*, **27**, 349
- Meier, W. M. and Olson, D. H. (1992), "Atlas of Zeolite Structure Types". 3rd Ed. USA, Butterworth-Heineman.
- Meisel, S.L., McCullough, J.P., Lechthaler, C.H., Weisz, P.B., (1967), *Chemtech*, **6**, 86
- Mochidzuki, K., Sakoda, A., Suzuki, M., Izumi, Jun., and Tomonoga, N., (2001), "Structural Behavior of Rice Husk Silica in Pressurized Hot-Water Treatment Processes", *Ind. Eng. Chem. Res.* **40**, 5705-5709

- Murayama N., Yamamoto H. and Shibata J., (2002), "Mechanisme of Zeolite Synthesis from Coal Fly Ash by Alkali Hydrothermal Reaction", *Int. J. Miller. Process.* **64**, 1-17
- Nadimi S. (1993) "Non-Aqueous Synthesis of Zeolites and Molecular Sieves"
Universiti of Toronto: PhD. Thesis
- Neils R. F. and Lovat V. C. R. (1995), "The Synthesis of Ferrierite, ZSM.5 and Theta-1 in the Presence of Diethanolamine: Experimental", *Zeolites*, **15**, 444-451
- Novotna, M., Satava, V., Maixner, J., Klouzkova, A., Kostka, P. , and Ležal, D., (2003) "Preparation And Characterisation Of Analcime Powders," *Journal of Optoelectronics and Advanced Materials*, **5**, 1405 - 1409
- Olah, G.A., (1964), Friedel-Crafts and Related Reactions, Vol III, Intersciences, New York, part 1
- Olson D.H., Hagg W.O., Lago R.M., (1980) "Chemical and Physical Properties of the ZSM-5 substitutional series", *Journal of Catalysis*, **61**, 390-396
- Oneystak, G., Valvon, J., Pal-Borbely, G., and Rees, L. V. C., (2002), "The Skeletal Isomerization of *n*-butene over ferrierite Catalysts", *Applied Surface Science*, **196**, 401-407
- Pais da Silva, M.I., Lins da Silva, F., and TellezS, S.A., (2002), "FT-Infrared Band Analysis and Temperature Programmed Desorption for The Y, L and Ferrierite Zeolites", *Spectrochimica Acta Part A*, **58**, 3159-3166
- Perego, G., Bellussi, G., Millini, R., Alberti, A., and Zanardi, S., (2002), "B-Containing Molecular Sieves Crystallized in the Presence of Ethylenediamine. Part I: Crystal Structure of as-synthesized B-Fer", *Microporous and Mesoporous Materials*, **56**, 193-202

- Prabir P.K., Roa K.M., Kresge C. T., Kennedy G.J., (1994) "Examination of the Growth Dynamics of Zeolite ZSM-5 and Mordenite from Inorganic Reactant Composition", *Microporous Materials*, **3**, 17-27
- Peixoto, D.P.B., Cabral de Menezes, S.M., and Pais da Silva, M.I., (2003), "Influence of Different Processes of Dealumination on Acid Properties of an H-Ferrierite Zeolite", *Materials Letters*, **4453**, 1 – 10
- Ramli Z., (1995), "Rhenium-Impregnated Zeolites: Synthesis, Characterization and Modification as Catalyst in the Metathesis of Alkenes" Universiti Teknologi Malaysia: Ph.D Thesis
- Rawtani, A.V., and Rao, M.S., (1989), "Synthesis of ZSM-5 Zeolite Using Silica from Rice Husk Ash", *Ind. Eng. Chem. Res.* **28**, 1411-1414
- Robert L. V., (2000), "Zeolites", *U.S. Geological Survey Minerals Yearbook*, **85**, 1-5
- Roeseler, J., Heitmann, G., Holderich, W., Chon, H.S.K., Uh, Y.S., (Eds), "Progress in Zeolites and Microporous Materials", *Studies in Surface Science and Catalysis, Part B*, Elsevier, Amsterdam, **105**, 1173
- Rollmann L. D., Schlenker J. L., Kennedy C. L., Kennedy G. J. and Doren D. J., (2000), "On the Role of Small Amines in Zeolite Synthesis. 2", *Journal of Physical Chemistry, B*, **104**, 721-726
- Rollmann L. D., Schlenker J. L., Lawton S. L., Kennedy C. L., Kennedy G. J. and Doren D. J., (1999), "On the Role of Small Amines in Zeolite Synthesis", *Journal of Physical Chemistry, B*, **103**, 7175-7183
- Sanyuang, Y. Vlessidis A. G. and Exmiridis N. P., (1997), "Synthesis of Zeolites in the System Na₂O-SiO₂- Al₂O₃-H₂O-Glycerol", *Mesoporous Material*, **9**, 273-286

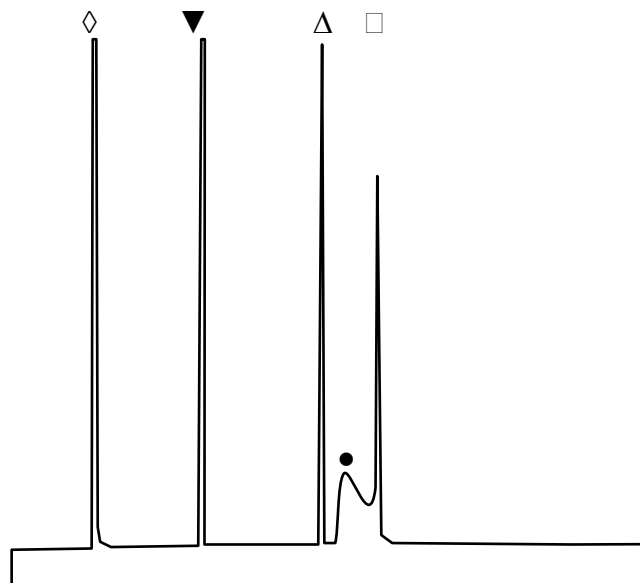
- Scott J. W., "Structure Direction in Microporous Materials: Synthesis and Characterization of Ferrierite Catalyst and Novel Phosphate Molecular Sieves", (1996), University of California, Ph.D. Thesis
- Seijger, G. B., Niekerk, P. V., Krishna, K.K., Calis, H. P. A., Bekkum H. V., and Bleek C. M. (2003), "Screening of Silver and Cerium Exchanged Zeolite Catalysts for the Lean Burn Reduction of NO_x with Propene", *Applied Catalysis B: Environmental*, **20**, 31-42
- Silva M. I. P.D, Silva F. L.D and Tellez C. A. S., (2002), "FT-Infrared Band Analysis and Temperature Programmed Desorption for the Y, L and Ferrierite Zeolites", *Spectrochimica Acta Part A*, **58**, 3159-3166
- Sing, K.S.W., Everett, D.H., Haul, R.A.W., Moscou, L., Pierotti, R.A., Rouquerol, J., and Siemieniewska, (1985), "Reporting Physisorption Data for Gas/Solid Systems with Special Reference to the Determination of Surface Area and Porosity", *Pure Applied Chemistry*, **57**, 603-619
- Smith, M.B, (1994). "Organic Synthesis", New York: McGraw-Hill
- Sobalik, Z., Dedecek, J., Kaucki, D., Wichterlova, B., Drozdova, L., and Prins, R., (2000), "Structure, Distribution, and Properties of Co Ions in Ferrierite Revealed by FTIR, UV-Vis, and EXAFS", *Journal of Catalysis*, **194**, 330-342
- Sugita, S., Shoya, M., and Tokuda, H. (1992), "Evaluation of Pozzolanic Activity of Rice Husk Ash", Proc. Of the Fourth CANMET ACI Int. conference. Turkey. 95-512
- Szoastak R., (1989) "Molecular Sieves, Principle of Synthesis and Identification", New York: Reinhold
- Tae J. K. Wha S. A. and Suk, B. H. (1996) "Synthesis of Ferrierite in the absence of Inorganic Cations", *Microporous and Mesoporous Materials*, **7**, 35-40

- Tanabe K. and Holderich W.F., (1999), "Industrial Application of Solid Acid-Base Catalyst", *Applied Catalysis A: General*, **181**, 399-434
- Taramasso, M., Manara, G., Fattore, V., and Notari, B., (1990), Assign to SnamProgetti S.p.A., GB Patent 2024790,
- Treacy, M.M.J., Higgins, J. B. and Von Bollmoos, R. (1996), "Collection of Simulated XRD Powder Patterns for Zeolite." 3rd ed. Amsterdam: Elsevier
- Ueda S. and Koizumi M., (1979), "Crystallization of Analcime Solid Solutions from Aqueous Solutions", *American Mineralogist*, **64**, 172-179
- West, A.R. (1988), "Basic Solid State Chemistry", New York: John Wiley and Sons Inc.
- Wichterlova B., Tvaruzkova Z., Sobalik Z. and Sarv P., (1998), "Determination and Properties of Acid Sites in H-Ferrierite. A Comparison of Ferrierite and MFI Structures", *Microporous and Mesoporous Materials*, **24**, 223-233
- Xu W. Q., Yin Y. G., Suib S. L., Edwards J. C. and O'Young C. L., (1995), "n-Butene Skeletal Isomerization to Isobutylene on Shape Selective Catalysis: Ferrierite/ZSM-35", *Journal of Physical Chemistry*, **99**, 9443-9451
- Xu, W.Q., Yin, Y.G., Suib, S.L., Edwards, J.C., and O'Young. C.L. (1996), "Modification of Non-template Synthesized Ferrierite/ZSM-35 for n-Butene Skeletal Isomerization to Isobutylene" *Journal of Catalysis*, **163**, 232-244
- Yokomori Y. Wachmuth J. and Koji N., (2001) "Structure and Bronsted Acid Sites of Ferrierite", *Microporous and Mesoporous Materials*, **50**, 137-143
- Zhdanov, S.P., Feoktissova, N.N., Vtjurina, L.M., Öhlman, G., Pfefer, H., Fricke R., eds., (1971), "Catalysis and Adsorption by Zeolites", *Studies in Surface Science and Catalysis*, 65, Elsevier, Amsterdam, 287.

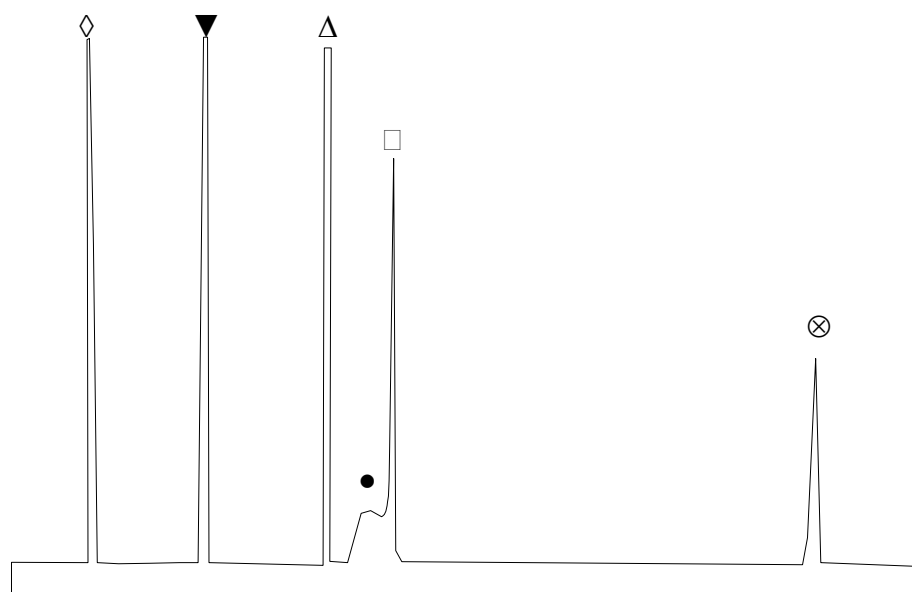
Appendix A

Gas Chromatography chromatogram for the reaction of propionic anhydride and anisole

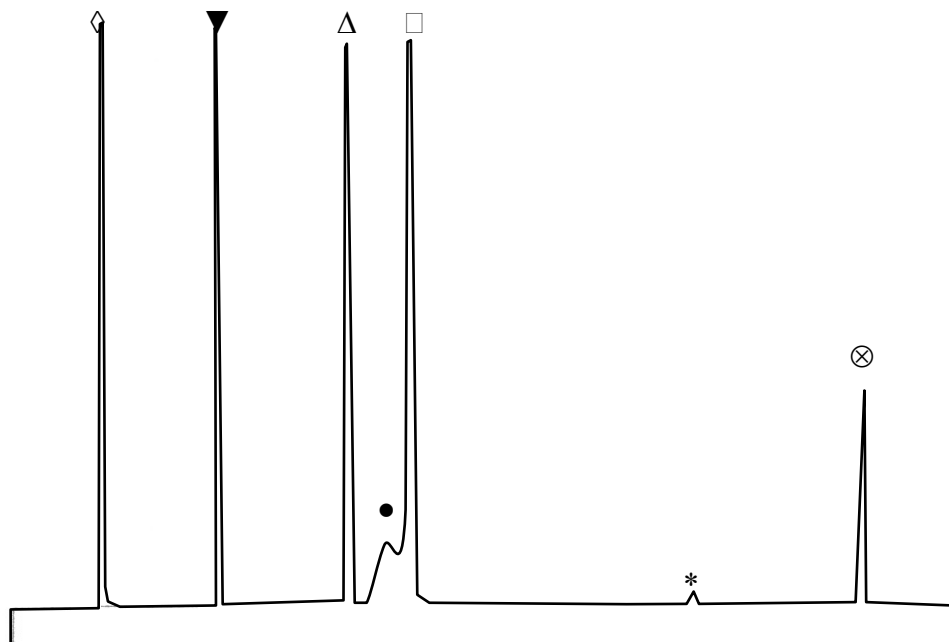
Notes - Δ = anisole, \bullet = propionic anhydride, \blacktriangledown = toluene, \diamond = n-hexane, \square = propionic acid, \otimes = *p*-methoxypropiofenone, * = unidentified product



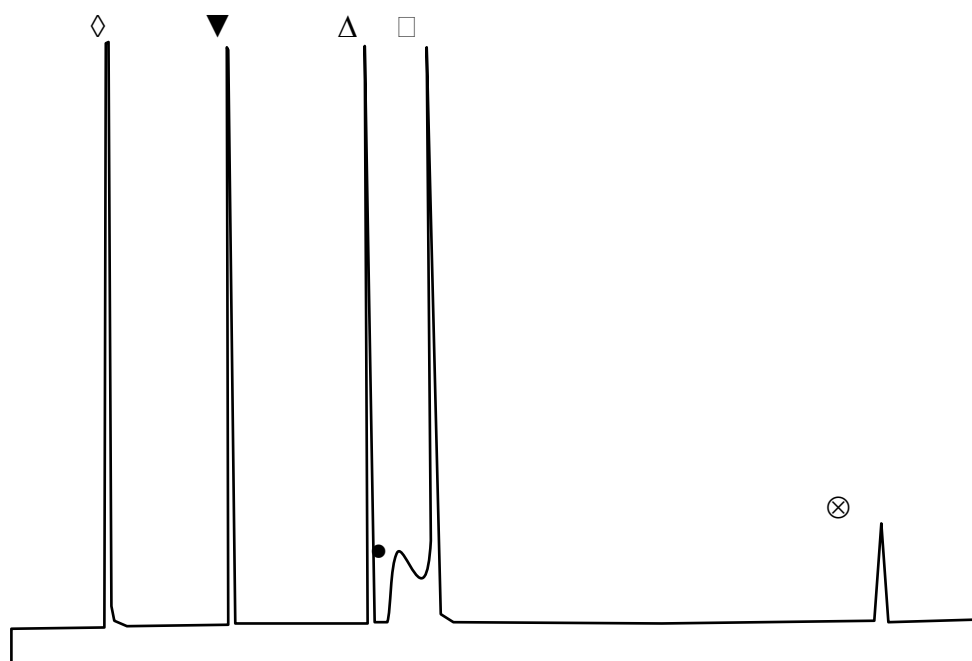
Reactant at 0 hour



H-Fer 12



H-Fer 20



H-Fer 30

Appendix B

Data obtained from GC-FID Chromatograms (Friedel-Crafts acylation of anisole and propionic acid)

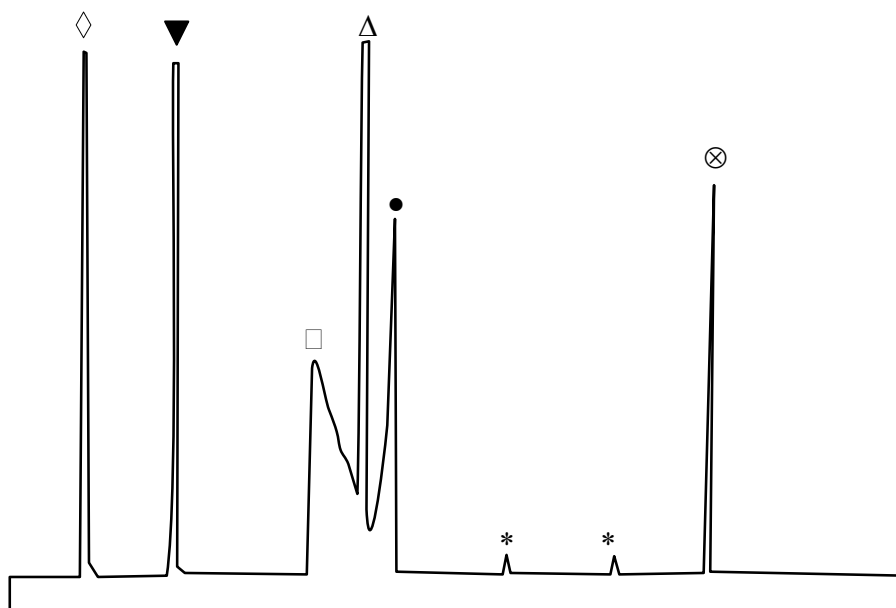
Time	0	0.25	0.45	1.5	2	2.5	4	20	24
anisole area, (9.09)	4126182	2932516	2107211	2067745	1990659	1952696	1557060	972419	869357
propionic acid area, (22.65)	0	36055	66580	73619	88183	125301	128898	145486	177283
propionic acid area, (10.72)	917274	1005548	856112	881992	856642	934367	530997	557586	551166
internal standard area, (5.46)	486262	400617	416126	433056	419923	450726	413502	327726	325957
Conversion, %	0	12.6	37.66	41.06	41.44	45.97	52.26	61.12	64.43
Selectivity, %	0	12.5	47.73	52.04	56.7	59.02	60.25	70.27	73.23

Reaction time	0	0.25	0.45	1.5	2	2.5	4	20	24
% anisole	67.53	56.73	52.37	51.1	50.3	47.33	43.76	37.77	34.75
% propionic acid	32.46	41.76	44.18	45.11	45	46.43	48.94	51.11	51.75
% <i>p</i>-methoxypropiofenone	0	1.49	3.45	3.77	4.6	6.23	7.29	11.03	13.5

Appendix C

GC chromatogram for the reaction of acetic anhydride and anisole using H-Fer 12 as catalyst

Notes - Δ = anisole, \bullet = acetic anhydride, \blacktriangledown = toluene, \diamond = n-hexane, \square = acetic acid, \otimes = *p*-methoxyacetophenone, * = unidentified product



Appendix D

- | NO. | PUBLICATIONS |
|-----|---|
| 1 | Synthesis of ZSM-5 type Zeolite using Crystallina Silica from Rice Husk Ash, (2003), <i>Malaysian Journal of Chemistry</i> , 5 , 048-055 |
| 2 | Effect of Molar Oxides Composition of Ferrierite from Rice Husk Ash, (2003), presented at Annual Fundamental Science Seminar, Institut Ibnu Sina, UTM |
| 3 | Effect of Ferrierite Support For TiO ₂ Loading as Photocatalysts, (2004), presented at Annual Fundamental Science Seminar, Institut Ibnu Sina, UTM |
| 4 | The reactivity of H-Ferrierite from rice husk ash as catalysts over Friedel-Crafts acylation of anisole, (2004), presented at Symposium on Science and Mathematics 2004, Faculty of Science, UTM, 14-15 December 2004 |